An Experimental and Numerical Investigation of Multiphase Flow Splitting at an Impacting T-Junction Between a Single Flowline And Two Risers

J.P.A. Beekers

Master of Science Thesis

TU Delft Delft University of Technology

Faculty of Applied Sciences

An Experimental and Numerical Investigation of Multiphase Flow Splitting at an Impacting T-Junction Between a Single Flowline And Two Risers

Master of Science Thesis

To obtain the degree of Master of Science in Applied Physics at Delft University of Technology

Author:

Name:	J.P.A. (Jaap) Beekers
Student number:	1357905
Project duration:	April 2015 - March 2016

Thesis committee:

Prof. dr. R.F. Mudde	TU Delft, supervisor
Prof. dr. ir. R.A.W.M. Henkes	TU Delft & Shell, supervisor
Dr. P.J. Hamersma	TU Delft
Dr. J. Ellepola,	Shell, supervisor (guest in committee)

Faculty of Applied Sciences (AS) · Delft University of Technology

Copyright ©
All rights reserved.

Abstract

In 2011, Royal Dutch Shell plc (Shell) took the final investment decision to develop the Prelude gas field using the world's first Floating Liquefied Natural Gas (FLNG) facility. FLNG poses some new technical challenges. For example, as the vessel is moored to the seabed, it is subject to movements induced by waves, winds and tides. Therefore, flexible instead of rigid risers are used to bring the gas from the seabed to the surface. However, these risers are limited in diameter. For Prelude each flowline is connected to a single riser. In new future projects it might be beneficial to have a single (larger diameter) subsea flowline at the sea floor which is split into two or more flexible risers. This flow split is complicated as gas wells produce a multiphase mixture of gas, hydrocarbon condensates and/or water. There thus is a need to understand how the different phases will distribute over the multiple risers, and how this will influence the whole operation.

In previous lab experiments [1], a horizontal symmetric impacting T-junction was used to divide the multiphase mixture from the horizontal flowline into two vertical risers. It was found that at low gas flow rates, for which the flow regime in the risers is hydrodynamic slug flow, non-symmetric distributions in the phase split are the rule rather than the exception. These maldistributions exhibit transient behaviour, and exhibit hysteresis. However, in gas production from dry fields with low Liquid to Gas Ratios (LGR), the gas flow rates generally are higher and the flow regime in the vertical risers is annular flow. In this flow pattern, liquids flow in the upward direction and no liquid buildup occurs at the riser base. As annular flow is more stable in time, it is expected that for these conditions the phase splits are evenly distributed over the two risers and no transient behaviour is present.

The main aim of the present study was to verify the hypothesis that if the gas flow rate is sufficiently high to sustain annular flow in both risers the phases will distribute evenly. Thereto experiments were performed in the Severe Slugging Loop (SSL) at the Shell Technology Centre Amsterdam. The loop consists of a 100 $[m]$ horizontal flowline connected via an impacting T-junction to two 1.25 $[in]$ diameter vertical risers of 16.8 $[m]$ height. The facility is operated with an air-water mixture at atmospheric pressure and ambient temperature.

As the SSL is not equipped with flow meters to measure the phase flow in the risers, a new method is developed to identify maldistribution in the phase split. In two phase flow in a

vertical riser, the flow rates in the pipe are not uniquely determined by the pressure drop. However, in the current dual riser experiments the total flow rate in the setup is known. It is found that, with the use of single riser benchmark data and visual inspection, one can distinguish between an equal and an unequal phase split.

Experiments are performed to test the stability of the phase split, and the effect of hysteresis for various gas and liquid flow rate combinations. It is observed that five different states exist for the flow split in the single flowline dual riser geometry. Out of these, only two are stable, which occur on opposite sides of a certain gas flow rate transition point. This point is identified as the minimum in the pressure gradient curve for a single vertical riser. This minimum can be linked to the transition from churn flow to annular flow.

In addition to the experiments, a computational model is proposed to predict the phase split. In this model, the Shell Flow Correlations (SFC) for multiphase pipe flow are used to propagate the boundary conditions of the system from the riser tops to the corresponding outlets of the splitter at the base of the risers. Next, all possible phase splits which satisfy the extended Bernoulli equation and the conservation of momentum in the splitter are identified. The model conserves mass implicitly. The extended Bernoulli equation is implemented as the Advanced Double Stream Model (ADSM) [2], the control volume approach is used for the conservation of momentum. All three sub-models assume 1D steady state fully developed flow in the different parts of the geometry.

By imposing different back pressures on the risers, for a constant gas and liquid flow, the model can generate phase split curves. These are compared to experimental data available in the literature and experimental results by Van de Gronden. It is found that the write-up of the derivations in the original ADSM paper [2] contains typos or errors. Therefore we have derived new relations, but they do not exhibit the same behaviour as the modelling results presented in the paper. From the comparison with the experimental results, it is concluded that the proposed computational model, which assumes 1D steady state fully developed flow, predicts a much too symmetric phase split. The modelling effort has not yet resulted in a reliable for the phase split prediction model.

Table of Contents

List of Figures

List of Tables

Nomenclature

Greek symbols

Symbol	Description	Units
α_G	Gas hold-up	$[-]$
α_L	Liquid hold-up	$[-]$
β	flow shape factor	$[-]$
ε	Wall roughness	$[m]$
θ	Wetted wall fraction	$[-]$
θ_G	Gutter angle	$[-]$
κ	Kinetic energy ratio	$[-]$
λ	Thermal conductivity	$[W/mK]$
λ_G	Mass fraction take off into the branch for the gas	$[-]$
λ_L	Mass fraction take off into the branch for the liquid	$[-]$
μ	Viscosity	$[kg/sm]$
ρ	Density	$[kg/m^3]$
σ	Surface tension	$[N/m]$
τ	Stress tensor	$[N/m^2]$
ϕ	Inclination angle, Angular coordinate	$[rad]$, $[rad]$

Latin symbols

Symbol	Description	Units
A	Pipe cross-section	$[m^2]$
A_G	Pipe cross-section occupied by the gas phase	$[m^2]$
A_L	Pipe cross-section occupied by the liquid phase	$[m^2]$
c_p	Heat capacity	$[J/kgK]$
D	Diameter	$[m]$
$\hat{E}_v$	Energy loss factor	$[J/s]$
f	Non-dimensional friction factor	$[-]$
F	Force	$[N]$
F_{BG}	Mass fraction take off into the branch for the gas	$[-]$
F_{BL}	Mass fraction take off into the branch for the liquid	$[-]$
g	Gravitational acceleration	$[m/s^2]$
h	Enthalpy	$[J]$
k	Friction loss coefficient	[]
L	Length	$[m]$
$\dot{M}_R$	Momentum flux ratio	$[-]$
n	normal coordinate	$[m]$
N	Number of unit cells	$[-]$
p	Pressure	$[Pa]$
Δp	Pressure drop	$[Pa]$
$\overline{\Delta p}$	Normalized pressure drop over the riser	$[-]$
$\dot{q}$	Internal heat source	$[J/s]$
Q_G	Volumetric flow rate of the gas	$[m^3/s]$
Q_L	Volumetric flow rate of the liquid	$[m^3/s]$
r	Radial coordinate	$[m]$
S	Internal perimeter	$[m]$
t	Time	$[s]$
T	Temperature	$[K]$
u_G	Actual velocity of the gas	$[m/s]$
u_L	Actual velocity of the liquid	$[m/s]$
u_{SG}	Superficial velocity of the gas	$[m/s]$
u_{SL}	Superficial velocity of the liquid	$[m/s]$
W_G	Mass flow rate of the gas	$[kg/s]$
W_L	Mass flow rate of the liquid	$[kg/s]$
x	Quality, Cartesian coordinate	$[-]$,$[m]$
y	Cartesian coordinate	$[m]$
z	Height of the centre of mass of the fluid	$[m]$

Preface

This report is the result of my graduation internship at Royal Dutch Shell and it serves as my thesis for the master Applied Physics at Delft University of Technology. Looking back at my time in Delft, I am happy to conclude that I have enjoyed every moment, it was a wonderful period of my life.

I consider the opportunity to graduate at Shell on multiphase flow splitting as a great experience. Not only did it offer me the possibility to perform research with a unique experimental setup, it also gave me an interesting inside look into how research is performed within a multinational.

First, I would like to thank Ruud Henkes who offered me this project, and who gave me the opportunity to write my thesis at a company. During my stay at Shell you were both a mentor and a supervisor to me, providing feedback on my scientific work and coaching my personal development.

Next, I would like to thank Jerome Ellepola who assisted and guided me through this research as my daily supervisor. Without your enthusiasm, critical questions and knowledge on performing experimental work, this project would not have been possible. I especially appreciated your endless devotion in providing feedback and taking time for me.

My time at the Shell would not have been the same without my fellow interns and the guys from finance. I have appreciated the many laughs we shared within and outside the office. Also I want to thank Christophe T'Joen, Patricio Rosen and Sebastiaan Olijerhoek who were great sparring partners during various stages of my project.

I also want to thank Rob Mudde, who was my thesis supervisor at Delft University and who allowed me to perform this research outside the walls of applied sciences. In our meetings you always managed to quickly address the issues in my work and guide me towards new solutions and viewpoints.

Last but not least, I would like to thank my dear family and friends for all the support. Especially my parents, Julie, Anne and Bas for the unconditional trust you gave me, thank you for everything!

Jaap Beekers, February 2016

Chapter 1

Introduction

In 2011, Royal Dutch Shell plc (Shell) took the final investment decision to develop the Prelude gas field using the world's first Floating Liquefied Natural Gas (FLNG) facility. This 488 $[m]$ long, 74 $[m]$ wide floating processing facility, is shown in Figure 1-1. The FLNG concept will help unlocking new offshore gas fields.

With FLNG it will become viable and profitable to operate remote gas fields far from the coast. As the FLNG vessel can float in the vicinity of the field, this concepts does not need compression platforms, long trunklines[1] or onshore processing facilities. This not only reduces the cost of developing remote gas fields, but also minimizes the environmental impact of the development and operation.

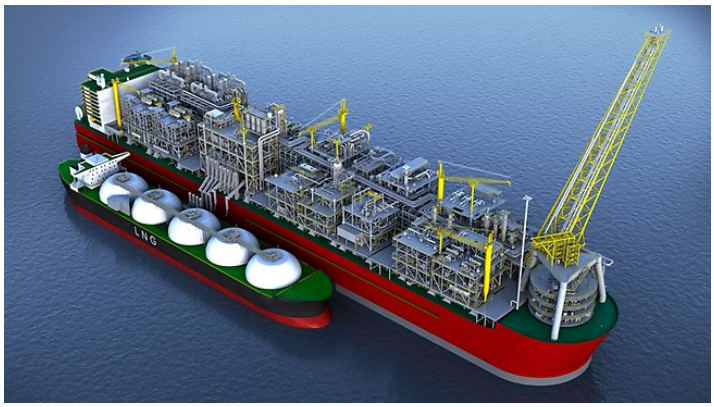

Figure 1-1: Artist impression of the FLNG facility *Prelude* with a LNG carrier docked alongside.

Besides new opportunities for Shell, FLNG introduces new technical challenges. Traditional fixed, static processing platforms use a stiff carbon steel riser to transport the gas from the seabed to the platform. As the FLNG facility is moored to the seafloor, there will be movements due to waves, winds and tides, and therefore it is difficult to use traditional carbon

[1] Transport pipelines to shore

steel rigid risers. Flexible risers can be used to mitigated this problem. These flexible risers have two important limitations:

- Due to material properties, construction constraints and maximum weight, current commercially available flexible risers have a maximum diameter of about 14 $[in]$.
- The fluid velocity in flexible risers is limited to 20 $[m/s]$. For higher fluid velocities mechanical failure can occur due to flow induced vibrations or erosion. Also unacceptable noise is generated for dry gas at to high fluid velocities.

The rigid subsea flowlines, attached to the flexible risers are not limited by constraints. For the Prelude project, it was decided to attach each 12 $[in]$ horizontal flowline to a 12 $[in]$ riser. This type of construction is shown in Figure 1-2a.

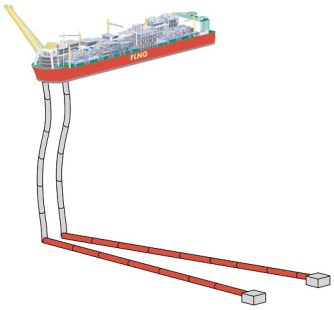

(a) Single riser, single flowline subsea construction designed for *Prelude*.

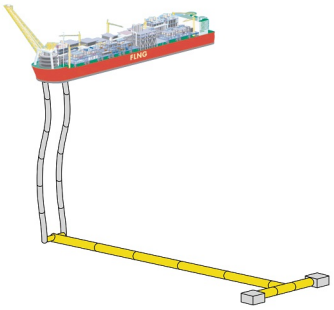

(b) Dual riser, single flowline subsea construction which has the potential to reduce CAPEX by 25%.

Figure 1-2

A rule of thumb for CAPEX of a subsea pipeline is 200 kUSD/mile/inch of diameter. For two, fifty miles, twelve $[in]$ pipelines, the total cost is $2 \cdot 200\text{k} \cdot 50$ miles $\cdot 12$ in $= 240$M USD. An alternative is, to replace the two flowlines with one 18 $[in]$ diameter pipe as shown in Figure 1-2b. The costs for such a single pipeline are $1 \cdot 200\text{k} \cdot 50$ miles $\cdot 18$ in $= 180$M USD, which is a CAPEX reduction of 25%.

However, this alternative subsea configuration introduces a new difficulty. As gas is extracted from the reservoir, liquids (e.g. condensate and water) are co-produced. When this multiphase mixture arrives at the end of the flowline, the question arises how the different phases will split across the risers. The processing equipment on the FLNG facility requires a steady production from all risers, as the capacity of their separators is limited. Therefore, a stable split of the gas phase and the liquid phase over the multiple risers is desired.

From previous research, it is known that at low gas flow rates unequal distributions in the phase split can occur. These maldistributions range from small asymmetries in the gas split, to situations where a stagnant liquid column forms in one of the risers, which forces all the gas and liquid production to the other risers. There are cases known, in which natural transients occur. Then, the asymmetries change unexpectedly over time without any identifiable cause or warning. Such phenomena can potentially damage processing facilities, and these can put the safe work environment for the staff at risk.

The Shell Multiphase Flow Team, where this master thesis study was performed, is responsible for defining the design criteria for the single flowline multiple riser configuration. Previous research on the topic in Shell is the work by Prickaerts[4] and the work by Van der Gronden[1]. Prickaerts used a branching T-junction to divide the multiphase mixture from the horizontal flowline over two vertical risers, Van der Gronden used an impacting T-junction. Both performed experiments at low gas flow rates, and both found unequal phase splits and transient behavior.

1-1 Research objectives

The goal of the current research is to test the hypothesis that:

The phase split from a single flowline into two vertical risers using an impacting T-junction will be symmetric and stable in time when the total gas flow rate is sufficiently high to sustain annular flow in both risers

To verify the hypothesis, experiments have been performed in the Severe Slugging Loop (SSL) at the Shell Technology Centre in Amsterdam. The experimental setup consists of a single 100 $[m]$ horizontal flowline followed by an impacting T-junction which splits the fluid flow into two 16.85 $[m]$ vertical risers. The working fluid in the experiments is an air-water mixture at ambient temperature and atmospheric pressure.

The research objectives are defined as follows:

1. Test recent changes made in the flow facility.
2. Carry out experiments for various liquid/gas flow rates that result into either slug flow, churn flow or annular flow in the risers.
3. Verify the basic assumption in the design rule (i.e. no maldistribution if the flow regime in both risers is annular flow.)
4. Carry out stability tests using topside chokes.
5. Carry out simulations using existing flow modeling tools. Particularly simulate how the risers downstream of the splitter can introduce maldistribution in the phase split.

1-2 Outline of the report

In Chapter 2 the theory of single phase and two phase fluid flow in pipes is presented. In Chapter 3 an overview of the literature on flow splitting at an impacting tee is given. Later, the influence of multiple operational parameters and fluid properties on the phase split is discussed separately. In Chapter 4 the experimental setup used in this research is introduced. Chapter 5 describes in detail how the experiments were performed. First single riser results are discussed, followed by dual riser results (which are the main part of this research). In

Chapter 6 a phase split prediction model is proposed and tested. In Chapter 7 the conclusions for this work, and the recommendations for further work are presented.

To improve the readability of this work, the report is written in a modular way. The reader can decide to skip certain chapters, and still comprehend the results presented. Therefore, some repetitiveness of concepts is encountered when reading the full report.

1-2-1 For the hurried reader

In order to understand the essence of the work (without having to read through all the details) the reader is advised to pay attention to at least the following sections:

1. Section 2-3, for a quick introduction of the additional implications in two phase pipe flow.
2. Figure 4-1, which gives a schematic overview of the experimental setup used in the current research.
3. Section 5-3-3, where the five different states of the flow split are identified and described. Their stability and their occurrence are discussed here too.
4. Figure 5-18, which shows the same trend in the location of the pressure drop minimum for a single riser at given liquid flow rates and the locations of the transitional gas flow rates.
5. Section 6-2, where the concept and the different components of the phase split predicting model are discussed.
6. Chapter 7, which summarizes the general conclusions drawn in this work and where recommendations for future research are given.

Chapter 2

Fundamentals of pipe flow

This chapter provides a short overview of the basic theory of fluid flow in pipes. First the governing equations are treated. Then, these are applied to single phase flow and to two phase flow. Both are addressed in the same way to emphasize the similarities and the differences between both types of flows.

2-1 Governing equations for transport phenomena

Transport phenomena form the common name for processes involving the transfer of mass, momentum and energy. The transport of these three quantities can be described using a similar mathematical framework. These conservation equations dictate that a change in the amount of mass, moment and energy in a certain control volume over time, can only be attributed to fluxes over the boundaries of the volume and to source or sink terms present within the control volume.

The most general representations for these conservation laws, in three dimensions, are listed below:

$$\frac{\partial}{\partial t}\rho + \nabla \cdot \rho\mathbf{u} = 0 \tag{2-1}$$

$$\left(\frac{\partial}{\partial t}\rho\mathbf{u} + \mathbf{u} \cdot \nabla\rho\mathbf{u}\right) = \nabla \cdot \tau + \sum \mathbf{F} \tag{2-2}$$

$$\rho\left(\frac{\partial}{\partial t}h + \mathbf{u} \cdot \nabla h\right) = \rho\dot{q} + \nabla \cdot \left(\frac{\lambda}{c_p}\nabla h\right) \tag{2-3}$$

Here, ρ is the density, t is time and $\mathbf{u}$ is the velocity vector. τ is the stress tensor and $\sum \mathbf{F}$ are all body forces. h is the enthalpy, $\dot{q}$ is the internal heat source and λ and c_p are the thermal conductivity and the heat capacity, respectively.

Equation 2-1 is known as the continuity equation which governs the conservation of mass. The 0 on the right hand side indicates that there are neither sinks nor sources of mass present. This is obvious as mass can neither be created or destroyed[1].

Conservation of momentum is described by Equation 2-2.This is Newton's second law, expressed per unit of fluid volume. The momentum related terms are on the left hand side. The total amount of momentum is subject to the forces on the right hand side.

The final equation, 2-3, represents the conservation of energy. In the current research the flow is assumed to be isothermal. Therefore this third conservation law will play a minor role.

2-2 Single phase pipe flow

Thanks to the axial geometry of the pipeline the three spatial dimensions in the governing equations can be reduced to one coordinate in the longitudinal direction s and still provide sufficient detail. In this so-called 1D-approximation the parameters of the flow are averaged over the cross section of the pipe.

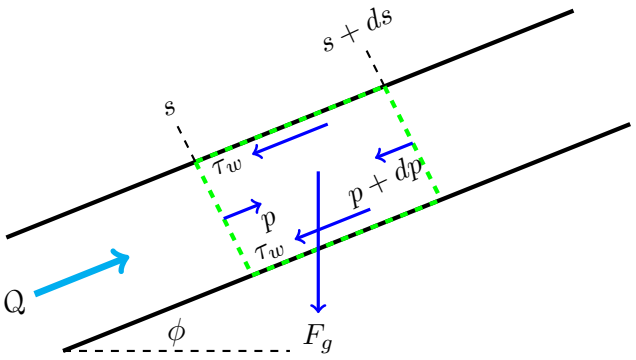

Figure 2-1: 1D-approximation for upward single phase flow in an inclined pipe.

With this approximation Equation 2-1 and Equation 2-2 for the single phase pipe flow in Figure 2-1 become:

$$\frac{\partial}{\partial t}\rho A + \frac{\partial}{\partial s}\rho u A = 0 \tag{2-4}$$

$$\frac{\partial}{\partial t}\rho u A + \frac{\partial}{\partial s}\rho u^2 A = -\frac{\partial p}{\partial s}A + \tau_w S + F_g \tag{2-5}$$

Combining the simplified mass and momentum equation and rewriting the gravity term results in:

$$\rho\frac{\partial}{\partial t}u + \rho u\frac{\partial}{\partial s}u = -\frac{\partial p}{\partial s} + \frac{\tau_w S}{A} - \rho g \sin\varphi \tag{2-6}$$

[1] When excluding relativistic effects

Where u is the averaged velocity, p is the pressure, τ represents the wall shear stress, S is the wetted surface of the pipe (which for single phase flow is equal to the internal perimeter), g is the gravitational acceleration and φ is the inclination angle of the pipe.

2-2-1 Flow regime

All parameters in Equation 2-6 can be determined in a straightforward manner, except for the wall shear stress. Usually, τ is modeled with a non-dimensional friction factor f.

$$\tau_w = f\frac{1}{2}\rho u^2 \tag{2-7}$$

Generally, this friction factor depends on the wall roughness ϵ and the non-dimensional ratio between the inertial and the viscous forces in the fluid. This ratio is called the Reynolds number and is defined as:

$$Re = \frac{\rho u D}{\mu} \tag{2-8}$$

where D is the diameter which is the characteristic length scale of the pipeline and μ is the dynamic viscosity. For low Reynolds numbers up to 2000 the flow in the pipe is laminar [5]. It can be derived analytically that for these conditions the following relation holds for the friction factor:

$$f = \frac{16}{Re}, \qquad Re \leq 2000 \tag{2-9}$$

Pipe flow with a Reynolds number of 4000 or higher will be turbulent flow and here no analytical solution is available for the friction factor. A widely used relation is the Churchill correlation [6]:

$$f = 2\left[\left(\frac{8}{Re}\right)^{12} + \frac{1}{(A+B)^{\frac{3}{2}}}\right]^{\frac{1}{12}} \tag{2-10}$$

with,

$$A = \left\{2.457 \ln\left[\left(\frac{7}{Re}\right)^{0.9} + 0.27\frac{\epsilon}{D}\right]\right\}^{16}, \qquad B = \left(\frac{37530}{Re}\right)^{16}$$

The advantage of this correlation is that it covers the friction factor for both laminar and turbulent flow since for low Reynolds numbers Equation 2-10 reduces to the analytical solution.

For Reynolds numbers between 2000 and 4000 the flow is neither fully laminar nor fully turbulent. This flow regime is therefore called transitional flow. The value of the friction factor at these conditions is subject to large uncertainties.

2-2-2 Pressure drop

Calculating the pressure drop in single phase pipe flow is quite straightforward when the flow is assumed to be fully developed and in steady state (hence $\rho\frac{\partial}{\partial t}u + \rho u\frac{\partial}{\partial s}u = 0$). Equation 2-6 can then be rearranged to:

$$\frac{\partial p}{\partial s} = \frac{2f\rho u^2}{D} - \rho g \sin\varphi \tag{2-11}$$

It is seen that the pressure drop consists of a frictional part which scales with the velocity and the diameter, and of a gravitational part which scales with the inclination of the pipe. For horizontal pipe flow the gravitational term is 0.

2-2-3 Scaling

Subsea pipelines in the oil and gas industry, can have a diameter up to 40 [in] and reach lengths of over 100 $[km]$. These dimensions can not be met in experimental setups. For the scaling of the flow conditions and geometry of the subsea pipeline to the laboratory setup non-dimensional numbers are used.

These numbers are identified using the Buckingham Π theorem [5]. This theorem states that the number of non-dimensional groups follows from subtracting the number of basic units from the total number of independent parameters. From the foregoing derivations for isothermal single phase pipe flow, five independent parameters are identified, as listed in Table 2-1.

Table 2-1: Governing parameters in isothermal single phase pipe flow.

Parameter	**Symbol**
Characteristic length	D
Characteristic velocity	u
Density	ρ
Viscosity	μ
Gravitational acceleration	g

The three basic units are time, length and mass. Therefore, two non-dimensional groups are needed to scale the single phase pipe flow conditions in the field to the laboratory. One of these two is the Reynolds number which was already mentioned above.

$$Re = \frac{\rho u D}{\mu} \tag{2-12}$$

The second non-dimensional group is the Froude number.

$$Fr = \frac{u^2}{gD} \tag{2-13}$$

This number is the ratio between the inertial and the gravitational forces in the fluid.

2-3 Two phase pipe flow

For two-phase flow a similar analysis can be performed as for single phase flow. However, in this case the cross section of the pipe is occupied by two different phases. The ratio of the cross section occupied by the gas and the total cross section is called the gas holdup (α_G). In a similar way the liquid holdup (α_L) is the ratio between the part of the cross section occupied with liquid and the total pipe cross section. The equations for the gas holdup and the liquid holdup are respectively:

$$\alpha_G = \frac{A_G}{A} \tag{2-14}$$

$$\alpha_L = \frac{A_L}{A} \tag{2-15}$$

The two variables are coupled by $\alpha_G + \alpha_L = 1$.

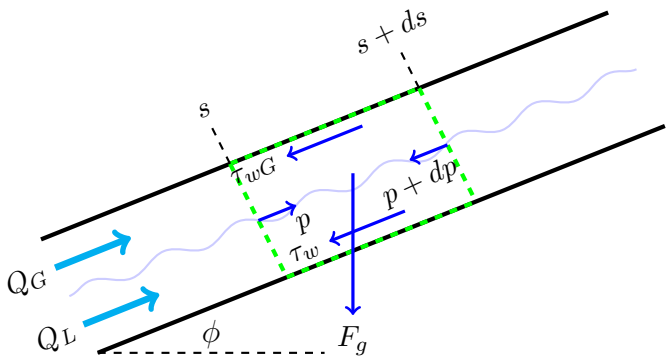

Figure 2-2: 1D-approximation for upward separated two phase flow in an inclined pipe.

Following the same approximations as for single phase pipe flow, the conservation laws for mass and momentum for the two phase flow in Figure 2-2 become:

$$\frac{\partial}{\partial t}\alpha_G\rho_G A + \frac{\partial}{\partial t}\alpha_L\rho_L A + \frac{\partial}{\partial s}\alpha_G\rho_G u_G A + \frac{\partial}{\partial s}\alpha_L\rho_L u_L A = 0 \tag{2-16}$$

$$\begin{aligned}\frac{\partial}{\partial t}\alpha_G\rho_G u_G A + \frac{\partial}{\partial t}\alpha_L\rho_L u_L A + \frac{\partial}{\partial s}\alpha_G\rho_G u_G^2 A + \frac{\partial}{\partial s}\alpha_L\rho_L u_L^2 A = \\ -\frac{\partial p}{\partial s}A + \tau_{wG}S_G - \tau_{GL}S_{GL} + \tau_{LG}S_{LG} + \tau_{wL}S_L + F_{g,G} + F_{g,L}\end{aligned} \tag{2-17}$$

Again both equations are combined and the gravity term is rewritten:

$$\begin{aligned}\alpha_G\rho_G\frac{\partial}{\partial t}u_G + \alpha_L\rho_L\frac{\partial}{\partial t}u_L + \alpha_G\rho u_G\frac{\partial}{\partial s}u_G + \alpha_L\rho u_L\frac{\partial}{\partial s}u_L = \\ -\frac{\partial p}{\partial s} + \frac{\tau_{wG}S_G}{A} + \frac{\tau_{wL}S_L}{A} - \alpha_G\rho_G g\sin\varphi - \alpha_L\rho_L g\sin\varphi\end{aligned} \tag{2-18}$$

here τ_{wG} and τ_{wL} are the shear stress between the wall and the corresponding phase. This stress is modeled the same as in Equation 2-7, equally for the friction factor f. The associated wetted perimeters S_G and S_L together are equal to the internal perimeter. Interestingly, the interfacial friction terms between both phases drop out of the equation due to Newton's third law. This does not mean that they do not influence the flow and in fact the exact opposite is true. The interfacial friction plays a role in the formation of flow patterns in the two phase mixture and thereby directly influences the gas holdup α_G and the liquid holdup α_L.

The models, and the corresponding sub-models, for determining the gas holdup α_G and liquid holdup α_G are shown in table 2-2. The liquid holdup follows automatically from $\alpha_G + \alpha_L = 1$.

2-3-1 Flow regime

In the previous section a general relation is derived for two phase pipe flow. The liquid holdup and the gas holdup are unknowns in this equation and they depend on the flow pattern in the mixture. A variety of flow patterns can be distinguished, their occurrence depends on the following parameters.

- Geometrical parameters: pipe diameter, wall roughness and pipe inclination.
- Physical parameters: density, viscosity and surface tension of the fluids.
- Operational parameters: flow rates of the phases.

In the literature a distinction is made between vertical and horizontal pipe flow when classifying the flow patterns.

For vertical flow the different flow patterns are classified as bubbly flow, slug or intermittent flow, churn flow and annular flow. Schematic drawings of the four are shown in Figure 2-3.

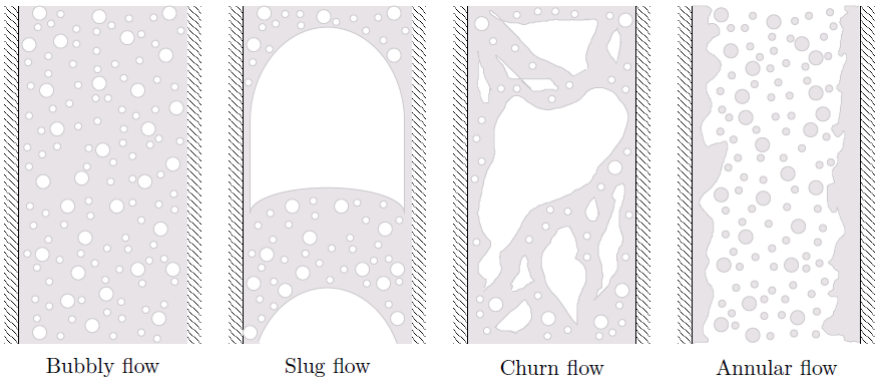

Figure 2-3: Flow patterns for upward gas-liquid flow in a vertical riser [7].

For a constant upward liquid flow rate, starting with a low and gradually increasing upward gas flow rate the following flow patterns are encountered. At low gas flow rates, the gas phase rises as small dispersed bubbles through the continuous liquid carrier and is therefore called bubbly flow. As the gas flow rate increases, the bubbles begin to coalesce forming larger bubbles which eventually occupy almost the full pipe cross section. In between these "Taylor

bubbles", liquid slugs with entrained gas bubbles form. They give rise to slug flow. When the gas flow rate increases further, the shear stress between the gas pockets and the liquid causes a breakdown of the interface. The resulting churning behavior of the mixture provides the name of this flow regime. For even higher gas flow rates the kinetic energy of the gas is sufficient to sustain a gas core in the centre of the pipe which sweeps all the liquid in the upward direction. A portion of the liquid is entrained in the gas core as droplets, while the other liquid flows upwards in a film surrounding the gas. The annulus shape of the liquid at the wall is the reason that this flow pattern is called annular flow. With an increasing gas flow rate, the liquid holdup decreases.

In horizontal pipe flow, gravity breaks the axi-symmetrical behavior found in vertical pipes. Generally, the heavier fluid is at the bottom of the pipe due to gravitational settling. The four different flow patterns in a horizontal pipe are: bubbly flow, slug flow, stratified flow and annular flow (see Figure 2-4).

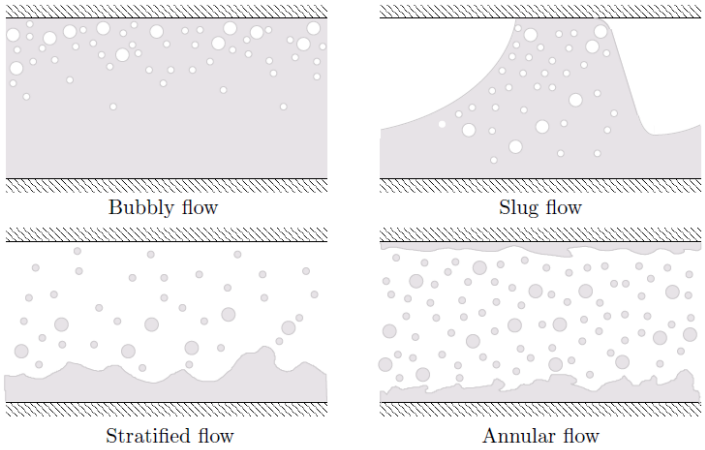

Figure 2-4: Flow patterns for gas-liquid flow in a horizontal flowline [7].

Starting with a sufficiently high liquid flow rate and a low gas flow rate in the same direction, gas bubbles will form and they will rise to the top part of the pipe. These small bubbles provide the name bubbly flow. When the gas flow rate is increased, the bubbles will coalesce as in the vertical pipe, and form gas pockets with liquid slugs between them, giving rise to the name slug flow. If the liquid flow rate is decreased, there will not be enough liquid to form slugs between the gas pockets and a separated pattern arises. The interface between the two phase is either stratified or stratified wavy, resulting in the name stratified (wavy) flow. When the gas flow rate is increased even more, the gas forms a core with entrained water droplets and pushes the liquid towards the wall creating an annuluar shape. However, due to the gravity this water film is much thicker in the bottom region. This flow pattern is called annular flow.

Since the flow patterns in two phase flow are strongly influenced by multiple parameters it is difficult to present their behavior in a 2D map. The most popular method is the flow pattern map where the superficial velocities, or parameters containing these velocities, are on the axes. An example of a flow pattern map is shown in Figure 2-5.

The superficial velocity mentioned above is the velocity that a phase would have if it would occupy the entire pipe cross section in the pipeline. It can be calculated by dividing the

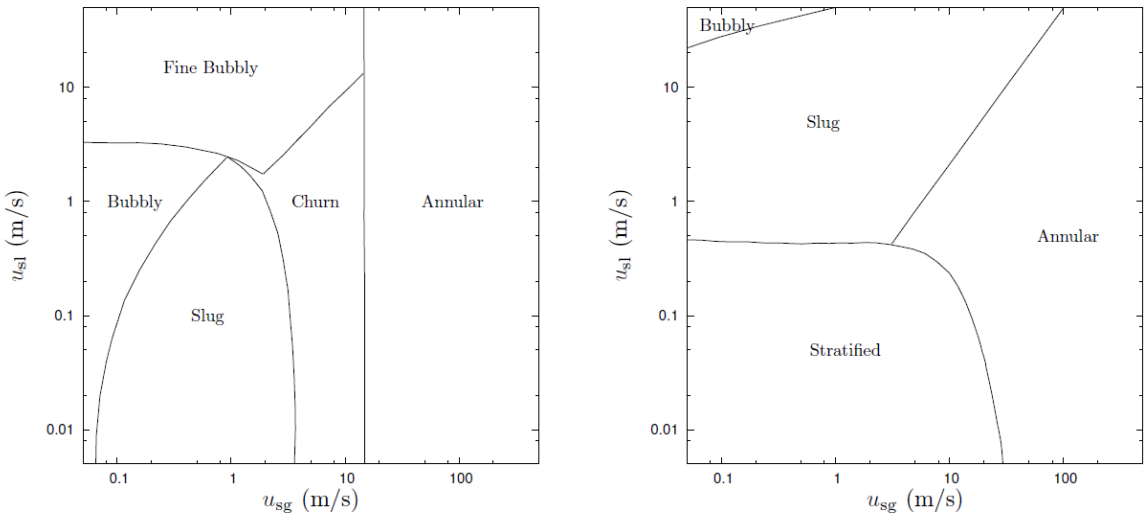

Figure 2-5: Flow pattern map for air-water pipe flow at atmospheric conditions, ambient temperature 25 [$^{\circ}C$] and with a diameter of 0.05 [m]. Left: Vertically upward flow. Right: Horizontal flow [7].

volumetric flow rate Q by the cross sectional area of the pipe A:

$$u_{SG} = \frac{Q_G}{A} \tag{2-19}$$

$$u_{SL} = \frac{Q_L}{A} \tag{2-20}$$

The superficial velocity is a practical parameter since only the geometry of the pipeline and the volumetric flow rate of the phase have to be known to calculate it.

The flow pattern in two phase pipe flow can be predicted by either of the two main approaches:

- Use an existing flow map from an equivalent pipeline with similar flow conditions.
- Systematically evaluate the stability of each flow pattern and determine which pattern is feasible.

The first approach is quick, but only possible when experimental data for an equivalent situation is available. The second approach is more generally applicable. Within Shell, the Shell Flow Correlations (SFC) are used to automatically evaluate the stability of each flow pattern. The order in which the different patterns are assessed is shown in Figure 2-6

Information on the various stability relations (e.g. Kevin-Helmholtz stability for horizontal stratified flow) can be found in [8].

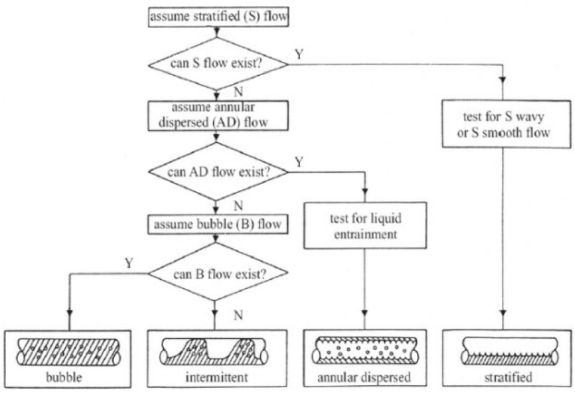

Figure 2-6: Decision tree used by the Shell Flow Correlations to identify the flow pattern.

2-3-2 Pressure drop

The calculation of the pressure drop for two phase pipe flow is more complicated than for single phase flow. It was found that the gas holdup or the liquid holdup is needed to solve for the pressure drop in Equation 2-18. In the previous section on two phase flow patterns it can be seen that these two parameters are flow pattern dependent. After the flow regime is determined, pattern specific models and sub-models are used to calculate the corresponding pressure drop. Table 2-2 provides an overview of these models.

Table 2-2: Classification of the mechanistic models and subs-models for calculating the pressure drop in two phase pipe flow.

Flow Pattern	**Model**	**Sub-models**
Dispersed bubble flow	Drift-flux model	Bubble rise velocity
		Distribution parameter
Separated flow	Two-fluid model	Interfacial friction
		Interfacial shape
		Interfacial velocity
		Liquid entrainment
Intermittent flow	Drift-flux + two-fluid model	Bubble rise velocity
		Bubble shape
		Distribution parameter
		Holdup in liquid slug
		Slug frequency
		Slug cylinder or film length

The classifications in table 2-2 was introduced by Wallis [9] and Taitel & Dukker [10]. The specific explanation of all these models is outside the scope of the current research. The reader is referred to classic textbooks such as Brennen [11].

For the single phase pipe flow case it was found that the pressure drop over an inclined pipe consists of a gravitational part and a frictional part. This distinction is also present in the two phase case. However, calculating the contribution of both parts to the total pressure drop is more complicated due to the different flow patterns.

In Equation 2-18 it is seen that the gravitational contribution to the pressure drop depends on the inclination of the pipe and the average mixture density ρ_m.

$$\rho_m = \alpha_G \rho_G + \alpha_L \rho_L \tag{2-21}$$

For higher gas flow rates, the liquid holdup decreases and thereby the mixture density decreases. The gravitational component therefore decreases.

The frictional contribution to the pressure drop increases for higher gas flow rates due to the higher velocity of the gas and the higher velocity of the liquid which is dragged along by the gas. The behavior of the total pressure drop, which is the sum of both contributions, is shown in Figure 2-7.

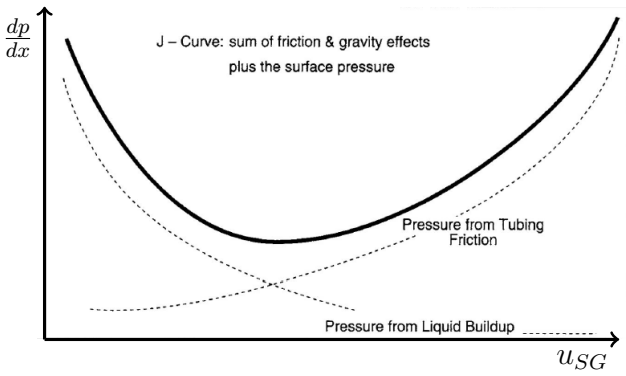

Figure 2-7: Pressure gradient for a constant superficial liquid velocity, as a function of the superficial gas velocity for an upward inclined pipe[12].

The important observation which can be made from this figure is that the two phase pressure drop for an upward inclined pipe has a minimum. The superficial gas velocity is therefore not uniquely defined by the pressure gradient. In this example, where the superficial liquid velocity is known, there are two possible solutions for the gas velocity for a certain pressure gradient. In Figure 2-8 the pressure gradient is shown for a range of superficial liquid and gas velocities. Here it is seen, that different combinations of fluid velocities can result in the same pressure gradient.

The location of the pressure drop minimum is of interest for the oil and gas flow in pipelines. Gas velocities on the right side of the minimum are associated with stable production conditions as they are high enough to transport the liquid phase (the film and the entrained droplets) upward. The pressure drop minimum itself is therefore linked to the transition from churn flow to annular flow.

In the literature on vertical flow, the location of the pressure drop minimum is predicted using the densimetric Froude number, the Kutateladze number or a combination of non-dimensional numbers.

For pipe diameters under 0.05 $[m]$, the densimetric Froude number Fr_G takes a value between 0.7 and 1.0 at the minimum of the pressure drop curve.

$$Fr_G = \sqrt{\frac{\rho_G u_{SG}^2}{gD\left(\rho_L - \rho_G\right)}} \tag{2-22}$$

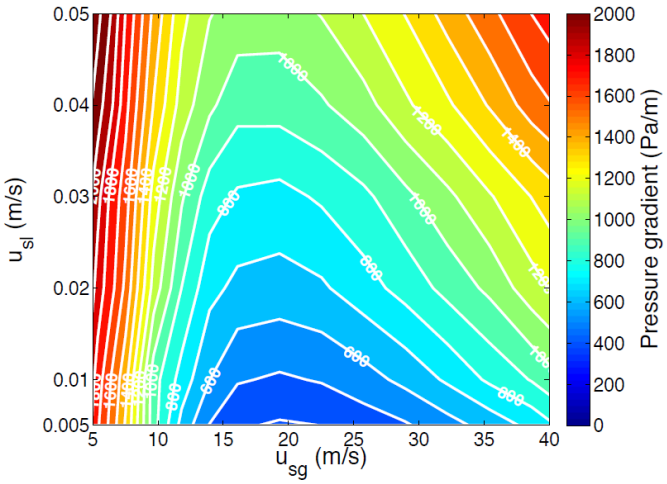

Figure 2-8: The pressure gradient as a function of the superficial gas and liquid velocities for a 34 $[mm]$ vertical riser with air-water at atmospheric conditions. [13]

For pipe diameters larger than 0.15 $[m]$, the pressure drop minimum is predicted by a Kutateladze number, Ku, of 3.2.

$$Ku = \frac{\rho_G^{1/2} u_{SG}}{\left(g\sigma\left(\rho_L - \rho_G\right)\right)^{1/4}} \tag{2-23}$$

These two dimensionless numbers contain a different choice on the parameters that are of interest. According to the densimetric Froude number the location of the minimum is independent of the surface tension, whereas the Kutateladze number predicts that the location of the pressure drop minimum is independent of the pipe diameter.

2-3-3 Scaling

From the above derivations for two phase pipe flow, nine independent parameters are identified which are listed in Table 2-3.

Table 2-3: Governing parameters in isothermal two phase pipe flow.

Parameter	Symbol
Characteristic length	D
Superficial gas velocity	u_{SG}
Superficial liquid velocity	u_{SL}
Gas density	ρ_G
Liquid density	ρ_L
Gas viscosity	μ_G
Liquid viscosity	μ_L
Surface tension	σ
Gravitational acceleration	g

Like in the single phase example the three basic units are those of time, length and mass. Therefore, (9-3=) 6 non-dimensional groups are needed for scaling. These additional non-dimensional numbers are an indication of the complex behavior of the two phase mixtures.

As before, the Reynolds numbers and the Froude numbers are defined for each phase:

$$Re_{SG} = \frac{\rho_G u_{SG} D}{\mu_G} \tag{2-24}$$

$$Re_{SL} = \frac{\rho_L u_{SL} D}{\mu_L} \tag{2-25}$$

$$Fr_G = \sqrt{\frac{\rho_G}{\rho_L - \rho_G} \frac{u_{SG}^2}{gD}} \tag{2-26}$$

$$Fr_L = \sqrt{\frac{\rho_G}{\rho_L - \rho_G} \frac{u_{SL}^2}{gD}} \tag{2-27}$$

The surface tension at the interface between both fluids are important in the formation of the flow patterns. This influence is captured by the Weber number:

$$We = \frac{\rho_G u_G^2 D}{\sigma} \tag{2-28}$$

This non-dimensional number is the ratio between the inertial and the surface tension forces in the fluid. Alternatives to the Webber number are the Eötvös number or the Morton number.

In Figure 2-8 it is seen that the ratio between the two fluid velocities has a large influence on the properties of the mixture. This aspect is incorporated in the volumetric quality:

$$\lambda = \frac{u_{SL}}{u_{SG} + uSL} \tag{2-29}$$

2-4 Industry units vs SI units

In the production of oil and gas, the flow rates of the condensate (oil), water and gas are key properties of the exploited field. Two non-dimensional numbers that are often used in describing these flow rates are the liquid to gas ratio (LGR):

$$LGR = \frac{Q_{Liquid}}{Q_{Gas}} = \frac{Q_{Condensate} + Q_{Water}}{Q_{Gas}} \tag{2-30}$$

and the condensate to gas ratio (CGR):

$$CGR = \frac{Q_{Condensate}}{Q_{Gas}} \tag{2-31}$$

These volumetric ratios are expressed in SI units as $[m^3/m^3]$, however in the oil and gas industry the common unit for these ratios is $[bbl/MMscf]$. Thes abbreviation stands for *barrels per million standard cubic feet*, where a standard cubic feet is the gas volume at 60 $[F]$ and 1 $[atm]$. The conversion between both units is made with the following formula:

$$LGR\left[\frac{bbl}{MMscf}\right] = 6.2467 \cdot 10^7 \cdot \frac{T}{p} \cdot LGR\left[\frac{m^3}{m^3}\right] \tag{2-32}$$

where T and p are the temperature and pressure of the mixture in SI units.

Chapter 3

Flow splitting at T-junctions

The chapter reviews the literature on two phase flow splitting. First, an introduction on the different types of junctions is given. Thereafter, the current state of the literature and the influence of each governing parameters on the phase split is presented. Finally, two models used to predict the phase split are discussed.

3-1 Junctions

Multiphase flows are encountered in many industrial applications. Chemical plants, refineries and power plants consist of complex networks of piping and junctions connecting reactors to other process equipment. The different junctions used in these pipe networks can be categorized by the following geometrical criteria:

1. **Number of branches**
   Common junctions in industry consist of three or four pipes.
2. **Shape**
   Different relative angles between the pipe segments and the curvature of bends influence the behavior of a junction.
3. **Orientation**
   Due to gravity effects, the orientation of the junction is relevant.(i.e. is it in the horizontal plane, vertical plane or any plane in between).

In the current research an impacting T-junction orientated in the horizontal plane is studied. As shown in Figure 3-1 the flow split can go in various directions:

- **Combining T-junctions** 3-1a & 3-1b
  Two inlets and one outlet. The two incoming flows are mixed into one outgoing flow.

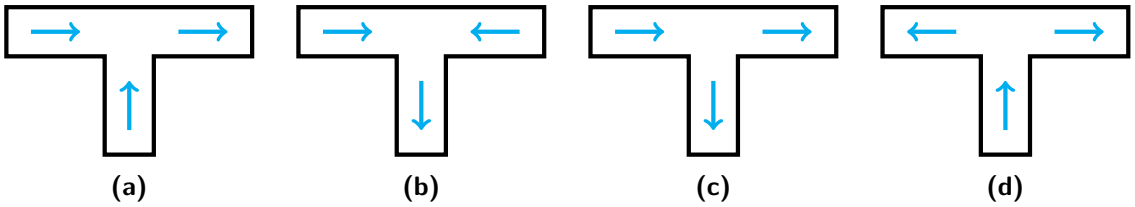

Figure 3-1: The four different flow configurations result in four different uses for the same geometrical shape.

- **Dividing T-junctions** 3-1c & 3-1d
  One inlet and two outlets. The incoming flow is split into two outgoing flows.
  - **Branching T-junction** 3-1c
    The branch arm is orthogonal to the inlet, the run arm is parallel to the inlet.
  - **Impacting T-junction** 3-1d
    Both the branch arm and the run arm are orthogonal to the inlet and parallel to each other.

  The convention is to indicate the three different pipe segments with numbers: inlet (1), run outlet (2) and branch outlet (3).

In the remaining sections only dividing T-junctions are discussed.

3-1-1 Displaying results

In the literature, two types of graphs are used to describe the behavior of dividing tees. Depending on the specific purpose of the junction, one of the two is chosen.

In steam distribution systems the extracted mass flow rate to the branch W_3 and the corresponding quality x_3 of the extracted mixture are the properties of interest. The quality is the ratio between the gas (vapor) mass flow rate and the total mass flow rate of the mixture:

$$x_3 = \frac{W_{G3}}{W_{G3} + W_{L3}} \tag{3-1}$$

In Figure 3-2a these two properties are displayed relative to the original conditions in the inlet. Such graphs can help to design the piping network.

For impacting T-junctions, often the exact distribution of both phases over the run and branch arm is of interest. This type of data is commonly displayed using a splitting curve shown in Figure 3-2b. The $(0.5, 0.5)$ point corresponds to an equal split of the phases between both outlets. The flow split is often expressed as a percentage value. For example, the colored marker in Figure 3-2b corresponds to a [30%][30%] split.

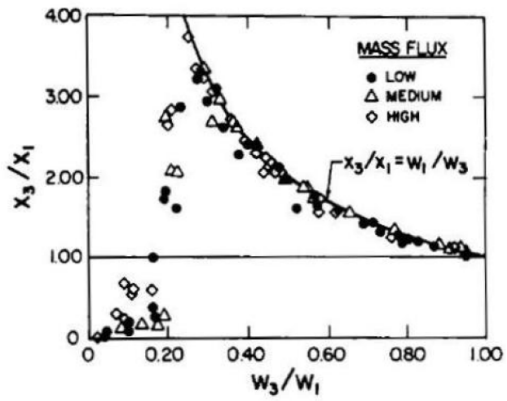

(a) The quality ratio for the branch (x_3/x_1) as a function of the corresponding mass extraction ratio (W_3/W_1) [14].

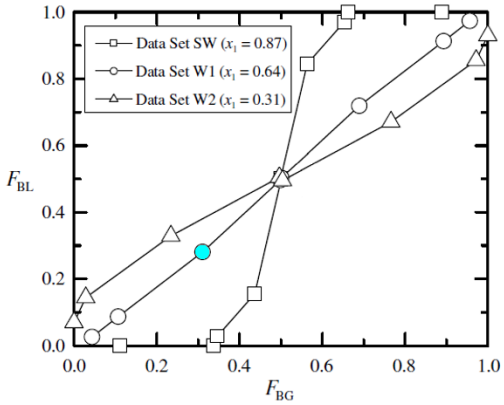

(b) The liquid mass fraction take-off for the branch ($F_{BL} = W_{L3}/W_{L1}$) as a function of the corresponding gas mass fraction take-off ($F_{BG} = W_{G3}/W_{G1}$) [15].

Figure 3-2

3-2 Literature review

Over the last three decades several experimental studies on the behavior of horizontal impacting T-junctions for gas-liquid mixtures were performed. A noteworthy selection of these papers is: Azzopardi et al. [16, 17], Hong et al. [3], Chin et al. [18] (internal Shell), Hart et al.[19], Ottens et al. [2] and El-Shaboury et al. [20]. For an extensive overview of the literature on impacting tees the reader is referred to the reference paper by El-Shaboury et al. They provide an excellent overview of all the work performed up to 2001.

Apart from Chin et al., who use steam-water, the remaining studies used an air-water mixture as working fluids. Air-water is a safe and cheap choice compared to working with steam-water, nitrogen-water or hydrocarbons mixtures. The operating conditions in these experiments are near atmospheric pressure and room temperature. An exception is the work of Chien and Rubel [21] who performed experiments with pressurized steam-water mixtures between 28.6-42.6 [bar]. Most studies use equal sized inlet and outlet pipes for which the diameter ranges from 0.009 [m] to 0.051 [m]. These lab conditions differ much from the operating conditions encountered in the upstream oil and gas industry, where hydrocarbons flow through large pipelines at pressures that are typically in the range between 10 to 120 [bar]. Apart from Hwong et al. all studies reported uneven phase splits. This remarkable result is discussed by Azzopardi et al. [17], who attributes it to the small diameter, 0.009 [m], of the pipes in the junction. For smaller dimensions, the surface tension effects at the interfaces dominate over inertia effects and pressure effects in the fluids. They dampen asymmetries in the flow, resulting in a more even phase split.

Besides the experimental work mentioned above, numerical research has been performed on two-phase flow splitting at impacting tees. Hatziavramidis et al. [22] looked at conformal mapping (potential flow) and two-fluid CFD modeling of tees. The commercial code used in their study gave poor results that did not match experimental data. Within Shell three reports [23, 24, 25] are available on the simulation of two phase flow at T-junctions. All three

conclude that the CFD packages FLUENT and OpenFOAM are promising for the simulation of multiphase flow, but they are not sufficiently developed yet to produce reliable results.

It can be concluded that the field of research on impacting T-junctions is still relatively immature. Experimental research is limited to lab scales and CFD tools need to become more mature.

For an extensive overview on branching tees, the reader is referred to *Phase separations at T junctions* [26], where Azzopardi summarizes and discusses all research on branching T-junctions up to 1999.

3-3 Governing parameters

The phase split at an impacting T-junction is influenced by the following parameters:

- Inlet quality
- Momentum of the incoming mixture
  - Flow pattern
  - Superficial liquid and gas velocities
  - Fluid properties
- Geometry of the junction
- Geometry of the upstream configuration
- Pressure drop in and downstream of the junction

Each parameter is discussed below.

Inlet quality

The quality of a two-phase flow mixture can vary between 0 to 1, where $x = 0$ implies single phase liquid flow and $x = 1$ implies single phase gas flow. At the two extremes the "mixture" is expected to behave as a single phase fluid, and to split equally over both branches. In practice, this behavior is not completely found in experiments. For low qualities an unequal distribution can occur. This maldistribution is attributed to the difference in inertia between both phases [18]. For these conditions the liquid split is less affected by a small difference in pressure between the outlets than the gas split.

Flow pattern

It was observed that the flow pattern at the inlet has a significant influence on the phase split. For equal qualities, but varying flow patterns, different phase splits occur.

Azzopardi [17] attributes this to the momentum flux ratio $\dot{M}_R$ of the two fluids and the spatial distribution of the phases over the cross section of the inlet. The momentum flux ratio is defined as:

$$\dot{M}_R = \frac{\rho_G u_{G1}^2}{\rho_L u_{L1}^2} \tag{3-2}$$

An interesting remark in his paper concerns the entrained liquid droplets in annular flow. Using a transparent acrylic tee, Azzopardi observed that the droplets impacted the back wall of the junction instead of being diverted with the gas flow. A pool of liquid formed at the bottom of the junction resulting in a flow pattern similar to stratified flow in the tee.

Other researchers [18, 21] found that stratified flows are influenced more than annular flows by changing operating conditions. Based on experimental data it was argued that this relates to whether the densimetric gas Froude number is less than, or larger than one. This indicates that the maldistribution in the flow split is related to the ratio between the inertia of the gas and gravitational effects.

Superficial liquid and gas velocities

El-Shaboury et al. [20] investigated the effect of varying either the gas or the liquid superficial velocity on the phase distribution when staying within the same flow regime.

They found for a constant u_{SG} and varying u_{SL} that in the range of $F_{BG}(= W_{G3}/W_{G1})$ between 0 and 0.5 increasing u_{SL} results in increasing the value of F_{BL} at the same F_{BG}. In the range of F_{BG} between 0.5 and 1 increasing u_{SL} results in decreasing the value of F_{BL}. This phenomenon is displayed in Figure 3-3a.

When varying u_{SG}, and keeping u_{SL} constant, the opposite behavior was found by El-Shaboury et al. An increasing u_{SG}, while keeping u_{SL} fixed, results in a decrease of the value of F_{BL} at the same F_{BG} in the range of F_{BG} between 0.5 and 1. This is displayed in Figure 3-3b.

The effect of varying the superficial gas and liquid velocity is summarized below:

- For a fixed superficial gas velocity, and an increased superficial liquid velocity, the splitting curve on an F_{BL} vs F_{BG} graph rotates in the clockwise direction around the $(0.5; 0.5)$ point.
- For a increased superficial gas velocity and a fixed superficial liquid velocity, the splitting curve rotates in the anti-clockwise direction around the $(0.5; 0.5)$ point.
- The effect of increasing u_{SG} is less significant for the phase distribution compared to increasing u_{SL}.

Fluid properties

In previous sections it was noted that the inertia of the fluid plays a large role in the phase splitting behavior of impacting T-junctions. It is therefore not surprising that the density difference of the two fluids influences the split. Decreasing the density difference between the

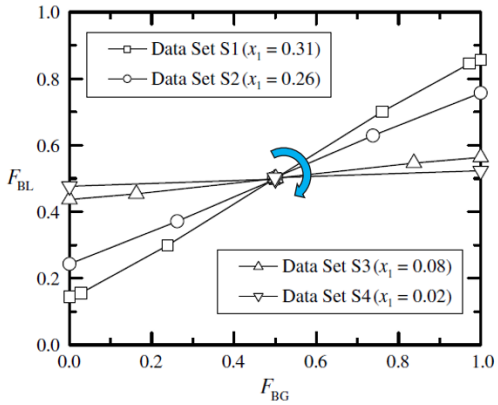

(a) For a fixed superficial gas velocity and an increasing superficial liquid velocity the phase splitting curve rotates in the clockwise direction around the $(0.5; 0.5)$ point [15].

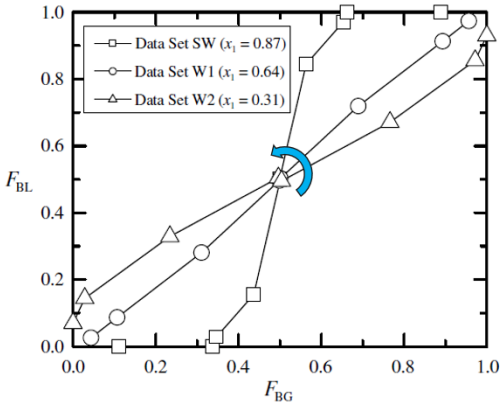

(b) For an increasing superficial gas velocity, and a fixed superficial liquid velocity the phase splitting curve rotates in the anti-clockwise direction around the $(0.5; 0.5)$ point [15].

Figure 3-3

gas and the liquid results in a more homogeneous mixture and consequently in a more even phase split.

The density of the compressible gas phase is affected by the pressure. Increasing the inlet pressure while keeping a constant superficial gas velocity, increases the inertia of the gas. This has a similar effect on the phase split as increasing the gas velocity at a constant inlet pressure. [20].

The second fluid property of interest is the surface tension. No specific research has been performed on the effect of this parameter for impacting T-junctions. Nevertheless, we know the evaluation by Azzopardi [17] of the experimental results obtained Hong [3] that the surface tension can not be neglected for small diameter junctions.

Geometry of the junction

Elazhary and Soliman [27] performed research on a mini-size impacting T-junction with a rectangular cross-sections of 1.87 [mm] height and a 20 [mm] width. They found the trend in the phase split to be consistent with earlier findings for macro-size junctions. However, the magnitude with which the phase split reacts to changing conditions is significantly smaller. This can be attributed to surface tension which has a larger influence on small scales.

Hong and Griston [28] investigated the effect of insert devices within the junction. They concluded that these devices have a significant influence on the phase split. The nozzles reduced tee, which is shown in Figure 3-4, produced equal phase splits over the widest range of gas and liquid ratios.

In private communication with Hamersma ([2], [19], [29]) the author has explained that the phase split in impacting T-junctions is sensitive to small asymmetries in the tee. Manufacturing defects as thickened welds, erosion of the tee or solid deposition are not present in the

milled junctions used in research. In industry however, these imperfections will be present. They can lead to unpredicted maldistribution in the phase split

When the outlets of the junction are not fully horizontal, gravity starts to affect the phase split. A higher liquid flow and a lower gas flow is found in the downward inclined outlet while a lower liquid flow and a higher gas flow is found in the upward inclined outlet.

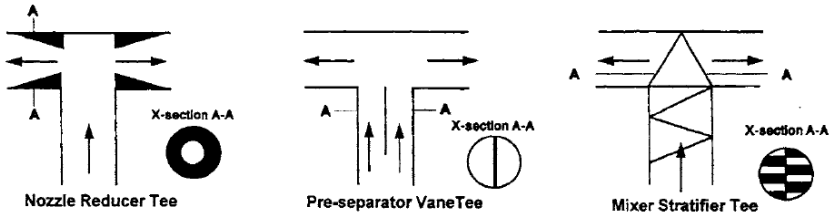

Figure 3-4: Improved tee split devices tested by Hong et al.[3].

Geometry of the upstream configuration

The upstream configuration influences the distribution of the phases over the cross section of the inlet. As described earlier this can have a positive or negative effect on the phase split. Bends upstream of the junction can lead to an asymmetric fluid distribution which negatively influences the phase split. Hong and Griston found that mixer-stratifier devices and especially pre-separator vanes upstream of the junction influence the phase split in a positive way by distributing the fluid mixture more evenly over the cross section of the inlet [28].

Pressure drop in and downstream of the junction

The pressure drop in the junction consists of a reversible part and an irreversible part. From the Bernoulli equation it is known that the reversible part corresponds to changes in velocities and gravitational effects between the inlet and outlet, whereas the irreversible part is due to friction within the tee. The magnitude of this frictional pressure drop depends on the flow pattern, mass split ratio and flow rates [15]. For an unequal phase split the pressure drop between the inlet and the outlet is unequal per branch, resulting in a pressure difference between the outlets. This pressure difference influences the phase split itself.

The influence of the downstream pressure drop was studied by Van der Gronden [1] who used the experimental setup as used in our study. He found that the downstream pressure drop, originating from a vertical riser equipped with a choking valve, has a large effect on the phase split.

3-4 Phase split models

Over the years various models for predicting the phase split and the pressure drop over the T-junction have been proposed. Different approaches are used in these models. However,

they share a common feature, namely that none of them is generally applicable. The models can be subdivided into the following three categories [30]:

- **Empirical models**
  Experimental correlations are used to describe the splitting behavior at the junction. Such correlations are based on specific experiments, and there is no or little theory behind them. They have a limited applicability and provide little insight into the physics.
- **Phenomenological flow regime based models**
  A theoretical base is used for these models, together with geometrical considerations and specific characteristic variables.
- **Mechanistic models**
  These models solve the governing equation of fluid dynamics presented in Section 2-1 and they use a limited number of empirical closure correlations.

In this report two mechanistic models are discussed. Saba and Lahey [31] stated that the phase split in a T-junction with a known geometry can be characterised by eight independent parameters: W_1, W_2, W_3, x_1, x_2, x_3, $p_{1\to2}$ and $p_{1\to3}$ [31]. This parameter set can be interchanged with another set as long as it comprises of eight degrees of freedom. Usually, three of these parameters are known, e.q. the inlet mass flow W_1, the outlet mass flow W_3 and the quality x_1 at the inlet. Then, five independent theoretical relations are needed to obtain the other five parameters and to uniquely determine the phase split. The exact choice of these theoretical relations varies per model. In this report, the Dividing Streamline Model and the (Advanced) Double Stream Model are discussed.

3-4-1 Dividing Stream Model

The main theoretical model for predicting the phase split at dividing T-junctions is the Dividing Stream Model (DSM) by Hwang et al. [32]. The basic idea behind this model is that for each phase a *zone of influence* exists which is bounded by the dividing streamline for the corresponding phase, as shown in Figure 3-5. Gas entering the junction on the left side of the dividing gas streamline will exit through the opposite outlet while the gas in the *zone of influence* will exit through the side outlet. The liquid phase behaves in a similar way and its split is determined by the dividing liquid streamline.

For their model Hwang et al. assumed that normally three of the eight independent variables are specified. Thus, five relationships have to be found to determine the phase split. Two of these equations are the steady state continuity equations:

$$W_1 = W_2 + W_3 \tag{3-3}$$

$$W_1 x_1 = W_2 x_2 + W_3 x_3 \tag{3-4}$$

and two are the steady state mixture momentum equations from the inlet to each outlet:

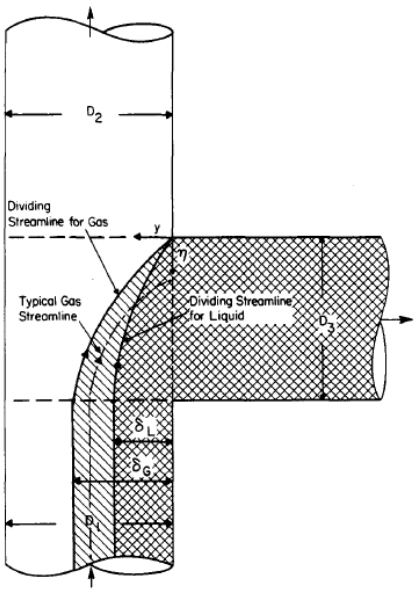

Figure 3-5: Dividing streamlines for the liquid and for the gas phase in a branching T-junction [14].

$$\Delta p_{12} = \Delta p_{1-1J} + (\Delta p_{12})_J + \Delta p_{2J-2} \tag{3-5}$$

$$\Delta p_{13} = \Delta p_{1-1J} + (\Delta p_{13})_J + \Delta p_{3J-3} \tag{3-6}$$

Here Δp_{i-iJ} is the static pressure change in the pipe section towards the junction, and $i = (1, 2, 3)$ corresponds to the inlet, run arm and branch arm of the tee. $(\Delta p_{1i})_J$ is the static pressure change within the junction. For the remaining (fifth) equation Hwang et al. uses the Euler equations of motion for a fluid parcel travelling on a curved streamline. The different forces working on a fluid parcel are shown in Figure 3-6

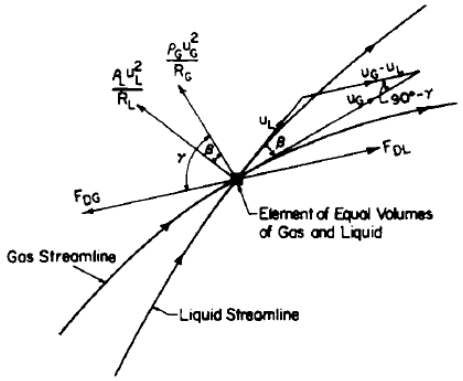

Figure 3-6: Schematic overview of the forces acting on each phase in a fluid parcel at a streamline crossing. The centrifugal forces are directed perpendicular to the streamline, the phasic drag forces can be split into forces parallel and perpendicular to the streamline [14].

In the s-direction, tangential to the streamline, the Euler equation of motion for each phase is:

$$\frac{\partial p}{\partial s} = -\rho_\beta u_\beta \frac{\partial u_\beta}{\partial s} + F_{D\beta,s} \tag{3-7}$$

where $F_{D\beta,s}$ is the part of the drag force on phase β in the s-direction. Similarly, for the n-direction, normal to the streamline:

$$\frac{\partial p}{\partial n} = -\rho_\beta u_\beta \frac{u_\beta^2}{R_\beta} + F_{D\beta,n} \tag{3-8}$$

where R_β is the radius of curvature for the streamline of phase β.

In dynamic equilibrium, the resultant forces acting on both phases are equal in magnitude and opposite in direction. From this Hwang et al. iteratively determine the shape of both dividing streamlines. The in-depth computation of these shapes and the corresponding phase split is beyond the scope of the current research; a complete description of the method of computation can be found in [14].

3-4-2 (Advanced) Double Stream Model

The Double Stream Model by Hart et al.[19] for an equal diameter T-junction is based on the assumption that both the gas flow and the liquid flow at the inlet of the T-junction are split over the two outlets. This allows for the existence of the following four streamlines:

- Inlet-to-run gas flow
- Inlet-to-branch gas flow
- Inlet-to-run liquid flow
- Inlet-to-branch liquid flow

These four streamlines are shown in Figure 3-7

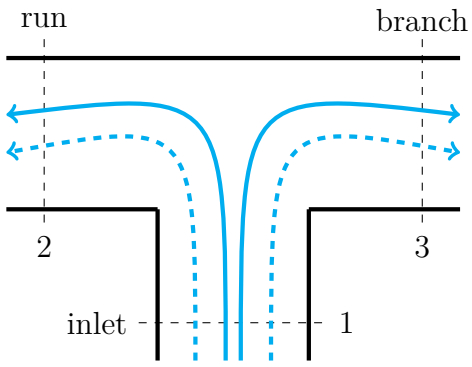

Figure 3-7: Schematic drawing of the four streamlines in the (Advanced) Double Stream Model. Dotted lines: gas flow, solid lines: liquid flow.

The steady-state macroscopic mechanical energy balance, which is an extended version of the Bernoulli equation with addition of a friction loss term $\hat{E}_v$, is applied to each of the four streamlines.

$$\frac{1}{2}\left[\frac{\langle u_1^3\rangle}{\langle u_1\rangle}-\frac{\langle u_2^3\rangle}{\langle u_2\rangle}\right]_G+\left[g\left(z_{1,2}-z_2\right)\right]_G+\left[\left(p_1-p_2\right)/\rho\right]_G=\left[\hat{E}_{v12}\right]_G \tag{3-9a}$$

$$\frac{1}{2}\left[\frac{\langle u_1^3\rangle}{\langle u_1\rangle}-\frac{\langle u_3^3\rangle}{\langle u_3\rangle}\right]_G+\left[g\left(z_{1,3}-z_3\right)\right]_G+\left[\left(p_1-p_3\right)/\rho\right]_G=\left[\hat{E}_{v13}\right]_G \tag{3-9b}$$

$$\frac{1}{2}\left[\frac{\langle u_1^3\rangle}{\langle u_1\rangle}-\frac{\langle u_2^3\rangle}{\langle u_2\rangle}\right]_L+\left[g\left(z_{1,2}-z_2\right)\right]_L+\left[\left(p_1-p_2\right)/\rho\right]_L=\left[\hat{E}_{v12}\right]_L \tag{3-9c}$$

$$\frac{1}{2}\left[\frac{\langle u_1^3\rangle}{\langle u_1\rangle}-\frac{\langle u_3^3\rangle}{\langle u_3\rangle}\right]_L+\left[g\left(z_{1,3}-z_3\right)\right]_L+\left[\left(p_1-p_3\right)/\rho\right]_L=\left[\hat{E}_{v13}\right]_L \tag{3-9d}$$

Combining the equations for the streamlines and the assumption that:

$$\left(p_2-p_3\right)_G=\left(p_2-p_3\right)_L \tag{3-10}$$

results into:

$$\begin{aligned}\frac{1}{2}\rho_G\left[\frac{\langle u_3^3\rangle}{\langle u_3\rangle}-\frac{\langle u_2^3\rangle}{\langle u_2\rangle}\right]_G-\frac{1}{2}\rho_L\left[\frac{\langle u_3^3\rangle}{\langle u_3\rangle}-\frac{\langle u_2^3\rangle}{\langle u_2\rangle}\right]_L+\rho_G\left[g\left(z_3-z_{1,3}+z_{1,2}-z_2\right)\right]_G\\-\rho_L\left[g\left(z_3-z_{1,3}+z_{1,2}-z_2\right)\right]_L=\rho_G\left[\hat{E}_{v12}-\hat{E}_{v13}\right]_G-\rho_L\left[\hat{E}_{v12}-\hat{E}_{v13}\right]_L\end{aligned} \tag{3-11}$$

With the introduction of new quantities as the gas phase split λ_G, the liquid phase split λ_L, the kinetic energy ratio κ, the flow shape factor β, the phase holdup α and by defining the energy loss factor as:

$$\hat{E}_v=k\frac{1}{2}\frac{\langle u_1^3\rangle}{\langle u_1\rangle} \tag{3-12}$$

Hart et al. rewrite Equation 3-11 as:

$$\begin{aligned}\kappa\left[\frac{\beta_{G2}\alpha_{G1}D_1^4}{\beta_{G1}\alpha_{G2}D_2^4}\left(1-\lambda_G\right)^2-\frac{\beta_{G3}\alpha_{G1}D_1^4}{\beta_{G1}\alpha_{G3}D_3^4}\lambda_G^2\right]-\left[\frac{\beta_{L2}\alpha_{L1}D_1^4}{\beta_{L1}\alpha_{L2}D_2^4}\left(1-\lambda_L\right)^2-\frac{\beta_{L3}\alpha_{L1}D_1^4}{\beta_{L1}\alpha_{L3}D_3^4}\lambda_L^2\right]\\+\frac{2g}{\beta_{L1}\langle u_{L1}\rangle^2}\left[\frac{\rho_G}{\rho_L}\left(z_{G2}-z_{G3}\right)-\left(z_{L2}-z_{L3}\right)\right]=\kappa\left(k_{13}-k_{12}\right)_G-\left(k_{13}-k_{12}\right)_L\end{aligned} \tag{3-13}$$

Hart et al. assumed, that for an inlet liquid holdup value lower than 0.06, the same value can be taken for the liquid holdup in the outlets. Thus, the heights z are equal within the tee. The ratio of the flow shape factors β is approximated by unity. Further, it was stated that

the difference of the friction loss coefficients k between both outlets are the same for each phase. Together with the introduction of the energy dissipation factor:

$$\lambda_0 = \frac{1}{2}\left(1 + k_{12} - k_{13}\right) \tag{3-14}$$

Equation 3-13 is simplified to what is known as the Double Stream Model (DSM):

$$\lambda_L = \lambda_0 + \kappa\left(\lambda_g - \lambda_0\right) \tag{3-15}$$

This simplified model generates acceptable results for low liquid holdup conditions.

In 1995 Ottens et al. [2] extended the model to make it applicable to different flow patterns. They started from Equation 3-13 and used semi-empirical correlations for the holdups, a geometrical model for the liquid heights and an empirical closure for the phase friction loss factor. With these additional sub-models it is possible to determine the shape of the initial equation. The derivation for this extended model, called the Advanced Double Stream Model (ADSM), is given in Appendix A.

The model by Hart et al. and the extended model by Ottens et al. are based on only two characteristic parameters which are defined initially. For both models these parameters are the phase velocities which together determine the ratio of the kinetic energies κ. Since the extended Bernoulli equations for the four streamlines are the only independent theoretical relations used in the derivation of the models, there remains a degree of freedom. This means that a relation is found between the gas phase split λ_G and the liquid phase split λ_L but no unique solution can be determined.

Chapter 4

Experimental setup

The experimental part of this research was performed in a air-water low pressure setup at the Shell Technology Center Amsterdam (STCA). This chapter describes the layout of the setup and the measurement techniques used in the experiments. Furthermore, the geometry and conditions of the SSL are compared with field conditions.

4-1 Severe Slugging Loop

The Severe Slugging Loop was built a few decades ago. The loop consists of a 100 $[m]$ horizontal flowline connected to two vertical risers of 16.8 $[m]$ height. The setup is operated with water and air as the liquid and gas phase. Water is recirculated through the loop, air is extracted from the STCA air supply system at 6 $[bara]$ and expelled to the atmosphere. The system is controlled and operated from a control room adjacent to the setup.

The layout of the SSL has been changed often over the years, to enable various studies to be conducted. In 2006, Groote and Haandrikman [33] worked on the development of Smart Choke Control of transient slugs. Malekzadeh et al. [34] performed research on severe slugging in 2012. Prickaerts [4] in 2011 and Van der Gronden [1] in 2013 studied two phase flow splitting from a horizontal flowline into two vertical risers, using a branching T-junction and an impacting T-junction, respectively.

In early 2015 the SSL was modified by installing two 1.25 $[in]$ risers and a larger air flow controller to achieve annular flow in both risers and to eliminate asymmetries from the flow loop. The top section of the flow loop was simplified at the expense of removing flow rate measurement capability. A schematic overview of the new layout is given in Figure 4-1 and some detailed photos are given in Appendix B. The different components and features of the SSL are discussed in the following sections.

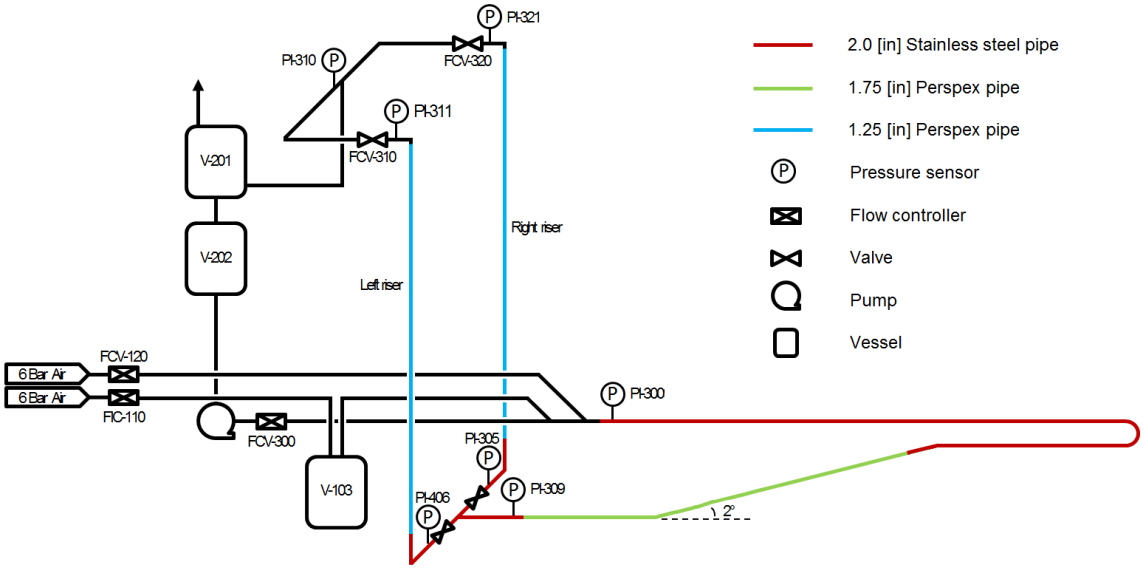

Figure 4-1: Schematic overview of the current configuration of the Severe Slugging Loop (SSL). Components of the flow loop not used in this research are left out for clarity.

4-1-1 Layout

The geometry of the setup is described along the path of the mixture through the system. First the air and water, which together form the two phase mixture, are combined in a double Y-sprout configuration. The mixture enters the 100 $[m]$ horizontal flowline which is composed of galvanized steel pipe segments with an inner diameter of 2.0 $[in]$, and transparent perspex pipe segments with an inner diameter of 1.75 $[in]$. The first 26 $[m]$ of the perspex section of the flowline has a downwards inclination of roughly 2 degrees. The final 6.1 $[m]$ perspex segment upstream of the tee is horizontal. This length corresponds to 120 pipe diameters which allows the flow to develop.

The symmetric impacting T-junction is shown in 4-2. A welded junction was installed instead of a machined junction as it is similar to the welded junctions used in industry. The inner diameter of the inlet and the outlets is 2.0 $[in]$. The mixture flows through a smooth bend and a gradual contraction into the 1.25 $[in]$ vertical polycarbonate riser with total length 16.85 $[m]$. At the top, pipes combines the flow from both risers, towards the release vessel V-201. In this vessels, the water and the air are separated by gravity. The air is released into the atmosphere and the water flows down into vessels V-202 which serves as a temporary storage tank upstream of the pump.

Flow control valves are installed at two locations in the flow loop. After both outlets of the junction a hand valve is present which can fully close off the corresponding riser. Directly downstream of each riser top a computer controlled valve is located which can choke the flow and thereby increase the back pressure on the riser.

The geometry of the SSL has been found to give the following undesired effects:

- **Uneven inflow distribution**

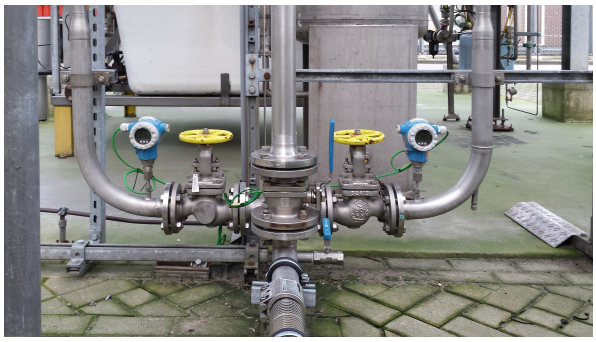

Figure 4-2: Front view of the symmetric impacting T-junction. Liquid and/or air can flow trough the left and/or right riser depending on the position of the corresponding valve. The middle riser is not used in this research and is closed off during experiments.

The declined perspex section and the horizontal perspex section upstream of the T-junction are connected with an S-bend. Van der Gronden [1] found that this has an effect on the distribution of the phases over the cross section of the incoming flow which can increase the maldistribution in the phase split.

- **Severe slugging**

  At low gas flow rates a severe slugging cycle is present. Fortunately the main part of this research focuses on high gas flow rates where this cycle is not present.

- **Pressure oscillations**

  It was found that pressure fluctuations occur in the flowline for certain combinations of the gas and liquid flow rate. These are relatively small in amplitude with a low frequency of 0.02 $[Hz]$. They do not have a significant influence on the measurements of this study.

4-1-2 Flow rates and flow conditions

The water is pumped from the storage vessel V-202 to flow controller FCV-300 and mass flow indicator FI-300. The flow is therefore determined by the chosen opening of the FCV-300 valve and the back pressure from the system instead of active control towards a set flow rate. The resulting liquid flow ranges from 0.15 to 3.0 $[m^3/h]$ with an accuracy of 0.02 $[m^3/h]$.

Since water can assumed to be incompressible the corresponding superficial velocity range can be calculated directly. For the 2.0 $[in]$ flowline and T-junction the superficial liquid velocity is in the range between 2.1 and 42.4 $[cm/s]$. Assuming that the water splits equally over both 1.25 $[in]$ risers the corresponding superficial velocity ranges from 2.6 to 52.6 $[cm/s]$

The air flow in the setup is extracted from the STCA air supply and regulated by two mass flow controllers. The FIC-110 (type: Brooks Instrument 5853E) has a range of 0-48 $[Nm^3/h]$ and the FCV-120 (TYPE) has a range of 30-200 $[Nm^3/h]$, the combined accuracy of the two controllers is 1.0 $[Nm^3/h]$. Both mass controllers are insensitive to fluctuations in the ambient temperature or back pressure. The air is compressible and hence the pressure of the system has to be taken into account when calculating the superficial gas velocity range. The

maximum superficial velocity for a 1, 2 and 4 $[bara]$ pressure at 15$[°C]$ is 37.8, 18.9 and 9.5 $[m/s]$ for the flowline, and 46.8, 23.4 and 11.7 $[m/s]$ per riser, respectively.

The Shell Flow Explorer simulation tool predicts that the mixture in the flowline will be in the slug flow, stratified wavy or annular flow regime for these flow rates. The flow pattern in the vertical risers can be bubbly, slug, churn or annular flow depending on the superficial velocities.

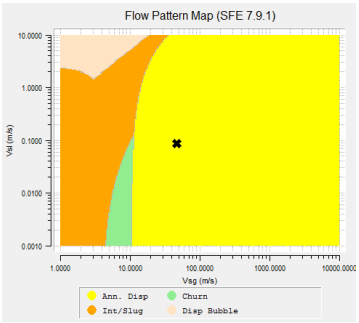

(a) At 1 $[bara]$, the maximum superficial gas velocity in double riser experiments with an equal gas split is 46.8 $[m/s]$.

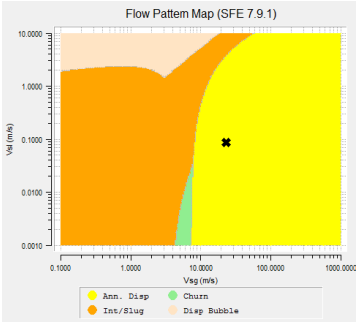

(b) At 2 $[bara]$, this maximum superficial gas velocity is 23.4 $[m/s]$.

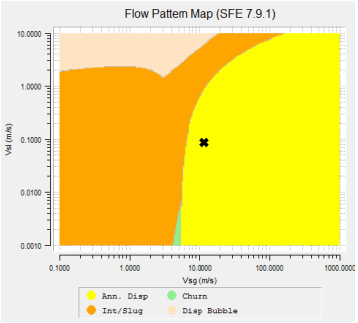

(c) At 4 $[bara]$, this maximum superficial gas velocity is 11.7 $[m/s]$.

Figure 4-3: Flow pattern maps generated with the Shell Flow Explorer simulation tool for a superficial liquid velocity of 0.10 $[m/s]$ and the maximum superficial gas velocity per riser for three different system pressures. It is found that for all three cases the gas flow rate is sufficient to sustain annular flow in both risers.

4-1-3 Measuring equipment

Multiple pressure indicators are placed along the flow loop, the exact locations of these are shown in Figure 4-1. The indicators along the flowline and at the riser base measure the absolute pressure. The three pressure indicators in the top section display the gauge pressure. The height difference of 16.85 $[m]$ between the top and bottom pressure indicator along the risers is used to determine the pressure gradient of the flow inside the vertical pipe. A typical pressure reading for the pressure sensors is shown in Figure 4-4. The fast fluctuations that have a period in the order of seconds, are caused by the specific flow pattern of the fluid. The low frequency fluctuations with a period between 30 seconds and a minute, are due to the pressure oscillations in the horizontal flowline. To filter such variations in pressure, a time averaged mean over 5 to 20 minutes is used. The flow in the setup is allowed to fully develop before pressure measurements are taken.

The flow pattern of a two phase mixture is not uniquely determined by its pressure gradient. The fluctuations in the pressure signal over time give an indication of the flow pattern but an additional method is needed to be more certain. The perspex segments of the loop allow visual inspection of the flow. This inspection is performed at 7.5 $[m]$ height, which is equal to 240 pipe diameter being sufficiently long for a stable flow pattern to develop. Besides inspection with the naked eye, visualisations are made with two GoPro HERO4 Black cameras (240 fps, 720p).

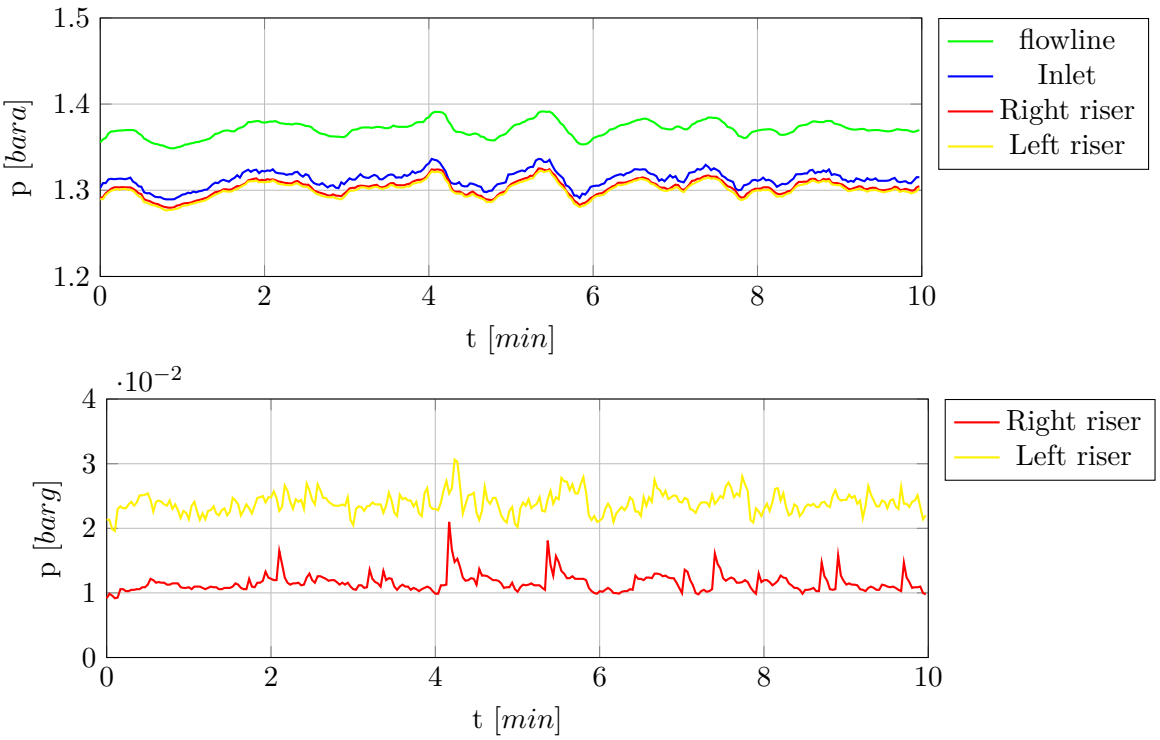

Figure 4-4: Typical pressure signals for an experiment with an unequal phase split. In the top graph the pressures in the flowline, the junction inlet, the left riser base and the right riser base are shown. The bottom graph displays the gauge pressures measured in the top section.

As the setup is not equipped with mass flow meters downstream of the risers, it was not possible to measure the phase split as could be done by Van der Gronden[1].

4-2 Safety

Safety is a key concern for all activities in and around the SSL. The following safety measures were incorporated in the design of the flow loop:

- The maximum operation pressure of the SSL is 6 [*bara*]. This is the maximum permitted pressure for the perspex pipe segments used in the horizontal flowline and vertical risers. The highest pressure in the system is located at the beginning of the flowline. A relief valve is installed which opens at high pressures.
- The strength of the perspex sections could decrease over time due to exposure to the weather and light, which resulted in a pipe rupture under 6 [*bara*] a few years ago. To protect people in the vicinity of the SSL, a metal grating has been installed around the perspex segments.
- The flow loop is controlled from a porto cabin situated next to the horizontal flowline. During operations, such as increasing the air and liquid flow rate or closing chokes, the operator works from the porto cabin.

- The SSL is designed to "fail safe" in the case of a power failure. The system then automatically shuts down the pump, the mass flow controllers for the air and valves.

Besides the above safety measures in the design of the loop, the operator has to meet the following requirements:

- A person has to pass the safety training for the outside plot before he or she is allowed on the outside plot. In this training hazards on the outside plot are identified. Next to the high impact risks, emphasis is placed on the ordinary "trips and falls" accidents.
- The operator of the loop has to wear Personal Protective Equipment (PPE) outside of the porto cabin. These include a helmet, safety glasses, lab coat and safety shoes.

Chapter 5

Experimental results

This chapter elaborates on the experiments performed. In Section 5-1 and 5-2 the result of single riser experiments with single phase flow and two phase flow are discussed. No single phase experiments were performed in the dual risers in this research, the work by Van der Gronden[1] addresses this topic in great detail. The two phase flow experiments in the dual risers, which form the main part of this experimental study, are presented in Section 5-3. Finally, the main conclusions drawn from the experiments are summarised in Section 5-4.

5-1 Single riser - single phase flow experiments

Before the start of this research, the experimental setup has been modified. Both risers have the same length and the top section from the riser top to the release vessel is now similar at both sides. The goal of the single riser single phase experiments is to test these modifications and thereby to validate the basic assumption that the setup is fully symmetric.

Compare riser height

The length of both risers can be verified by pumping a low liquid flow rate through one riser while the other is closed off. A liquid column forms in the riser and produces a pressure difference. This pressure consists of a gravitational part and a frictional part. Since the latter is negligible at low liquid velocities and the liquid is incompressible, the pressure difference is a direct measure of the riser height.

In Figure 5-1 the resulting pressure drops along both risers are shown. It is concluded that the length of both risers is equal.

Test for symmetry

The same experiment is performed with a high gas flow rate. The pressure drop between the inlet of the T-junction and the release vessels is compared for both risers. The results are

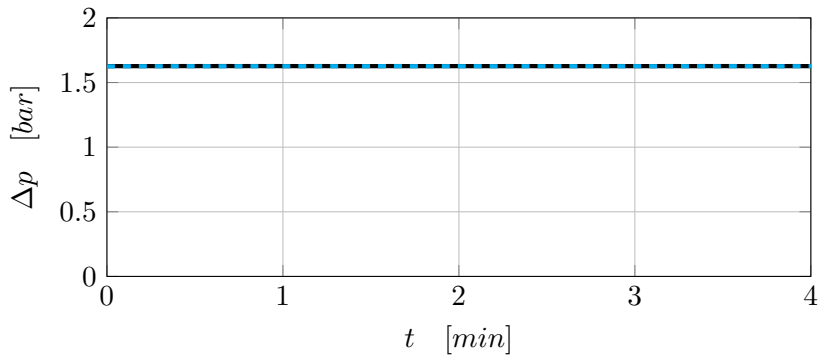

Figure 5-1: Pressure drop along the left riser and the right riser for single phase liquid flow with a superficial velocity of 0.12 $[m/s]$. The measurements were done at different time instances, within half an hour. Both lines overlap.

shown in Figure 5-2. The pressure drop is equal for both pathways, therefore it is concluded that the geometry of the setup is symmetric downstream of the T-junction.

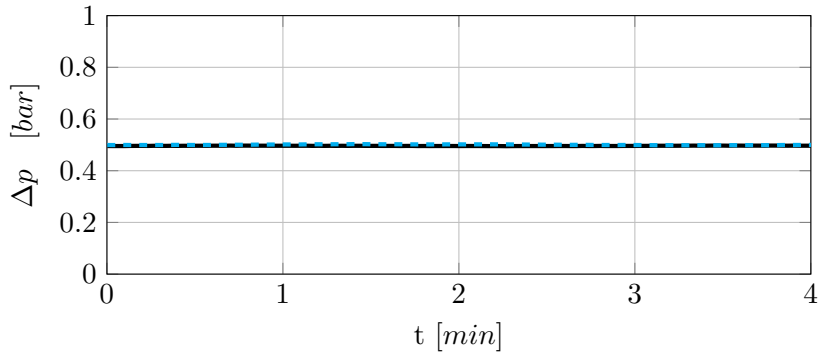

Figure 5-2: Pressure drop from the junction to the release vessel along the left riser and the right riser for single phase gas flow with a superficial velocity of 97.6 $[m/s]$ in the riser at normal conditions. The measurements were done at different time instances, within half an hour. Both lines overlap.

5-2 Single riser - two phase flow experiments

Since the liquid and gas flow rates cannot be measured after the splitter an indirect method is needed to quantify the phase split. The pressure drop over a single vertical riser does not uniquely define the phase flow rates (Section 2-3). However, in the double riser experiments the total flow rate through both risers is known. Using visual inspection of the flow patterns it is possible to distinguish a symmetric split from an asymmetric split in the current setup.

The goal of the single riser, two phase flow, experiments is to generate pressure drop data which can be used in the double riser experiments. The pressure gradient curve is determined for three different superficial liquid velocities. These three velocities are chosen, based on the range of the liquid flow rate controller.

Superficial liquid velocity of 0.06 [m/s]

The superficial velocity of 0.06 $[m/s]$ corresponds to a liquid flow rate of 0.17 $[m^3/h]$ through a single riser; this flow rate is on the low end of the range of the liquid controller. In the experiment the water flow rate is constant and the air flow is increased from zero to 240 $[Nm^3/h]$. The 20 data points are spaced evenly on a log scale, which results in a fine resolution at low gas velocities.

Figure 5-3 shows the pressure gradient found for $u_{SL} = 0.06$ $[m/s]$. The errorbar in the pressure gradient at low gas velocities is due to the occurrence of severe slugging. The large error in the datum point at $u_{SG} = 17$ $[m/s]$ is due to an oscillating pressure in the flowline.

The values of the superficial gas velocities are calculated from the air mass flow rate by means of the interpolated pressure halfway the riser and the ambient temperature of the flow loop. This is the procedure for the calculation of all superficial gas velocities in this research.

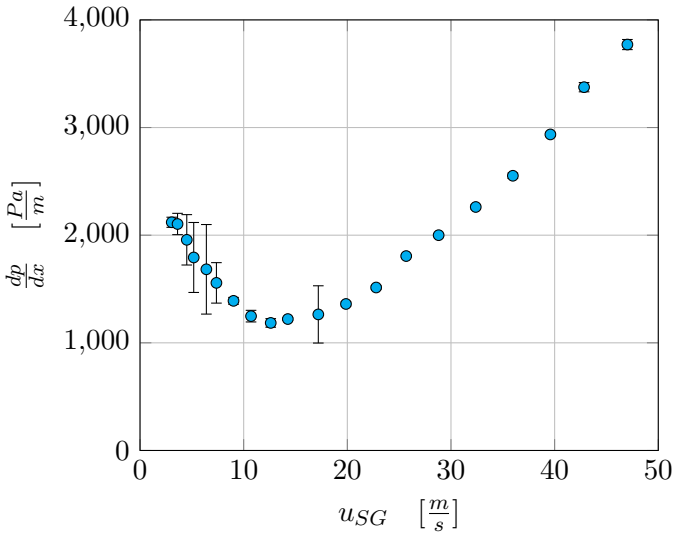

Figure 5-3: The pressure gradient as function of the superficial gas velocity at a constant superficial liquid velocity of 0.06 $[m/s]$.

The measured pressure gradients, can be compared with work by Van Nimwegen [13]. He performed experiments at Delft University in a 34 $[mm]$ diameter vertical riser, with air-water flow at ambient conditions. The 1.25 $[in]$ risers of the SSL have an equivalent diameter and therefore the same pressure gradients are expected for equal superficial velocities. The comparison between both experiments is shown in Figure 5-4.

The pressure gradients from both experiments are in very good agreement. The two SSL data points between 30 and 40 $[Nm/s]$ have a slightly larger pressure gradient, which is due to a higher superficial liquid velocity. It is concluded that the pressure gradients from the work by Van Nimwegen for the same superficial liquid velocity match the results found in the current research. It is therefore likely that the pressure gradients measured by Van Nimwegen for lower liquid velocities can be used in this research as well.

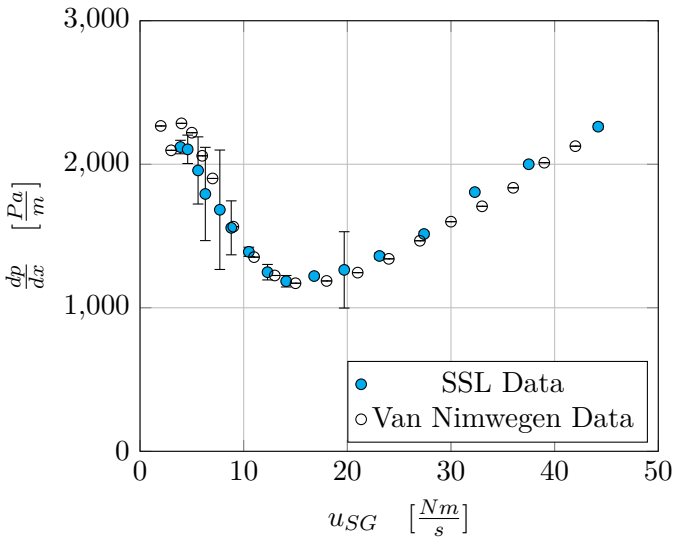

Figure 5-4: Comparison of our single riser pressure drop data, for a constant superficial liquid velocity of 0.06 $[m/s]$, with results by Van Nimwegen. The superficial gas velocity in this figure is given in $[Nm/s]$ as Van Nimwegen presents his data at normal conditions.

Superficial liquid velocity of 0.17 [m/s]

The superficial liquid velocity of 0.17 $[m/s]$ corresponds to a total liquid flow rate of 0.50 $[m^3/h]$ for single riser experiments and to 1.0 $[m^3/h]$ for double riser experiments. The tests are performed with the same data points for the air mass flow rate as in the previous experiment (with exception of the two lowest air flow rates, for which the amount of liquid in the setup was too low to perform these two tests). The results of the experiment are shown in Figure 5-5.

The errorbar in the pressure gradient for the 4 lowest displayed data points originates from severe slugging in the riser. The errorbars in the following 4 points are due to oscillations in the flowline which influence the pressure at the bottom of the riser.

Superficial liquid velocity of 0.34 [m/s]

The superficial liquid velocity of 0.34 $[m/s]$ corresponds to a liquid flow rate of 1.0 $[m^3/h]$ for one riser and to 2.0 $[m^3/h]$ for experiments with two risers. The second flow rate is at the high end of the liquid flow controllers range. For this liquid velocity it was not possible to perform test at the lowest air flow rates as there was not enough liquid in the setup. Figure 5-6 shows the pressure gradient for the various superficial gas velocities. The errors in the pressure gradient of the two data points at the low gas velocities are due to severe slugging.

Comparison of the results

Comparing the pressure gradient curves for the three superficial liquid velocities, it is seen that the pressure minimum moves towards a lower superficial gas velocity for increasing superficial

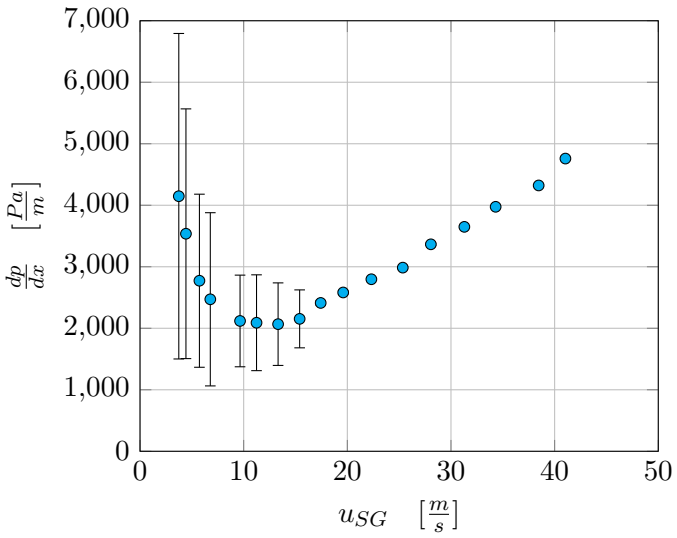

Figure 5-5: The pressure gradient as function of the superficial gas velocity at a constant superficial liquid velocity of 0.17 $[m/s]$.

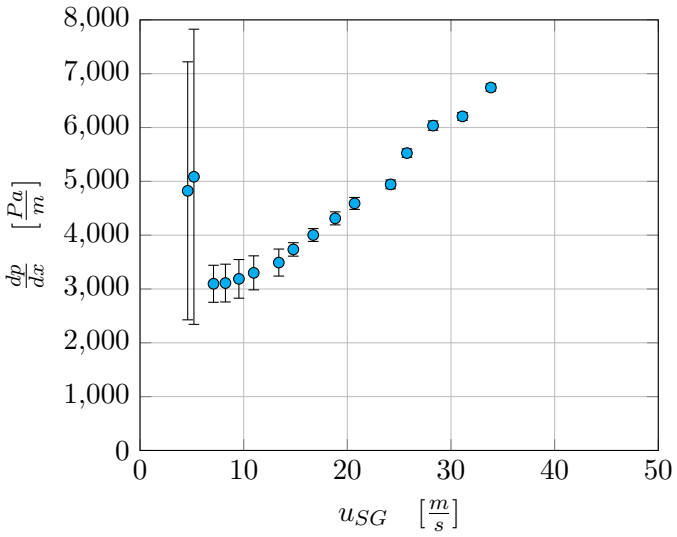

Figure 5-6: The pressure gradient as function of the superficial gas velocity at a constant superficial liquid velocity of 0.34 $[m/s]$.

liquid velocity. Van Nimwegen did not find the same behaviour in his experiments with a 34 $[mm]$ riser. The change between subsequent superficial gas velocities in his experiments is in the order of the expected shift in the location of the minimum in the pressure gradient and therefore the phenomenon is not detected. He did find this phenomenon in experiments with the 50 $[mm]$ vertical riser. It is expected that, when more liquid is present in the riser, the liquid film will be thicker and a lower u_{SG} is needed to move the film in the upward direction. For Van Nimwegen's experiment with a 80 $[mm]$ vertical riser, the pressure drop minimum shifted towards higher superficial gas velocities for an increasing superficial liquid velocity. This difference is attributed to a larger influence of the entrainment on the transition from

churn flow to annular flow transition in larger diameter pipes.

5-3 Dual riser - two phase experiments

The goal of the dual riser, two phase flow experiments is to validate the hypothesis that the phase split will be symmetric when the total gas flow rate is sufficient to sustain annular flow in both risers.

First, exploratory tests were done to confirm the assumption that the flow split over an impacting T-junction with risers downstream can be symmetric for high gas flow rates. Next the double riser data were compared with single riser pressure gradients to check if it is possible to distinguish between symmetric and asymmetric phase splits. Then the influence of hysteresis and the stability of the phase splits was tested. Finally, the required minimum gas flow rate to obtain a stable symmetric split was determined.

5-3-1 Exploratory tests

In the literature, only one experimental study was found on the splitting of two phase flow from a horizontal flowline into two vertical risers with an impacting T-junction. This is the research by Van der Gronden [1]. The gas flow rates used in those experiments were not sufficient to achieve annular flow in one or both risers. The hypothesis that the phase split will be symmetric when the total gas flow rate is sufficient to sustain annular flow in both risers could therefore not be tested in the layout of his experimental facility (i.e. the SSL at STCA). The goal of our exploratory experiments is to test if the hypothesis is valid, using the new layout of the SSL.

The behaviour of the flow split is tested for four characteristic gas flow rates at two different liquid flow rates. These four flow rates are:

- The maximum total gas flow rate of the setup: 200 $[Nm^3/h]$.
- A moderate total gas flow rate which is sufficient to sustain annular flow in both risers: 80 $[Nm^3/h]$.
- A moderate total gas flow rate which is insufficient to sustain annular flow in both risers: 60 $[Nm^3/h]$.
- A low total gas flow rate which gives the same condition as used by Van der Gronden: 20 $[Nm^3/h]$.

If the hypothesis is valid, the flow split for the first two characteristic flow rates should be symmetric. The hypothesis does not exclude a symmetric flow split for the other two flow rates. However, an asymmetric split is expected based on previous results by Van der Gronden.

The results of the exploratory tests are shown in Figure 5-7. In the experiment, the flow split is regarded as symmetric when the pressure drop over both vertical risers is equal, and their flow regime is the same. In the four cases with high air flow rates, the flow pattern in both

risers was annular and the pressure drop was equal for both sides. In the other four cases the flow pattern and the pressure drop varied per riser.

From this, it is concluded that a symmetric flow split is possible in an impacting T-junction with two vertical risers downstream. The flow patterns in the risers, during the symmetric split, were in agreement with the expectations from the hypothesis. The asymmetric splits occurred at low gas flow rates which are insufficient to sustain annular flow in both risers. This thus gives no reason to falsify the hypothesis.

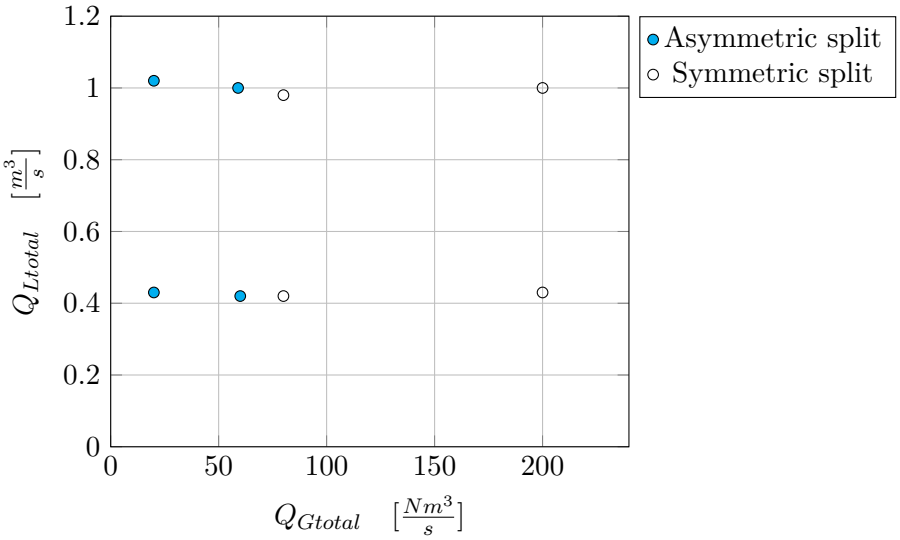

Figure 5-7: The splitting behaviour of eight flow rate combinations. The flow rates on the horizontal axis denotes the combined flow rate of both risers.

5-3-2 Comparison between dual and single riser results

When the gas and liquid of the incoming two phase flow split evenly over the left and right riser, the pressure drop should be the same for both sides and equal to the pressure drop found in a single riser with an equivalent flow. The results for the pressure gradient generated in Section 5-2 are now compared to the results generated in the dual riser experiments with equal superficial velocities in the risers.

The pressure gradients found in a dual riser experiment with superficial liquid velocity of 0.06 $[m/s]$, are shown in Figure 5-8. The pressure gradient in the two risers is equal for each data point to the right of the pressure drop minimum as the black markers precisely overlap the white markers. These gradients also agree with the results of the single riser tests. The values of two data point pairs on the left side of the pressure gradient minimum are not equal to one another or to the single riser results.

For a dual riser experiment with superficial liquid velocity of 0.17 $[m/s]$, the pressure gradients are shown in Figure 5-9. For all dual riser data point pairs to the right of the pressure drop minimum, the pressure gradient in the left and right riser is equal to the gradient in the equivalent single riser experiment. This is also the case, for for the first data point pair to the left of the pressure drop minimum. For the other low gas flow rate tests the pressure gradients are unequal for the left and right riser.

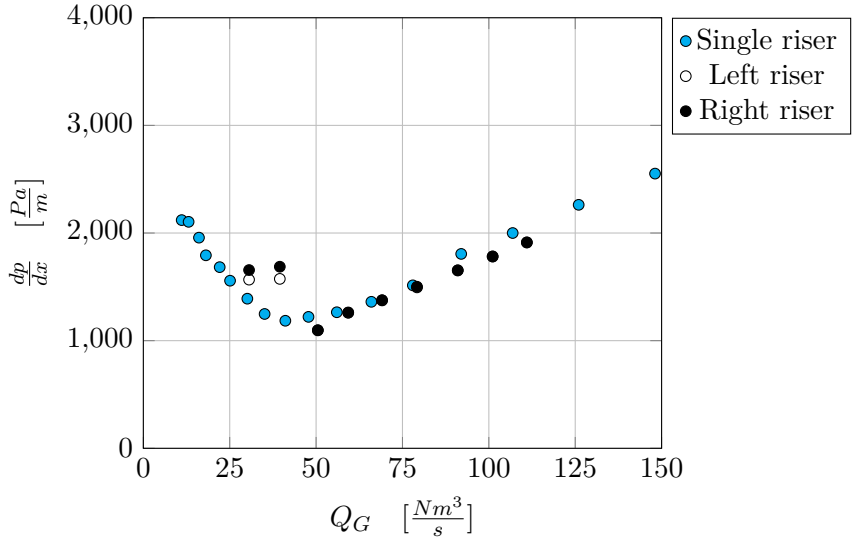

Figure 5-8: The pressure gradient as function of the gas flow rate per riser, at a constant superficial liquid riser velocity of 0.06 $[m/s]$.

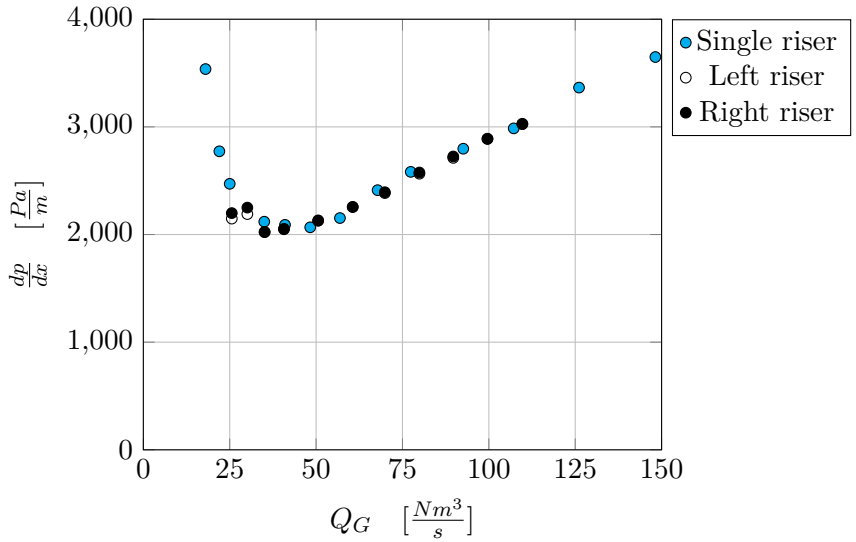

Figure 5-9: The pressure gradient as function of the gas flow rate per riser, at a constant superficial liquid riser velocity of 0.17 $[m/s]$.

Figure 5-8 and Figure 5-9 show that, for all data point pairs to the right of the single riser pressure drop minimum the flow split can be regarded as symmetric. The pressure drop minimum is associated with the transition from churn flow to annular flow. Therefore is concluded that, when the gas flow rate is sufficient to sustain annular flow in both risers, the flow split tends to be symmetric.

In Figure 5-10, the red line indicates all superficial velocity combinations, on the right side of the pressure drop minimum, which result in the same pressure gradient. The hypothetical situation is shown, for which the pressure gradient for a single riser S is equal to the pressure

gradient for two dual risers $D2$ and $D3$, and the combined flow rates of the dual riser are double of a single riser. However, there is a maldistribution in the phase split between the dual risers. As the phase split in a horizontal symmetric impacting T-junction is governed by the pressure difference between both outlets, the following conditions should be true:

$$p_2 > p_3 \qquad \text{since } u_{SG3} > u_{SG2}$$
$$p_3 > p_2 \qquad \text{since } u_{SL2} > u_{SL3}$$

These two inequalities for the pressure can not occur simultaneously. Therefore, it is expected that the phase split between $D2$ and $D3$ is equal for both phase or nearly equal. As their total flow rate is double of the value of the single riser, this also means that the flows in the single and dual risers are equal.

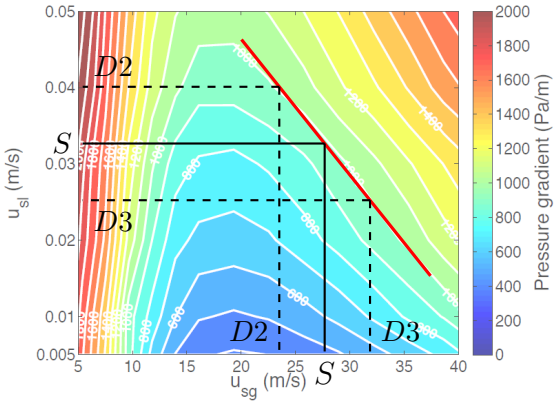

Figure 5-10: Hypothetical situation where the pressure drop (red line) over a single riser S is equal to the pressure drop over two dual risers $D2$ and $D3$. The image in the background is the pressure drop sheet which was also shown in Figure 2-8.

From these findings it is concluded that for future experiments in the SSL a distinction can be made between an asymmetric and a symmetric phase split based on the pressure drop over each riser and visual inspection. This does not hold for similar setups where the downstream section of both risers towards a release vessel is unequal. The different pressure drop over both downstream sections will then interfere with the pressure drop over the riser.

Furthermore it was found in both experiments that the pressure at the base of the risers was not equal for single riser tests and double riser tests with equal superficial velocities. This difference originates from the pressure drop over the final pipe segment from the top section towards the release vessel (shown in Figure B-10a). The flow through this pipe doubles for experiments where both risers are used. The resulting additional pressure drop does influence the total pressure drop over the system but it has a negligible effect on the pressure gradient measurements and on the flow splitting.

5-3-3 Hysteresis and stability

The previous experiments were focused on how to distinguish between a symmetric and an asymmetric phase split. No special attention was paid to the flow condition prior to taking the experiments or to the stability of the results over time.

From the work of Van der Gronden, it is known that hysteresis can occur and this influences the flow split. When hysteresis is present in a system the question arises which state or states are stable over time. In the next experiments these effects are investigated.

Figure 5-11 displays the experiment that captures the influence of the hysteresis. The goal is to localise the point, marked X in the figure, where the phase split changes from symmetric to asymmetric for a certain liquid flow rate. The point is approached starting from a high and a low gas flow rate. The high value of the total gas flow rate is 160 $[Nm^3/h]$ and the initial phase split is symmetric. The low value of the total gas flow rate is 43 $[Nm^3/h]$ which results in an asymmetric split. In addition to the asymmetric split, a standing water column is created in the right riser as an extra asymmetry (with use of the bottom hand valve). After some time, the high or low gas flow rate is changed instantaneously to its new value. The new conditions are allowed to develop for 20 minutes.

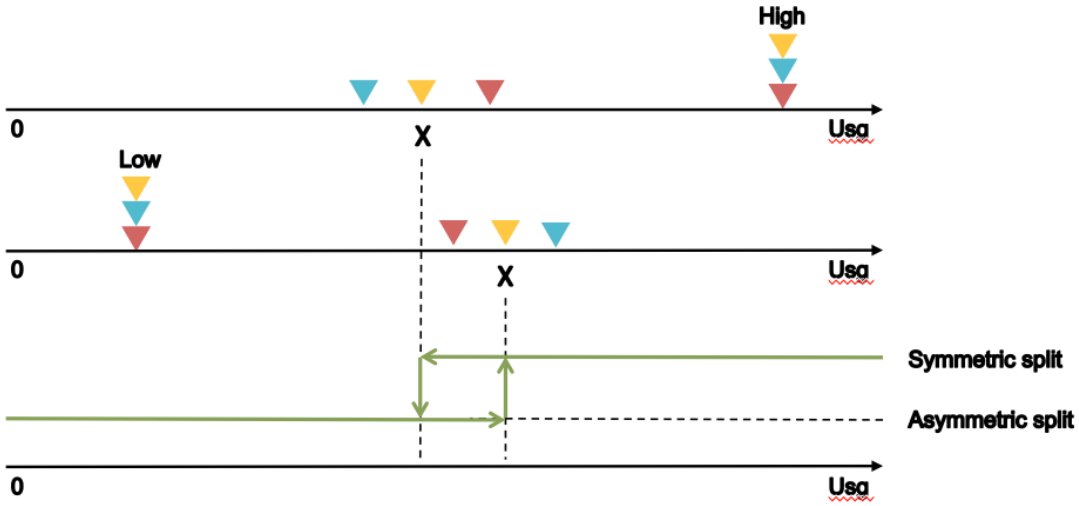

Figure 5-11: Visualization of the hysteresis and stability tests

After the hysteresis test, the stability of the flow split is tested by perturbing the flow. The riser with the highest gas flow rate is choked for 1 minute, and the new conditions are allowed to develop for 9 minutes. In total the flow split is perturbed three times.

In Section 5-3-2 it was concluded that, for experiments with the SSL, the pressure drop can be used to distinguish between a symmetric and an asymmetric phase split. Therefore a new quantity is introduced: the normalized pressure drop, $\overline{\Delta p_i}$

$$\overline{\Delta p_i} = \frac{2 \cdot \Delta p_i}{\Delta p_L + \Delta p_R}$$

where the i in Δp_i is L or R for the left and right riser, respectively. This quantity is a measurement of the difference in pressure drop for both risers. In the case of a symmetric phase split this quantity is equal, or almost equal, to one.

Superficial liquid velocity of 0.06 [m/s]

The normalized pressure drops for experiments with superficial liquid velocities of 0.06 $[m/s]$, as obtained for the low and the high gas flow rates, are shown in Figure 5-12. In both cases the flow split is symmetric for gas flow rates over 40 $[Nm^3/h]$ per riser. The corresponding pressure drops and flow patterns (annular) are the same for the low and high gas flow rate tests and they remain stable after choking.

For flow rates of 40 $[Nm^3/h]$ and lower the splits are asymmetric and depend on which gas flow rate was used. In the low gas flow rate cases the water column in the right riser becomes a bubble column which produces only gas. After the first perturbation, the additional liquid of the bubble column is blown out and the results coming from both test flow rates are indistinguishable. The flow regime in the one riser now is annular/churn flow and in the other riser slug flow. Interestingly it is possible to flip the flow patterns in both risers by using the top chokes.

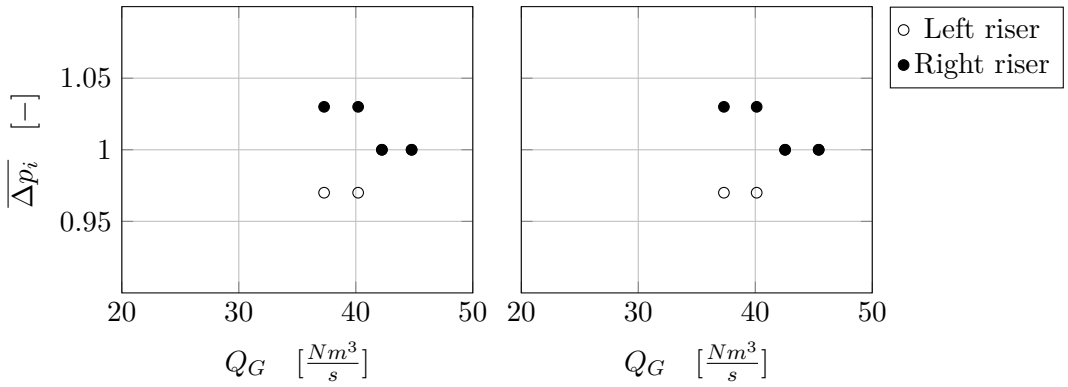

Figure 5-12: The normalized pressure drop of the left and the right riser as function of the gas flow rate per riser, at a constant superficial liquid velocity of 0.06 $[m/s]$. Results corresponding to the low and high gas flow rates are shown in the left and right plot, respectively.

Superficial liquid velocity of 0.18 [m/s]

The normalized pressure drops coming from the high and low gas flow rates, for experiments with superficial liquid velocities of 0.18 $[m/s]$ are shown in Figure 5-13.

In this experiment the same behavior is found as before. Above a certain gas flow rate the split is symmetric and independent of which initial gas flow rate is used. Below this flow rate initially two states are found. After the first perturbation, the water bubble column is blown out and only the churn/annular and slug state is found. For this experiment with a higher superficial liquid velocity, symmetry breaking occurs at a lower gas flow rate, namely at 30 $[Nm^3/h]$ per riser.

In the two experiments shown in Figure 5-12 and Figure 5-13 no asymmetric phase split was found above a certain gas flow rate. However, the initial instantaneous jump found when going from the low gas flow rate towards the new value can be regarded as a perturbation. Therefore an experiment is conducted where the gas flow rate is slowly increased from the low value. In this test, with $u_{SL} = 0.18$ $[m/s]$, the initial asymmetric split and the associated

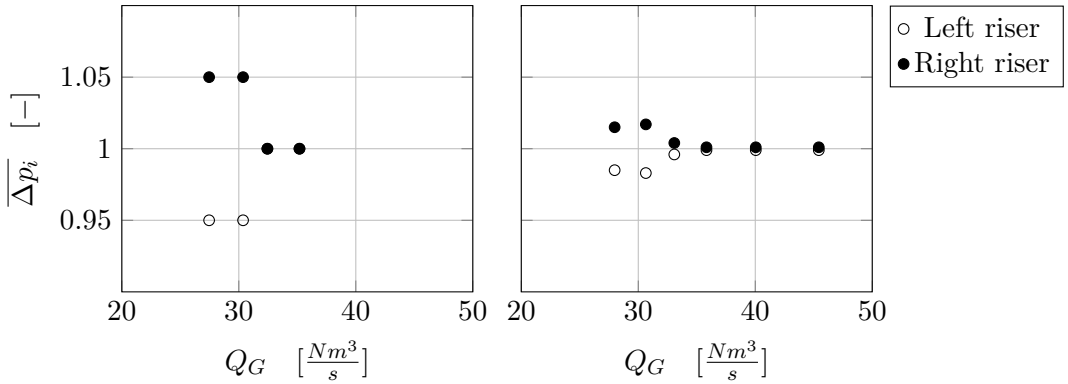

Figure 5-13: The normalized pressure drop of the left and the right riser as function of the gas flow rate per riser, at a constant superficial liquid velocity of 0.18 $[m/s]$. Results corresponding to the low and high gas flow rates are shown in the left and right plot, respectively.

bubble column were preserved up to a gas flow rate of 89 $[Nm^3/h]$ per riser. Then the asymmetric situation collapsed and became symmetric.

Flow split states

Based on the results from the hysteresis and stability tests, the following conclusions can be drawn for a situation where the liquid flow rate is kept constant.

- For every liquid flow rate there is one gas flow rate which can be considered as a transition point. For gas flow rates above this point, the most stable phase split is symmetric. For gas flow rates below the transition flow rate, the most stable phase split is asymmetric.
- Five different states are distinguished for the flow split:

  1. **Annular-Annular (A-A)**
     stable symmetric phase split 5-14a

     This state is most likely to be found when the gas flow rate is above the transition flow rate. Perturbations have no effect on this state.
  2. **Bubble-Annular (B-A)**
     highly unstable asymmetric phase split 5-14b

     This state can only appear when the gas flow rate for a B-CS state is increased in a quasi static manner to above the transition flow rate. The hydrostatic head of the bubble column counteracts the pressure drop over the other riser. Small perturbations will make this state collapse to A-A.
  3. **Churn/Slug-Annular/Churn/Slug (CS-ACS)**
     stable asymmetric phase split 5-14c

     Below the transition flow rate this is the only stable state. Perturbations have no effect on this split other than flipping the riser flows.

4. **Bubble-Annular/Churn/Slug (B-ACS)**
   unstable asymmetric phase split 5-14d

   This state can occur below the transition flow rate. In the current research this state was forced on the system with the use of the bottom hand valves, Van der Gronden encountered this state in experiments where all valves were open. The hydrostatic head of the bubble column counteracts the pressure over the other riser. Perturbations make let this state collapse to S-ACS. This state is not as unstable as B-A.

5. **Churn-Churn & Slug-Slug (C-C & S-S)**
   highly unstable symmetric phase split 5-14e

   This state was only encountered a few times during the extensive hours of experimentation. Probably, the unstable character of the slug flow and the churn flow is a large enough perturbation to make this state collapse to S-ACS.

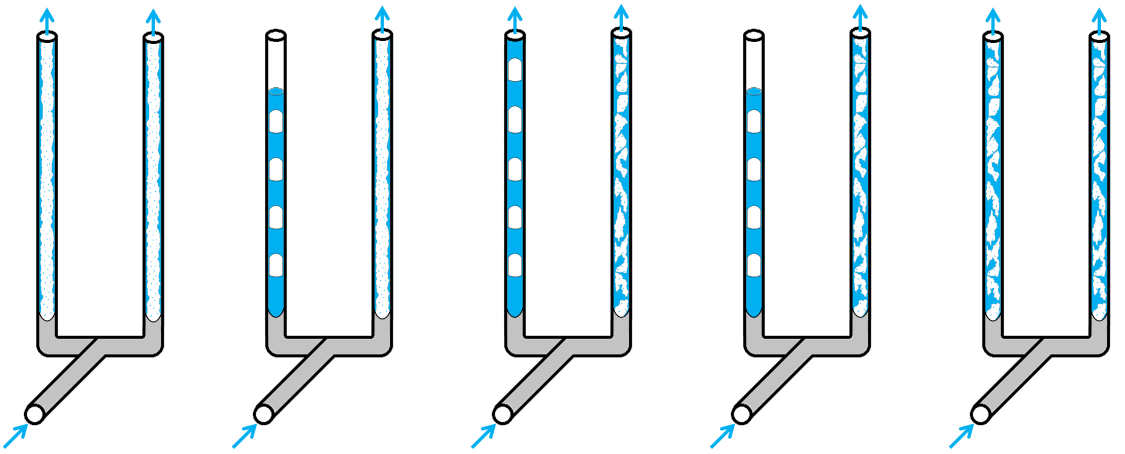

(a) A-A **(b)** B-A **(c)** CS-ACS **(d)** B-ACS) **(e)** C-C & S-S

Figure 5-14: Schematic overview of the five states of the flow split

From the results of the stability tests performed in the previous experiments a flow split transition chart is constructed, which is shown in Figure 5-15.

5-3-4 Transition flow rate

In the previous subsection it was found that, for each liquid flow rate, there exists a specific gas flow rate which acts as the transition boundary for the type of flow split. The two following experiments are aimed at finding this specific gas flow rate for other liquid values and to determine the behavior of the transition point. The experiments are similar to the previous test, except that now only one initial condition is considered. It was decided to approach the transition point from the high gas flow rate for practical reasons.

The two superficial liquid velocities tested are 0.12 $[m/s]$ and 0.26 $[m/s]$. The results of the experiments are shown in Figure 5-16 and 5-17. Again it is found that for higher liquid flow rates the corresponding gas flow rate of the transition point is lower.

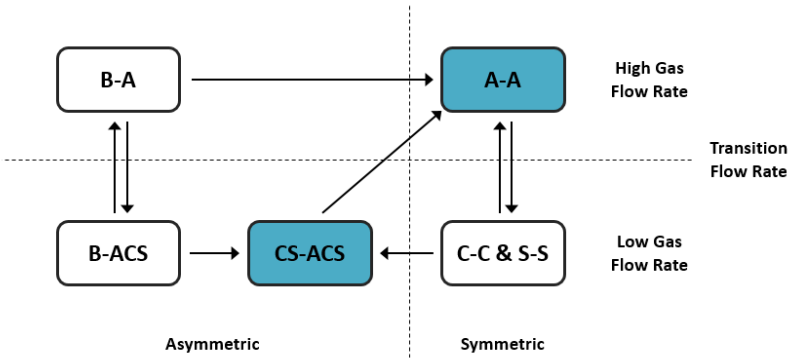

Figure 5-15: Overview of the five states and the directions of the possible transition. The colored states are the most stable states for the corresponding flow rate.

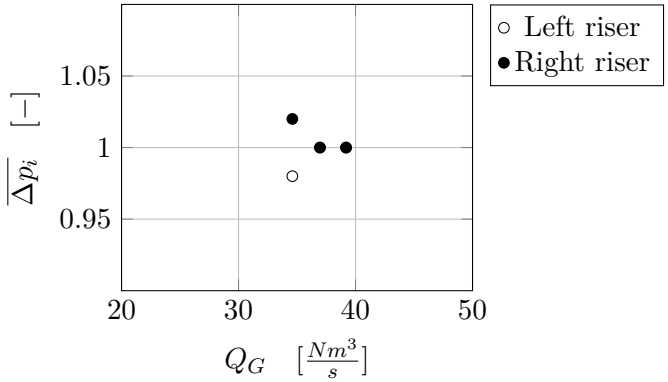

Figure 5-16: The normalized pressure drop over the left and the right riser as function of the gas flow rate per riser. The results shown correspond a superficial liquid velocities of 0.12 $[m/s]$. The splits in the experiment follow the phase split transition chart of Figure 5-15.

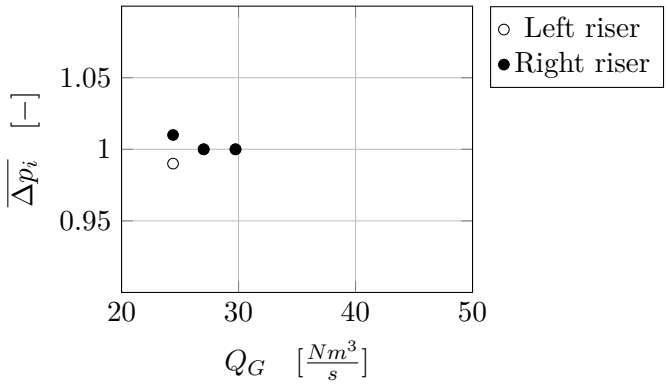

Figure 5-17: The normalized pressure drop over the left and the right riser as function of the gas flow rate per riser. The results shown correspond a superficial liquid velocities of 0.26 $[m/s]$. The splits in the experiment follow the phase split transition chart of Figure 5-15.

The hypothesis at the start of the experiments was that the phase split will be symmetric when the total gas flow rate is sufficient to sustain annular flow in both risers. Therefore, the

flow split transition points and the locations of the pressure drop minima are plotted in the same graph in Figure 5-18.

All points but one are situated on the same trend line. The deviating point corresponds to a superficial liquid velocity for the which severe slugging interfered with the pressure drop measurements at low gas flow rates. It is assumed that the true location of the minimum was not captured in the single riser experiment. The point depicted in this graph therefore corresponds to a gas flow rate above the pressure drop minimum.

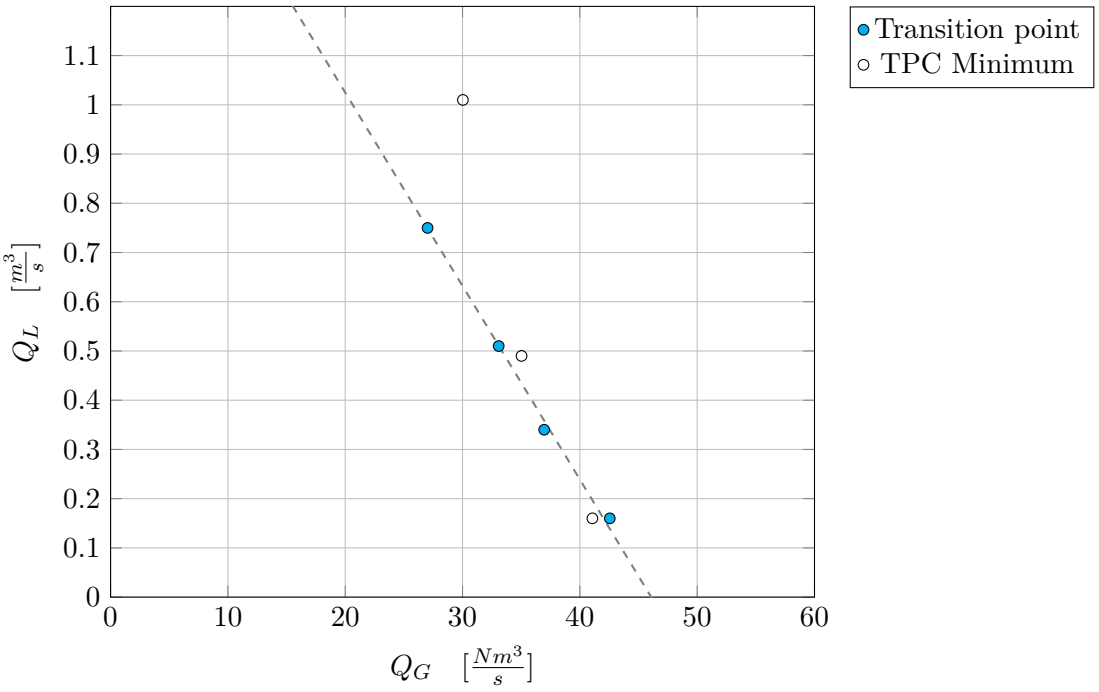

Figure 5-18: Combined plot of the transition points found in dual riser experiments and the pressure drop minima found in single riser experiments. The units on the axis are the flow rates per riser.

Based on the data shown in Figure 5-18 and the visual inspections of the flow patterns in all experiments it is concluded that the transition from a stable asymmetric flow split to a stable symmetric flow split occurs at the pressure drop minimum which is an indication of the transition to annular flow.

5-4 Experimental conclusions

The main conclusions of this experimental study are summarized below:

- It is concluded in Section 5-1 that the flow loop downstream of the impacting T-junction is symmetric. No geometrical asymmetries where found between the splitter and the release vessel.
- The pressure drop curve is generated for three different superficial liquid velocities in

Section 5-2. When the superficial liquid velocity is increased, the superficial gas velocity corresponding to the pressure drop minimum decreases.

- It is concluded in Section 5-3-2 that, for the current setup, which is symmetric downstream of the T-junction, the pressure gradient data combined with visual inspection of the flow patterns in both risers is sufficient to determine whether a phase split is symmetric.
- It is found in Section 5-3-3 that there are five possible states in which the flow can split in the current setup. Of these five splits only two are stable and they occur on opposites sides of a specific transition gas flow rate. A schematic overview of the five states and how they develop is shown in Figure 5-14 and Figure 5-15.
- The transition gas flow rates are compared to the gas flow rates corresponding to pressure drop minima in equivalent single riser experiments in Section 5-3-4. For both characteristic flow rates the same behavior is found.

From these points and their corresponding results it is concluded that the flow split in an impacting T-junction with vertical risers will be symmetric when the gas flow rate is sufficiently high to sustain annular flow in both risers.

Chapter 6

Phase split modelling

In this chapter a new model to predict the phase split at an impacting T-junction with vertical risers downstream of the tee is developed. In Section 6-1 a short overview of previous research is given. In Section 6-2 the new modelling approach is introduced and the different sub-models are presented. In Section 6-3 results generated with the model are compared with the literature and with experimental results by Van der Gronden [1]. Finally, the main conclusions are summarised in Section 6-4.

6-1 Literature review

In the literature only two studies were found on predicting the phase split of two phase flow from a horizontal flowline into two vertical risers with an impacting T-junction.

- Van der Gronden [1] developed a phase split predicting model in the *Honeywell UniSim Design* environment. The *Unisim* process simulation tool provides solutions for steady state and dynamic process conditions. Essential to his model, is a specific experimental correlation which describes the gas and liquid fraction take off into the left riser (i.e. the phase split curve). This empirical model is not applicable to other configurations and operating conditions.
- Worthen [23] performed a computational fluid dynamics (CFD) study using the experimental data generated by Van der Gronden as a benchmark. She used the Volume of Fluid (VOF) interface tracking method in ANSYS Fluent 15.0. The CFD simulations showed that, if the back pressures on the two risers are held constant in time, the flow split is only stable when all the flow is exiting through one riser. At the same flow rate, Van der Gronden found an equal split in his experiments. The experiments, however, did give that all flow goes through one riser if the gas flow rate was taken a bit lower. Worthen concluded, that the software is not sufficiently developed yet to model the complex interaction of the interface between the two fluids in the vertical riser.

In the following section, a new approach is followed to find a model to predict the phase split.

6-2 Computational model

The geometry of interest in this research is schematically illustrated in Figure 6-1a. In the computational model it is assumed that this geometry can be split in two parts, the junction and the vertical risers, which are evaluated separately. The influence of the upstream horizontal flowline is neglected.

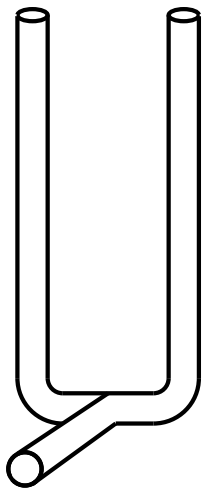

(a) Schematic drawing of the considered geometry.

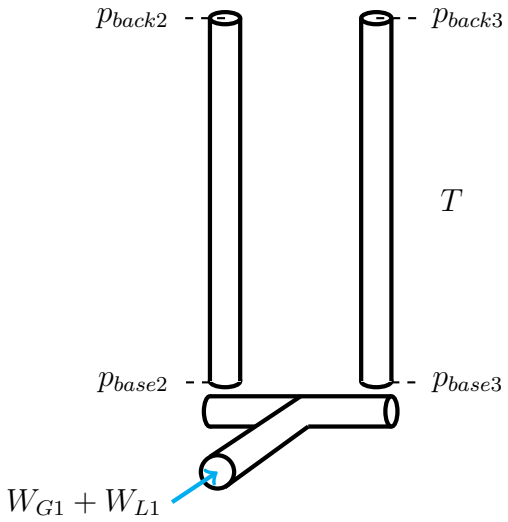

(b) Schematic drawing of the modelled geometry: the impacting T-junction and the two vertical risers.

Figure 6-1

For the model the following five parameters are set: the incoming gas mass flow rate W_{G1}, the incoming liquid mass flow rate W_{L1}, the temperature T, and the back pressures on the two risers p_{back2} and p_{back3} which originate from the pressure drop between the riser head and the release vessel. Parameters λ_G and λ_L, which represent the mass fraction take off into the right riser for the gas and liquid respectively, are defined as:

$$\lambda_G = \frac{W_{G3}}{W_{G1}} = \frac{W_{G3}}{W_{G2} + W_{G3}}, \qquad \lambda_L = \frac{W_{L3}}{W_{L1}} = \frac{W_{L3}}{W_{L2} + W_{L3}} \tag{6-1}$$

From these definitions, the mass flow rates in the riser W_{G2}, W_{L2}, W_{G3} and W_{L3} are calculated. The temperature T, together with the local pressure and the equation of state, determines the local density ρ_G of the compressible gas.

The two vertical risers are modelled using the Shell Flow Correlations (SFC). Starting from the back pressure at the riser head, the pressure at the base of the riser is calculated. The base pressure of the left and right riser is then used as an input for two independent phase split models for the flow at the junction. Using the Advanced Double Stream Model (ADSM) [2], the relation between the gas and liquid take off is determined for the tee at the specific flow conditions. Now, all possible phase splits corresponding to the given initial parameters are identified. However, which phase split the system will select from this set is yet to be determined.

The ADSM is based on the extended Bernoulli equation, which incorporates the conservation of energy for an isothermal junction. By the definition of λ_G and λ_L, conservation of mass is automatically satisfied. Unique to the developed model is the use of the conservation of momentum to select the exact phase split from the set of possible splits generated by the ADSM. Here, the influence of the two downstream vertical risers is incorporated as pressure forces imposed on the control volume, which affect the phase split.

The three models described above, all assume 1D steady state fluid flow. Flow transients are not accounted for. Detailed information on the single riser model, the ADSM and the momentum constraint is presented in the next three sections: 6-2-1, 6-2-2 and 6-2-3 respectively.

Saba and Lahey [31] stated that the phase split in a T-junction with a known geometry (no risers), is characterised by eight independent parameters: W_1, W_2, W_3, x_1, x_2, x_3, $p_{1\to2}$ and $p_{1\to3}$, where x_i is the mixture quality. However, for the newly developed model only seven parameters are mentioned: W_{G1}, W_{L1}, p_{back2}, p_{back3}, T, λ_G and λ_L. This can be explained by two additional independent parameters in the ADSM, i.e. the energy loss factors k_G and k_L for the gas and the liquid, respectively. This brings the total number of degrees of freedom to nine. The extra parameter, compared to the eight of Saba and Lahey, is the gas density which is allowed to vary in the vertical risers of the current model.

6-2-1 Single riser model

Within Shell the Shell Flow Correlations (SFC) [8] are used to predict the steady state characteristics of fully developed flow in pipelines and risers. This set of correlations is a harmonized collection of published and internal models. Given the flow rates of the phases, the fluid properties and the pipe geometry, the SFC returns steady state pointwise solutions for the flow conditions. The input parameters for air-water flow in one riser are shown in table 6-1.

Table 6-1: Input parameters for the Shell Flow Correlations (v7.9.1. Most parameters are assumed constant, only u_{SG}, u_{SL} and ρ_G are varied.

Parameter	Value	Unit
Superficial liquid velocity	0 - 0.35	$[m/s]$
Superficial gas velocity	0 - 60	$[m/s]$
Water cut	1	[-]
Density of air	1.2 - 3.0	$[kg/m^3]$
Density of water	998	$[kg/m^3]$
Viscosity of air	$1.845{\cdot}10^{-5}$	$[Ns/m^2]$
Viscosity of water	$1{\cdot}10^{-3}$	$[Ns/m^2]$
Surface tension water/air	$7.2{\cdot}10^{-3}$	$[N/m]$
Pipe hydraulic diameter	0.03175	$[m]$
Pipe inclination	90	$[deg]$
Wall roughness	$1{\cdot}10^{-8}$	$[m]$

The fluid flow input parameters for the main model are the incoming gas mass flow rate W_{G1} and the incoming liquid mass flow rate W_{L1}. As water can assumed to be incompressible, and as the pipe diameter is known W_{L1} is easily converted into u_{SL}. The density of the gas

ρ_G and thereby the superficial gas velocity u_{SG} depend on the pressure and temperature at the specific cross section of the pipe. The absolute local pressure is the sum of the back pressure on the riser head and the pressure drop in the riser. Since the pressure drop in the riser depends on the superficial gas velocity and the density, an iterative scheme is used to determine all three values for the single point at the specific cross section of the pipe.

In Figure 6-2, the unit cell used in the iterative scheme is shown. Using the pseudo algorithm 1 as listed below, the average flow conditions at the cell center are calculated (from the downstream conditions). Since the average pressure drop over the unit cell is known now, the back pressure p_{back} at the top of the riser can be extrapolated to the bottom of the unit cell to finally calculate p_{base}.

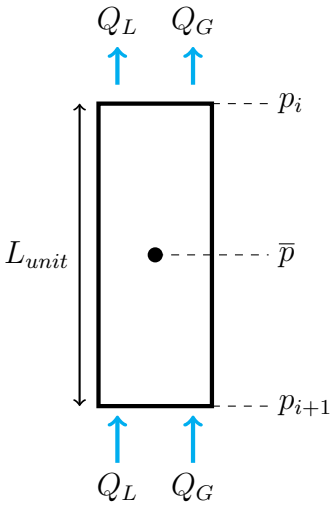

Figure 6-2: Schematic representation of the unit cell used in determining u_{SG}, ρ_G and $\overline{p}$ for the vertical riser. The riser can be divided into multiple unit cells and therefore L_{unit} is equal to, or smaller than the riser height.

Algorithm 1 Iterative algorithm

```
procedure FLOWCONDITIONS
    calculate u_SL
    guess p̄
    for iterations < 50 do
        calculate ρ_G
        calculate u_SG
        if |Δu_SG| < 0.5% then
            break
        interface with SFC to determine dp̄/dx
        calculate new p̄
    return flow conditions at p_{i+1}
```

As a test case, the model for determining the flow conditions is compared to the experimental data from Section 5-2. In Figure 6-3, the experimental data for the single riser with a superficial liquid velocity of 0.06 $[m/s]$ is shown. This data set is chosen as it is the one that

is the least influenced by severe slugging and flowline oscillations.

First, the model was run with the default settings. It was found that, with the default settings, the SFC failed to predict the correct pressure drop for vertical slug flow. This shortcoming is known (within Shell), hence an alternative model was developed for improving the predictions for vertical pipe flow: the *Novati* model [35]. The *Novati* model is the new default setting for churn flow and annular flow in the SFC (v7.9.1). As this model gave better prediction of the experimental data, it is used for slug flow in the vertical riser.

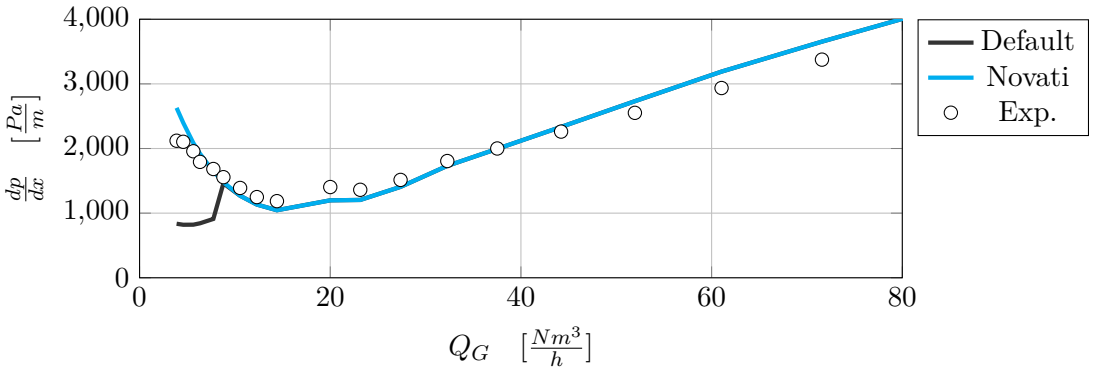

Figure 6-3: Comparison of the flow condition model with experimental data for vertical single riser flow with a superficial liquid velocity of 0.06 $[m/s]$.

The pressure drop prediction found by using a single unit cell with a length of 16.85 $[m]$ gives a reasonable match with the experimental data. The forward extrapolation, used in algorithm 1, can introduces an error which scales with the length of the unit cell. A sensitivity analysis is performed where the riser is divided into multiple unit cells. By using the pseudo code in algorithm 2, the performance of 1, 2, 4 and 8 unit cells is tested.

Algorithm 2 Single Riser Model

procedure SINGLERISER
  N = number of unit cells
  $L_{unit} = L_{riser}/N$
  $p_i = p_{back}$
  for N **do**
    calculate $d\overline{p}/dx$ ▷ use algorithm 1
    $p_{i+1} = p_i + L_{unit} \cdot d\overline{p}/dx$
    $p_i = p_{i+1}$
  $p_{base} = p_{i+1}$
  return flow conditions at p_{base}

The results are shown in Figure 6-4. For low gas flow rates, the number of unit cells has a negligible influence since the pressure will not change much over the height of the riser. For gas flow rates above 50 $[Nm^3/h]$, the single unit cell introduces the largest error as the pressure changes significantly along the riser. However, this error has the same order of magnitude as the overall accuracy of the SFC.

The computation time of the single riser model scales linearly with the number of unit cells.

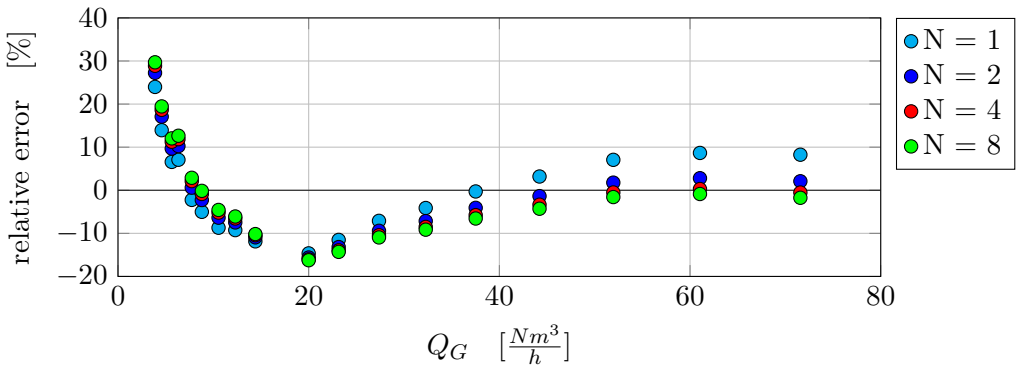

Figure 6-4: Relative error, compared to experimental data, for N unit cells.

Thus, it was decided to use only one unit cell to predict the flow conditions at the bottom of the riser as the single unit cell produces equally good results for low gas flow rates and acceptable results for high gas flow rates.

6-2-2 Advanced Double Stream Model

The Advanced Double Stream Model (ADSM) is based on the extend Bernoulli equation which includes an (empirical) closure for the energy loss factors in addition to the usual terms. The model assumes that both the gas flow and the liquid flow at the inlet of the T-junction are split over the two outlets. Therefore, four streamlines exist. They are:

- Inlet-to-run gas streamline
- Inlet-to-branch gas streamline
- Inlet-to-run liquid streamline
- Inlet-to-branch liquid streamline

The four streamlines are shown in Figure 6-5

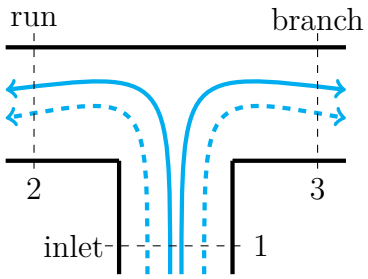

Figure 6-5: Schematic drawing of the four stream lines in the Advanced Double Stream Model. Dotted lines: gas flow, solid lines: liquid flow.

The steady-state macroscopic mechanical energy balance is shown below. Here, i could be either 2 or 3 for the run and branch arm, β could be either L or G for the liquid and gas phase and $\hat{E}_v$ is the frictional loss term.

$$\frac{1}{2}\left[\frac{\langle u_1^3\rangle}{\langle u_1\rangle}-\frac{\langle u_i^3\rangle}{\langle u_i\rangle}\right]_\beta+\left[g\left(z_{1,i}-z_i\right)\right]_\beta+\left[\left(P_1-P_i\right)/\rho\right]_\beta=\left[\hat{E}_{v1i}\right]_G \tag{6-2}$$

With the assumption that:

$$\left(P_2-P_3\right)_G=\left(P_2-P_3\right)_L \tag{6-3}$$

the equations of the four stream lines are combined into one equation:

$$\begin{aligned}\frac{1}{2}\rho_G\left[\frac{\langle u_3^3\rangle}{\langle u_3\rangle}-\frac{\langle u_2^3\rangle}{\langle u_2\rangle}\right]_G-\frac{1}{2}\rho_L\left[\frac{\langle u_3^3\rangle}{\langle u_3\rangle}-\frac{\langle u_2^3\rangle}{\langle u_2\rangle}\right]_L+\rho_G\left[g\left(z_3-z_{1,3}+z_{1,2}-z_2\right)\right]_G\\ -\rho_L\left[g\left(z_3-z_{1,3}+z_{1,2}-z_2\right)\right]_L=\rho_G\left[\hat{E}_{v12}-\hat{E}_{v13}\right]_G-\rho_L\left[\hat{E}_{v12}-\hat{E}_{v13}\right]_L\end{aligned} \tag{6-4}$$

By introducing the following new quantities: the gas take off in the branch arm λ_G, the liquid take off in the branch arm λ_L, the kinetic energy ratio κ, the flow shape factor β, the phase holdup ϵ and the energy loss factor as $\hat{E}_v$:

$$\hat{E}_v=k\frac{1}{2}\frac{\langle u_1^3\rangle}{\langle u_1\rangle} \tag{6-5}$$

Equation 6-4 is rewritten as:

$$\begin{aligned}\kappa\left[\frac{\beta_{G2}\alpha_{G1}D_1^4}{\beta_{G1}\alpha_{G2}D_2^4}\left(1-\lambda_G\right)^2-\frac{\beta_{G3}\alpha_{G1}D_1^4}{\beta_{G1}\alpha_{G3}D_3^4}\lambda_G^2\right]-\left[\frac{\beta_{L2}\alpha_{L1}D_1^4}{\beta_{L1}\alpha_{L2}D_2^4}\left(1-\lambda_L\right)^2-\frac{\beta_{L3}\alpha_{L1}D_1^4}{\beta_{L1}\alpha_{L3}D_3^4}\lambda_L^2\right]\\ +\frac{2g}{\beta_{L1}\left\langle u_{L1}\right\rangle^2}\left[-\left(z_{L3}-z_{L1,3}+z_{L1,2}-z_{L2}\right)\right]=\kappa\left(k_{13}-k_{12}\right)_G-\left(k_{13}-k_{12}\right)_L\end{aligned} \tag{6-6}$$

The full derivation for this equations and the definitions of other introduced quantities are presented in Appendix A. The geometrical relation for calculating the liquids heights z, is a superposition of a liquid film model and a liquid gutter model. These two models are presented in Figure 6-6 and discussed in Appendix A.

The empirical closures for the energy loss factors k in Equation 6-5 are a key element of the ADSM. Ottens et al. [2] used the loss factor relations in Equations 6-7 and 6-8 based on work by Ito and Imai [36] for single phase turbulent gas flow in impacting T-junctions.

$$k_{12,G}=0.59+\left(1.18-1.84\sqrt{R}+1.16R\right)\left(1-\lambda_G\right)-\left(0.68-1.04\sqrt{R}+1.16R\right)\left(1-\lambda_G\right)^2 \tag{6-7}$$

$$k_{13,G}=0.59+\left(1.18-1.84\sqrt{R}+1.16R\right)\lambda_G-\left(0.68-1.04\sqrt{R}+1.16R\right)\lambda_G^2 \tag{6-8}$$

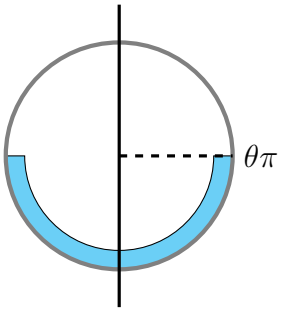

(a) Geometry of the film model, in which θ is the wetted wall fraction.

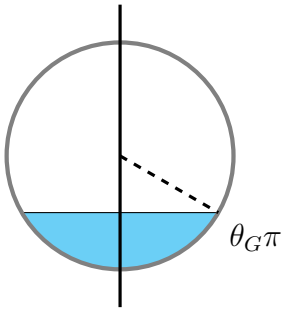

(b) Geometry of the gutter model, in which θ_G is the gutter angle.

Figure 6-6

R is the rounding radius from the inlet to the branch arm.

No energy loss factor for the liquid film at a junction was found in the literature. To overcome the lack of empirical closure relations, Ottens et al. [2] performed a multi-parameter non-linear fit with the following model:

$$k_{12,L} = \left(a_1 + \frac{a_2}{1 + Re_{L,2}} + a_3\kappa\right) k_{12_G}, \qquad k_{13,L} = \left(a_4 + \frac{a_5}{1 + Re_{L,3}} + a_6\kappa\right) k_{13_G} \tag{6-9}$$

Using a data set of 89 experimental data points for an impacting T-junction at atmospheric conditions with diameter 0.0295 $[m]$, u_{SG} = 15.7-15.8 $[m/s]$ and u_{SL} = 0.00063-0.030 $[m/s]$ the following a_i values were calculated: a_1=a_4=-1.109, a_2=a_5=-13.77 and a_3=a_6=1.646.

Using the above relations, the fluid properties and the superficial velocities for both phases, it is possible to predict the phase split behavior at an impacting tee.

Unfortunately, the geometrical relations to calculate the liquid heights described by Ottens et al. in their article which introduces the ADSM [2] as well as in their follow-up publication [29], do not produce the results featured in their articles. Multiple typing errors were found in the derivations reported in the two articles. Therefore, new geometrical relations were derived by the present author. These are described in Appendix A. However, for these new relations, the film model fails at high fluid velocities. Therefore it was decided to use the gutter model to calculate the liquid heights.

The results, obtained with these new relations with and without the film model, are shown in Figure 6-7 together with the results featured in the original article.

Results based on the newly derived relations, with and without the film model, exactly overlap the the results presented in the original paper by Ottens et al. for case (A) and (B). For case (C) with the higher superficial liquid velocity, the new relations do not match the original results but show similar behaviour. For case (D), the original data and the the newly calculated results differ significantly, especially when only the gutter model is used.

The film model fails to predict the liquid heights at higher fluid velocities. When only the gutter model is used instead of a linear superposition of both, the result is a sufficiently good match in case (A), (B), and (C). As there is no viable alternative, it was decided to incorporate the ADSM using only the gutter model.

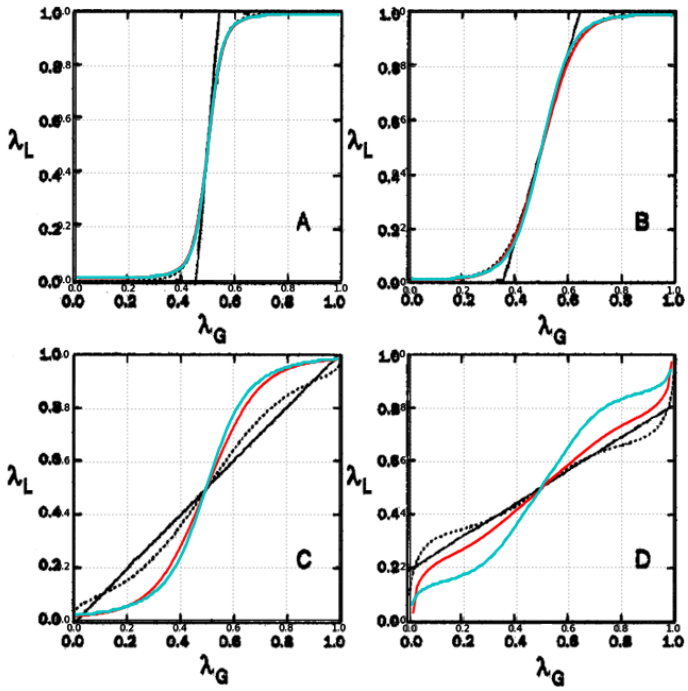

Figure 6-7: Phase split prediction results for the DSM (solid black), and the ADSM (dashed black), featured in the original article by Ottens et al. [2]. (A) $u_{SL} = 0.00063$ $[m/s]$, (B) $u_{SL} = 0.00302$ $[m/s]$, (C) $u_{SL} = 0.012$ $[m/s]$, (D) $u_{SL} = 0.030$ $[m/s]$. In all four cases $u_{SG} = 15.8$ $[m/s]$.
The red and cyan curves correspond to the phase split predictions using the new geometrical relations with, and without the film model, respectively.

6-2-3 Momentum model

In the momentum model, the fluid flow is assumed to be 1D steady state (consistent with the other two models). Thus, the flow in the inlet has momentum only in the $\hat{y}$ direction, and the flow in the outlets has momentum only in the $\hat{x}$ direction. For the control volume shown in Figure 6-8, the following two relations are derived from the conservation of momentum (Equation 2-2):

for the momentum the $\hat{x}$ direction:

$$\sum_{\beta} \left(\alpha_{\beta 3} \rho_{\beta 3} u_{\beta 3}^2 - \alpha_{\beta 2} \rho_{\beta 2} u_{\beta 2}^2 \right) = -p_3 + p_2 + \sum_{\beta} \left(\tau_{w\beta 2} S_{\beta 2} L - \tau_{w\beta 3} S_{\beta 3} L \right) / A \tag{6-10}$$

for the momentum the $\hat{y}$ direction:

$$\sum_{\beta} \left(\alpha_{\beta 1} \rho_{\beta 1} u_{\beta 1}^2 - 0 \right) = -p_1 + 0 + \sum_{\beta} \left(0 - \tau_{w\beta 1} S_{\beta 1} L \right) / A \tag{6-11}$$

where the subscript β could be either G or L for the gas phase and the liquid phase.

Because split of the phases over the two outlets is the property of interest, the momentum model focuses on Equation 6-10. This equation is rewritten as:

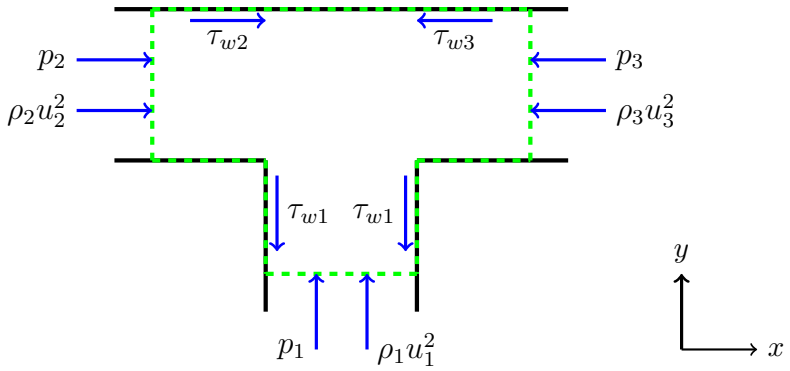

Figure 6-8: Schematic overview of the control volume used in the momentum model, and the forces working on the mixture.

$$\sum_{\beta}\left(\alpha_{\beta 3}\rho_{\beta 3}u_{\beta 3}^2-\alpha_{\beta 2}\rho_{\beta 2}u_{\beta 2}^2\right)+p_3-p_2-\sum_{\beta}\left(\tau_{w\beta 2}S_{\beta 2}L-\tau_{w\beta 3}S_{\beta 3}L\right)/A=K \tag{6-12}$$

For a phase split which is steady in time, the sum of all terms K is equal to zero.

Approximations, similar to those in the ADSM are made. The liquid holdup and the void fraction are determined by the solving the same empirical relation as for the ADSM:

$$\frac{\alpha_L}{1-\alpha_L}=\frac{u_{SL}}{u_{SG}}\left\{1+10.4\cdot Re_{SL}^{-0.363}\sqrt{\frac{\rho_L}{\rho_g}}\right\} \tag{6-13}$$

The gas and liquid momentum flux terms are rewritten using the square of the average velocity multiplied with a shape factor β:

$$\rho u^2=\rho\frac{<u^3>}{<u>}=\rho\beta<u>^2 \tag{6-14}$$

This shape factor is equivalent to the shape factor described in Appendix A by Equation A-11. The average velocity is calculated from the incoming mass flow of the phase W, the phase take off λ, the density ρ and the cross section occupied by the phase αA. For the liquid in the branch this becomes:

$$u_{L3}=\frac{W_1\lambda_L}{\rho_L\alpha_L A} \tag{6-15}$$

As there are no entrained liquid droplets in the outle[17], no liquid momentum flux term is required.

The friction terms are modelled using the relations below:

$$\tau_w=f\left(Re\right)\frac{1}{2}\rho<u>^2,\qquad\frac{S_L L}{A}=\frac{\pi D\theta}{\frac{\pi D^2}{4}},\qquad\frac{S_G L}{A}=\frac{\pi D\left(1-\theta\right)}{\frac{\pi D^2}{4}} \tag{6-16}$$

with θ the wetted wall fraction.

A phase splits satisfies the momentum model when the term K in Equation 6-12 is equal to zero. Thanks to the global convexity of K, which is shown in Figure 6-9, finding these solutions can be done using a 2D bisection method. The accuracy of this method scales with the step size of the bisections which decreases quadratically with the number of iterations performed. For 8 iterations, the accuracy is $1/2^8 = 1/256$.

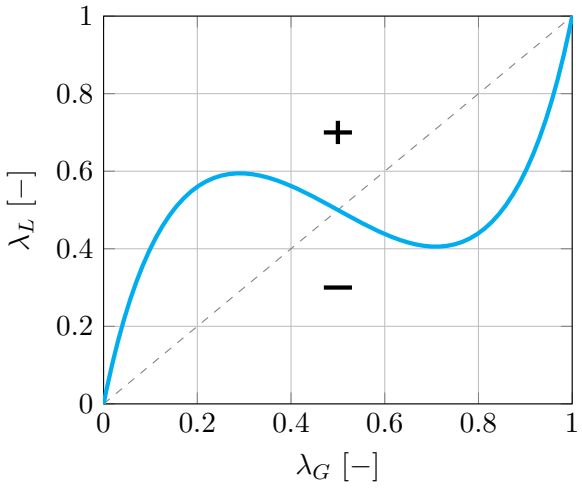

Figure 6-9: The value of K, for arbitrary input parameters, as a function of λ_G and λ_L. The cyan line, indicates where K is equal to zero and the corresponding phase split satisfies the momentum model. For all points above this line, K has a positive value. For all point below the line, K is negative.

6-2-4 Model implementation

The three sub-models presented above are built and linked in the Python 3.5.1 environment. The structure of the main model is shown in Figure 6-10.

The initial parameters of the main model are p_{back2}, p_{back3}, W_{G1}, W_{L1} and T. Initially, all λ_L λ_G combinations which satisfy the momentum model are calculated in a computational step which combines the single riser model and the momentum model. The single riser models transfers the back pressure information for both risers to the corresponding outlet of the junction from where it serves as an input to the momentum model. As the single riser model has to interface with the Shell Flow Correlations each time, the main model is discrete and not continuous. In the combined computational step, three arrays are generated containing the values for $\lambda_{L,MM}$, λ_G and $p_{junction}$.

Finally, the Advanced Double Stream Model calculates, for each λ_G generated in the previous step, the corresponding $\lambda_{L,ADSM}$ which satisfies the model. The density of the air in this step is calculated with T and $p_{junction}$ and the equation of state.

In the last computational step, the liquid fraction off takes generated by each model are compared. For each pair of λ_G and $\lambda_{L,MM}$, if the absolute difference between $\lambda_{L,MM}$ and $\lambda_{L,ADSM}$ is smaller than a tolerance ε, it is regarded as a feasible steady state phase split for

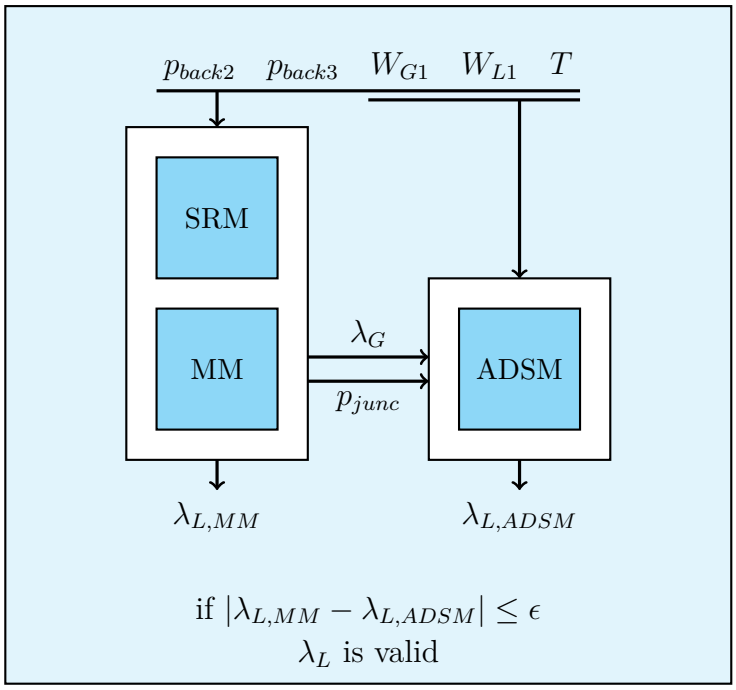

Figure 6-10: Overview of the structure of the computational model. The single riser model (SRM) and the momentum model (MM) are combined in the same computational step. The Advanced Double Stream Model (ADSM) is incorporated after this step.

the chosen initial parameters. Here, ε is chosen to be equal to half the spatial accuracy of the model: $\varepsilon = 1/2^{iterations}$.

The main model generates two outputs, namely a data file and a plot as shown in Figure 6-11. The file contains the initial parameters, each feasible phase split and its corresponding flow conditions (e.g. pressure drop over the risers, value of the different terms in Equation 6-12). The plot displays all λ_L's generated by the momentum model (colored) and the ADSM (yellow). The different colors of the momentum model curve correspond to flow regimes in the left and right riser and the legend to these colors is shown in table 6-2.

Although the plot in Figure 6-11 may resemble the phase split introduced in Figure 3-2b, it does not contain splitting curves. The plot generated by the main model shows which phase split(s) are feasible for a certain inflow and back pressure combination: the value(s) where both curves cross.

6-3 Model results

In the previous section the difference between a phase split plot and the plot generated by the model was described. The model can be used to generate phase split plots for a given inflow. In rhe experiments, phase split curves can be generated by varying the back pressure on the outlets of the junction for a certain inflow. Using the model, a similar approach results in a computer generated phase split plot. An example is shown in Figure 6-12 for an air flow rate of 100 $[Nm^3/h]$ and a water flow rate of 1 $[m^3/h]$ at room temperature.

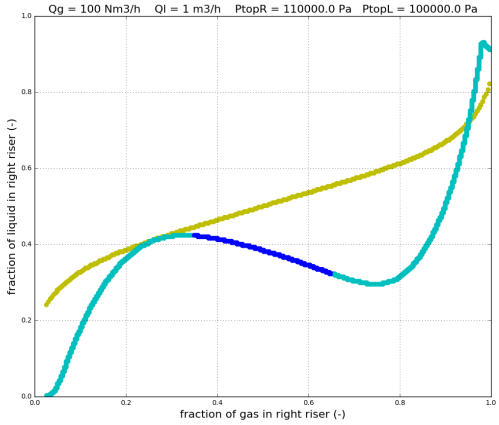

Figure 6-11: Example of plot generated by the main model. The two curves are the liquid mass fraction take offs predicted by both models.

Table 6-2: Table with colors corresponding to different flow pattern combinations.

Color	Flow regimes
Blue	Annular - Annular
Red	Churn - Churn
Green	Slug - Slug
Magenta	Annular - Churn
Cyan	Annular - Slug
Black	Churn - Slug
Yellow	Other

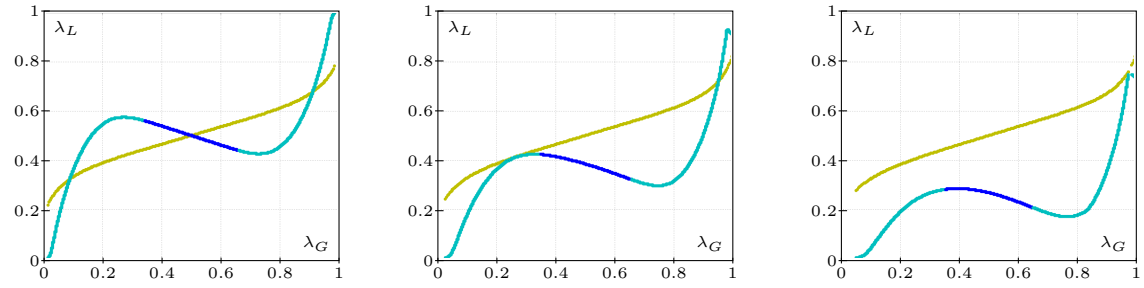

(a) $Q_G = 100\ [Nm^3/h]$
$Q_L = 1.0\ [m^3/h]$
$p_{back2} = 1.0 \cdot 10^5\ [Pa]$
$p_{back3} = 1.0 \cdot 10^5\ [Pa]$

(b) $Q_G = 100\ [Nm^3/h]$
$Q_L = 1.0\ [m^3/h]$
$p_{back2} = 1.0 \cdot 10^5\ [Pa]$
$p_{back3} = 1.1 \cdot 10^5\ [Pa]$

(c) $Q_G = 100\ [Nm^3/h]$
$Q_L = 1.0\ [m^3/h]$
$p_{back2} = 1.0 \cdot 10^5\ [Pa]$
$p_{back3} = 1.2 \cdot 10^5\ [Pa]$

Figure 6-12: Graphs generated by the model for a certain inflow with different back pressures on the risers.

Sixteen cases, with varying back pressures, are run for the inflow conditions specified above. The back pressure on the left riser is fixed at 1 $[bara]$, while the back pressure on the right riser is varied between 1.0 and 1.3 $[bara]$. In the three plots, shown in Figure 6-12, it is

seen that the shape of the ADSM curve remains unchanged. The different back pressures strongly influence the shape of the momentum model curve, and thereby the intersection and the feasible phase splits. Combining the phase splits generated in the sixteen cases results in the the left plot in Figure 6-13.

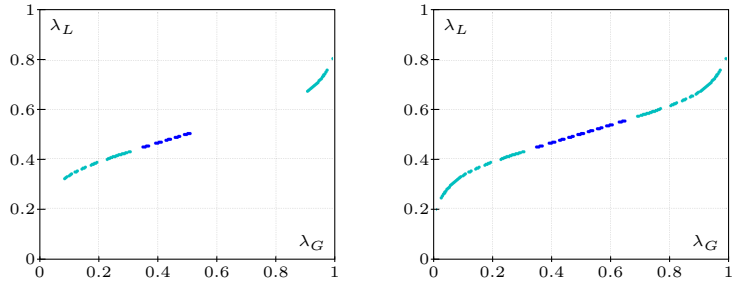

(a) Half phase split plot for:
$Q_G = 100\ [Nm^3/h]$
$Q_L = 1.0\ [m^3/h]$

(b) Full phase split plot for:
$Q_G = 100\ [Nm^3/h]$
$Q_L = 1.0\ [m^3/h]$

Figure 6-13: The left phase split plot is generated with the computational model. The right plot is constructed by mirroring the results from the other plot.

As the junction-riser geometry is symmetric, the plot is mirrored to obtain the results for varying the back pressure on the left riser while the right back pressure is fixed. Note that, the generated phase split curve is not continuous. This is because of the limited number of cases (the plot on the right side is constructed from the results of 16 computed cases and 15 mirrored results).

6-3-1 Comparison with literature findings

Figure 6-14 shows a series of computer generated phase split plots is shown for liquid flow rates of 1.0, 0.5 and 0.25 $[m^3/h]$ versus gas flow rates of 40, 60, 80, 100 and 150 $[Nm^3/h]$.

In the literature it was found that for increasing superficial liquid velocities the phase split curve should rotate in the clockwise directions around the (0.5;0.5) point. As the liquid flow rate increases from the bottom row to the top row, the superficial liquid increases in the same direction. It is seen in the matrix of splitting plots that, for all fixed gas flow rates, the phase split curve rotates in the clockwise direction with increasing liquid velocities. For a fixed liquid flow rate, increasing the superficial gas velocity results in the phase split curve to rotate in the anticlockwise direction around the (0.5;0.5) point according to literature. The opposite effect is seen in the matrix of splitting plots.

In the computational model, the exact shape of the phase split curve is determined by the ADSM. The momentum model only selects points on this curve that correspond to the given back pressures on the risers. The different behavior of the model for increasing superficial gas velocities is therefore attributed to the ADSM.

From the limited information presented in the original paper by Ottens et al. [2] on the principles of the ADSM for impacting T-junctions it can not be determined whether the model produces valid phase split predictions. Only the results in Figure 6-7 are presented in the article (fixed u_{SG}, increasing u_{SL}), and they are in line with the literature. The case of

increasing u_{SG} and fixed u_{SL}, where the models fails in the current implementation, is not treated by Ottens et al.

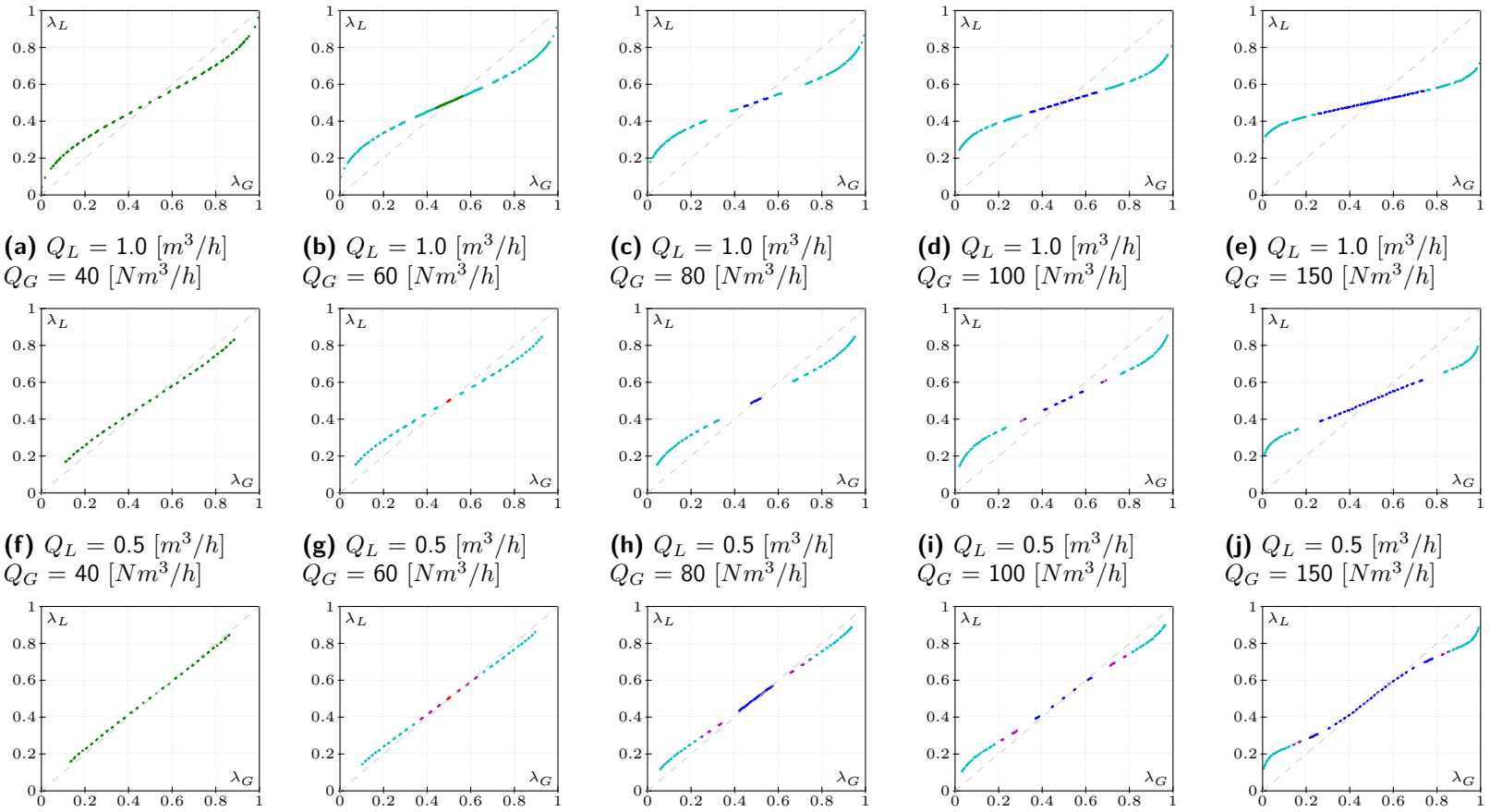

(a) $Q_L = 1.0\ [m^3/h]$ $Q_G = 40\ [Nm^3/h]$ **(b)** $Q_L = 1.0\ [m^3/h]$ $Q_G = 60\ [Nm^3/h]$ **(c)** $Q_L = 1.0\ [m^3/h]$ $Q_G = 80\ [Nm^3/h]$ **(d)** $Q_L = 1.0\ [m^3/h]$ $Q_G = 100\ [Nm^3/h]$ **(e)** $Q_L = 1.0\ [m^3/h]$ $Q_G = 150\ [Nm^3/h]$

(f) $Q_L = 0.5\ [m^3/h]$ $Q_G = 40\ [Nm^3/h]$ **(g)** $Q_L = 0.5\ [m^3/h]$ $Q_G = 60\ [Nm^3/h]$ **(h)** $Q_L = 0.5\ [m^3/h]$ $Q_G = 80\ [Nm^3/h]$ **(i)** $Q_L = 0.5\ [m^3/h]$ $Q_G = 100\ [Nm^3/h]$ **(j)** $Q_L = 0.5\ [m^3/h]$ $Q_G = 150\ [Nm^3/h]$

(k) $Q_L = 0.25\ [m^3/h]$ $Q_G = 40\ [Nm^3/h]$ **(l)** $Q_L = 0.25\ [m^3/h]$ $Q_G = 60\ [Nm^3/h]$ **(m)** $Q_L = 0.25\ [m^3/h]$ $Q_G = 80\ [Nm^3/h]$ **(n)** $Q_L = 0.25\ [m^3/h]$ $Q_G = 100\ [Nm^3/h]$ **(o)** $Q_L = 0.25\ [m^3/h]$ $Q_G = 150\ [Nm^3/h]$

Figure 6-14: Computer generated phase split plots for increasing gas (horizontal) and liquid flow rates (vertical).

6-3-2 Comparison with experimental data

To test the performance of the momentum model, it was decided to apply the model for the experimental conditions used by Van der Gronden [1]. Although it was found in the previous section that the model does not behave as described in the literature, some insight can be gained from this comparison. Table 6-3 shows the experimental conditions and results from Van der Gronden (for experiments with churn/slug flow in both risers). The phase split predictions by the computational model, are displayed in the two most right columns. An important note is that the risers used by Van der Gronden are not equal in length (16.3 $[m]$ and 15.4 $[m]$). This is accounted for in the model.

Table 6-3: The experimental conditions and the results obtained by Van der Gronden are shown on the left of the two vertical lines. The phase split predictions by the main model are shown in the two right columns.

Q_L m^3/h	Q_G Nm^3/h	p_{back2} $bara$	p_{back3} $bara$	λ_G $-$	λ_L $-$	λ_G $-$	λ_L $-$
1.01	56.31	1.860	1.089	-0.02	0.00	-	-
1.02	56.70	1.744	1.522	0.05	0.35	0.83	0.71
1.04	56.96	1.612	1.591	0.17	0.44	0.50	0.50
1.03	57.00	1.608	1.586	0.18	0.48	0.51	0.50
1.07	57.06	1.533	1.556	0.26	0.51	0.42	0.46
1.03	57.11	1.520	1.540	0.26	0.59	0.42	0.46
1.08	57.28	1.444	1.461	0.35	0.53	0.43	0.46
1.03	57.13	1.449	1.458	0.33	0.58	0.45	0.47
1.11	57.45	1.398	1.408	0.40	0.58	0.45	0.47
1.14	57.62	1.288	1.303	0.54	0.57	0.44	0.47
1.15	57.78	1.225	1.228	0.64	0.70	0.46	0.48
1.05	57.36	1.209	1.224	0.65	0.68	0.44	0.47
1.05	57.36	1.218	1.226	0.66	0.71	0.45	0.47
1.05	57.29	1.278	1.269	0.76	0.67	0.48	0.49
1.04	57.20	1.295	1.325	0.86	0.77	0.41	0.45

Looking at the different phase splits found in the experiment and determined by the model, it is seen that the model predicts a much more equal phase split. This is also shown in Figure 6-15.

It is expected that the assumption made in the model that the flow is fully developed is not valid for churn or slug flow in the outlets. This approximation fails due to:

- **The short length of the outlets**
  0.5 $[m]$ corresponds to 10 pipe diameters which is not enough length for the flow to fully develop.
- **Liquid build up at the riser base**
  Shortly after the outlets the flow orientation changes from horizontal to vertical. In the momentum model semi-empirical correlations are used to determine the hold-up, however they are derived for long pipe lines. The assumption of fully developed flow therefore does not hold.

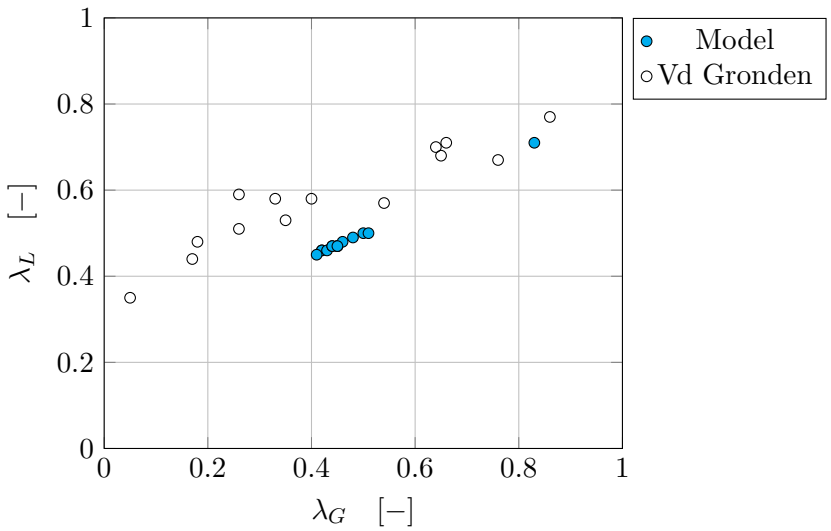

Figure 6-15: The liquid mass fraction take off as a function of the gas mass fraction take off as found by Van der Gronden and as predicted by the model.

- **Small pressure transients**
  It is expected that the small pressure transients between both outlets play a more significant role in the phase split than predicted by the control volume approach. The steady state flow approximation therefore does not hold here.

Based on the considerations above, it is concluded that the application of the control volume approach over the splitter as done in the momentum model has a limited accuracy in predicting the phase splits. This is due to the presence of risers and the short development lengths, which have a significant effect on the flow conditions and which are difficult to capture in the model.

6-4 Modeling conclusions

A new phase split prediction model is proposed, which uses the Advanced Double Stream Model for the conservation of energy in the isothermal junction and a control volume approach for the conservation of momentum in the tee in Section 6-2. The main conclusions of the computational study are summarized below:

- It is found in Section 6-2-1, which compares experiments and modelling results for twophase flow in a single riser, that using the *Novati* setting in the Shell Flow Correlations gives better results at low gas flow rates than the default settings.
- It is found in Section 6-2-2, that the write-up of the derivations in the original paper on the Advanced Double Stream Model contains errors in the geometrical models. New relations are derived, but for high flow rates the new ADSM fails to predict the phase splits when a linear combination of the film and gutter model is used to calculate the liquid heights. Further investigation is needed to find the cause for this.

- The behaviour of the phase split curves generated with the computational model are compared with the behaviour described in the literature in Section 6-3-1. The phase split curve rotates in the clockwise direction for increasing fluid velocities with our ADSM. This is not in agreement with the theory described in the literature. This misalignment requires further investigation.
- Predictions with our ADSM are compared to experimental data generated by Van de Gronden in Section 6-3-2. It is seen that the phase split predicted by the model is more symmetric than what is found in the experiments. It is concluded that the assumption of fully developed flow in the control volume approach is not valid.

Based on the points above a general conclusion can be that the modelling effort has not yet resulted in a reliable prediction model for the phase split.

Chapter 7

Conclusions & Recommendations

In this final chapter the general conclusions from the experimental and computational work are summarized. Furthermore, recommendations for further research are given.

7-1 General conclusions

The goal of the current research was to test the hypothesis (which can serve as a design criterion, if valid) that: The phase split, from a single flowline into two vertical riser using an impacting T-junction, is symmetric and constant in time when the total gas flow rate is sufficient to sustain annular flow in both risers.

Based on air-water flow experiments from a 2 $[in]$ diameter horizontal flowline into two 16.85 $[m]$ vertical risers of 1.25 $[in]$ diameter, the main conclusion is that the hypothesis above is true. Further conclusions from the experimental part and the computational part of this work are summarized below.

7-1-1 Experiments

The main conclusions of the experimental study are summarized below.

- The pressure drop curve is generated for three different superficial liquid velocities. As the superficial liquid velocity is increased, the superficial gas velocity corresponding to the pressure drop minimum is decreased.
- It is concluded that, for the current setup, which is symmetric downstream of the T-junction, the pressure gradient data combined with visual inspection of the flow patterns in both risers is sufficient to determine whether a phase split is symmetric.
- It is found that there are five possible states in which the flow can split (in the current setup). Of these five states only two are stable. They occur on opposites sides of a

specific transition gas flow rate. A schematic overview of the five states and how they develop was shown in Figure 5-14 and Figure 5-15.

- The transition gas flow rates are compared to the gas flow rates corresponding to the pressure drop minima in equivalent single riser experiments. For both characteristic flow rates the same behavior is found.

Based on these findings it can be concluded that the flow split at an impacting T-junction with vertical risers (downstream) will be stable symmetric when the gas flow rate is sufficiently high to sustain annular flow in both risers.

7-1-2 Modeling conclusions

A new prediction model for the phase split is proposed which applies the Advanced Double Stream Model for the conservation of energy in the isothermal junction and a control volume approach for the conservation of momentum in the tee. The influence of the two vertical risers is incorporated in the momentum model as pressure forces. The main conclusions of the computational study are summarized below:

- It is found in Section 6-2-2, that the write-up of the derivations in the original paper on the Advanced Double Stream Model contains errors in the geometrical models. New relations are derived, but for high flow rates the new ADSM fails to predict the phase splits when a linear combination of the film and gutter model is used to calculate the liquid heights. Further investigation is needed to find the cause for this.

- The behaviour of the phase split curves generated with the computational model are compared with the behaviour described in the literature in Section 6-3-1. The phase split curve rotates in the clockwise direction for increasing fluid velocities with our ADSM. This is not in agreement with the theory described in the literature. This misalignment requires further investigation.

- Predictions with our ADSM are compared to experimental data generated by Van de Gronden in Section 6-3-2. It is seen that the phase split predicted by the model is more symmetric than what is found in the experiments. It is concluded that the assumption of fully developed flow in the control volume approach is not valid.

From the points above, it is concluded that the modelling effort has not resulted in a reliable phase split prediction model.

No successful implementation of the ADSM for impacting T-junctions was found in the literature other than the original article by Ottens et al. [2], which contains erroneous geometrical relations. In their overview El-Shaboury et al. [20] evaluated the performance of what they call the Ottens model, although that Double Stream Model was derived by Hart et al.[19]. With only the information presented in the original article by Ottens et al., one can not rebuild a valid prediction model for the phase split.

7-2 Recommendations

As for the general conclusions, the recommendations are also categorized with respect to the experiments and the modelling.

7-2-1 Experiments

- Currently the SSL is not equipped with mass flow meters downstream of the risers, therefor phase flow rates after the split are not measured. If flow meters were installed, their time series data could be used for:
  - **Quantifing results**
    In Section 5-3-2 a hypothetical case was discussed from which it is concluded that, for experiments where the flow regime in both risers is annular, the pressure drop over the risers can be used to determine whether a phase split is equal.
  - **Model development**
    The only available experimental data on multiphase flow splitting at an impacting tee are from the work by Van der Gronden [1]. As the superficial gas velocities were relatively low in his experiments, this data set does not contain cases where the flow regime in either or both risers is annular. For the development and benchmarking of phase splitting models, the available data have to be expanded.
  - **Transient behavior**
    In the current research, only steady state experiments were performed, which means that the total mass flow rate in the two risers is equal to the air and water mass inflow in the setup. Identifying the transient behaviour of the phase split is of high importance for the development of operational procedures since transients during start-up can have a major impact on the safety of the operation.
- When in experiments the gas flow rate is set to a fixed value, the air flow controllers will deliver this amount of gas irrespectively of the system pressure. However, this is not in line with the conditions in the field, where the gas flow rate is not fixed, but a result of the pressure difference between the reservoir and the bottom hole location of the well. This dependency can be introduced in the experimental setup by a feedback loop which incorporates pressure indicator PI-309. The author expects that this introduces new forms of hysteresis.
- In the current research, an air-water mixture at atmospheric pressures is used as the working fluid and the density ratio between the two phases is in the order of 500. In the field, where oil and gas are the phases and pressure can rise above 150 [*bara*] this ratio is two orders of magnitude smaller (8:1). This changes the momentum ratio between the two phases in the flow and thereby the splitting behavior at the junction. Also the increased viscosity of the liquid will have an effect on the phase split. As a scale up step, experiments can be performed at medium pressures using hydrocarbons as the working fluid.
- In the computational part of the research, it was found that the flow in the junction and the riser cannot be treated separately. To investigate the influence of the risers on the

shape of the flow in the junction it would be interesting to replace the metal tee with a transparent one. Then phenomena as back flow from the risers and pressure effects in the upward bends can be studied using visualisation.

- As the flow between the junction and the risers is not fully developed, the flow structure inside the junction outlets is unknown. This could be resolved by inserting a wire mesh with capacitance sensor arrays downstream of the junction to obtain cross-sectional measurements of the liquid profile and the hold-up of the two phase flow.
- It was observed in the experiments with gas flow rates just below the flow rate transition point, where the most stable phase split is asymmetric, that "active" control can force the phase split in the unstable symmetric state. Each time when the unstable symmetric phase split changed to asymmetric, the back pressure on the riser with the higher gas flow rate was increased with choking. This increased pressure, forces more air to flow into the other riser. As active control of the phase split is outside the scope of the present research. no additional effort is put in this observation.
- The impacting T-junction used in the current research, can be considered as an idealization of the tees to be deployed in the field. In gas flowlines, wax may build up in the junction, and sand in the flow may erode the back wall. These all negatively influence the symmetric shape of the junction. They potentially introduce an unexpected maldistribution in the phase split. It is advised to perform tests on imperfect junctions and to assess the size of the maldistribution before the single flowline dual riser concept is deployed in the field.

7-2-2 Modeling

- In the current work, no agreement was found between the model predictions presented in the ADSM paper and the results computed using the ADSM that was derived in the present study. It is recommended to redetermine the empirical energy loss closure relations used in the ADSM to make that the results are valid. The experimental data from El-Shaboury et al. [15] can be used for this.
- As the results from the current model and literature suggest that small pressure transients between the outlets of the junction can have a large effect on the phase split, it is advised to look into dynamic modelling for future phase split predictions in the single flowline dual riser geometry. Dynamic modelling allows to represent possible hysteresis in the phase split as in the dual riser experiments in Section 5-3-3 hysteresis was observed.
- In a vertical gas well, the production depends on the *Tubing Performance Curve* (TPC) of the vertical pipe and the *Inflow Performance Relation* (IPR) of the reservoir. Here the production is stable when the gas flow rate is to the right of the pressure drop minimum. A similar analysis can be made for the single flowline dual riser geometry.

Appendix A

Derivations for the Advanced Double Stream Model

In 1991, Hart et al. [19] introduced the Double Stream Model (DSM). Four years later, Ottens et al. [2] published the Advanced Double Stream Model (ADSM), which is an improved version of the model by Hart et al. and which can be applied to a larger variety of flow conditions.

The Advanced Double Stream Model is based on the assumption that both the gas flow and the liquid flow at the inlet of the T-junction are split over the two outlets. This allows for the existence of the following four streamlines:

- Inlet-to-run gas flow
- Inlet-to-branch gas flow
- Inlet-to-run liquid flow
- Inlet-to-branch liquid flow

These four streamlines are shown in Figure A-1

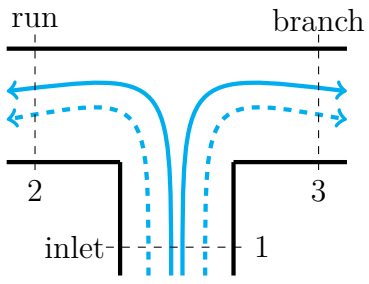

Figure A-1: Schematic drawing of the four stream lines in the Advanced Double Stream Model. Dotted lines: gas flow, solid lines: liquid flow.

The steady-state macroscopic mechanical energy balance, which is an extended version of the Bernoulli equation, i.e. with addition of a friction loss term $\hat{E}_v$, is applied to each of the four streamlines.

$$\frac{1}{2}\left[\frac{\langle u_1^3\rangle}{\langle u_1\rangle}-\frac{\langle u_2^3\rangle}{\langle u_2\rangle}\right]_G+\left[g\left(z_{1,2}-z_2\right)\right]_G+\left[\left(p_1-p_2\right)/\rho\right]_G=\left[\hat{E}_{v12}\right]_G \tag{A-1a}$$

$$\frac{1}{2}\left[\frac{\langle u_1^3\rangle}{\langle u_1\rangle}-\frac{\langle u_3^3\rangle}{\langle u_3\rangle}\right]_G+\left[g\left(z_{1,3}-z_3\right)\right]_G+\left[\left(p_1-p_3\right)/\rho\right]_G=\left[\hat{E}_{v13}\right]_G \tag{A-1b}$$

$$\frac{1}{2}\left[\frac{\langle u_1^3\rangle}{\langle u_1\rangle}-\frac{\langle u_2^3\rangle}{\langle u_2\rangle}\right]_L+\left[g\left(z_{1,2}-z_2\right)\right]_L+\left[\left(p_1-p_2\right)/\rho\right]_L=\left[\hat{E}_{v12}\right]_L \tag{A-1c}$$

$$\frac{1}{2}\left[\frac{\langle u_1^3\rangle}{\langle u_1\rangle}-\frac{\langle u_3^3\rangle}{\langle u_3\rangle}\right]_L+\left[g\left(z_{1,3}-z_3\right)\right]_L+\left[\left(p_1-p_3\right)/\rho\right]_L=\left[\hat{E}_{v13}\right]_L \tag{A-1d}$$

With the assumption that:

$$\left(p_2-p_3\right)_G=\left(p_2-p_3\right)_L \tag{A-2}$$

these are combined in one equation:

$$\begin{aligned}\frac{1}{2}\rho_G\left[\frac{\langle u_3^3\rangle}{\langle u_3\rangle}-\frac{\langle u_2^3\rangle}{\langle u_2\rangle}\right]_G-\frac{1}{2}\rho_L\left[\frac{\langle u_3^3\rangle}{\langle u_3\rangle}-\frac{\langle u_2^3\rangle}{\langle u_2\rangle}\right]_L+\rho_G\left[g\left(z_3-z_{1,3}+z_{1,2}-z_2\right)\right]_G\\-\rho_L\left[g\left(z_3-z_{1,3}+z_{1,2}-z_2\right)\right]_L=\rho_G\left[\hat{E}_{v12}-\hat{E}_{v13}\right]_G-\rho_L\left[\hat{E}_{v12}-\hat{E}_{v13}\right]_L\end{aligned} \tag{A-3}$$

The friction loss $\hat{E}_v$ for both phases is defined using a friction loss coefficient k which depends on the Reynolds number and geometry of the junction [37]:

$$\hat{E}_v=k\frac{1}{2}\frac{\langle u_1^3\rangle}{\langle u_1\rangle} \tag{A-4}$$

The kinetic energy ratio κ of the gas and the liquid at the the inlet is defined as:

$$\kappa=\frac{\rho_G\left\langle u_{G1}^3\right\rangle/\left\langle u_{G1}\right\rangle}{\rho_L\left\langle u_{L1}^3\right\rangle/\left\langle u_{L1}\right\rangle} \tag{A-5}$$

The gas phase split λ_G, and the liquid phase split λ_L are defined using the average velocity $< u >$ and the phase holdup α:

$$\lambda_G=\frac{\langle u_{G3}\rangle\,\alpha_{G3}D_3^2}{\langle u_{G1}\rangle\,\alpha_{G1}D_1^2} \tag{A-6}$$

$$\lambda_L=\frac{\langle u_{L3}\rangle\,\alpha_{L3}D_3^2}{\langle u_{L1}\rangle\,\alpha_{L1}D_1^2} \tag{A-7}$$

Substitution of the above equations into Equation A-3 results into:

$$\kappa\left[\frac{\beta_{G2}\alpha_{G1}D_1^4}{\beta_{G1}\alpha_{G2}D_2^4}\left(1-\lambda_G\right)^2-\frac{\beta_{G3}\alpha_{G1}D_1^4}{\beta_{G1}\alpha_{G3}D_3^4}\lambda_G^2\right]-\left[\frac{\beta_{L2}\alpha_{L1}D_1^4}{\beta_{L1}\alpha_{L2}D_2^4}\left(1-\lambda_L\right)^2-\frac{\beta_{L3}\alpha_{L1}D_1^4}{\beta_{L1}\alpha_{L3}D_3^4}\lambda_L^2\right]$$
$$+\frac{2g}{\beta_{L1}\left\langle u_{L1}\right\rangle^2}\left[\frac{\rho_G}{\rho_L}\left(z_{G3}-z_{G1,3}+z_{G1,2}-z_{G2}\right)-\left(z_{L3}-z_{L1,3}+z_{L1,2}-z_{L2}\right)\right]=$$
$$\kappa\left(k_{13}-k_{12}\right)_G-\left(k_{13}-k_{12}\right)_L \quad \text{(A-8)}$$

Equation A-8 is the governing equation for the mechanical energy in the junction. It contains all information from the four streamlines.

Approximations

To simplify the governing equation, which will also reduce the amount of parameters, Ottens et al. applied the following approximations.

The difference in the heights of the gas streamlines is neglected, as the contribution of this term is small since $\rho_G << \rho_L$ for the air-water mixture.

$$\kappa\left[\frac{\beta_{G2}\alpha_{G1}D_1^4}{\beta_{G1}\alpha_{G2}D_2^4}\left(1-\lambda_G\right)^2-\frac{\beta_{G3}\alpha_{G1}D_1^4}{\beta_{G1}\alpha_{G3}D_3^4}\lambda_G^2\right]-\left[\frac{\beta_{L2}\alpha_{L1}D_1^4}{\beta_{L1}\alpha_{L2}D_2^4}\left(1-\lambda_L\right)^2-\frac{\beta_{L3}\alpha_{L1}D_1^4}{\beta_{L1}\alpha_{L3}D_3^4}\lambda_L^2\right]$$
$$+\frac{2g}{\beta_{L1}\left\langle u_{L1}\right\rangle^2}\left[-\left(z_{L3}-z_{L1,3}+z_{L1,2}-z_{L2}\right)\right]=\kappa\left(k_{13}-k_{12}\right)_G-\left(k_{13}-k_{12}\right)_L \quad \text{(A-9)}$$

The velocity term in the kinetic energy ratio κ is approximated as:

$$\frac{\left\langle u^3\right\rangle}{\left\langle u\right\rangle}=\beta\left\langle u\right\rangle^2 \quad \text{(A-10)}$$

Here, the velocity shape factor β is 1.54 in the laminar flow regime, β is 1.00 in the turbulent flow regime, and a linear interpolation is used for the transition area in between.

$$\beta=\begin{cases}1.54 & Re<1500\\ 1.54-0.54\frac{(Re-1500)}{500} & 1500<Re<2000\\ 1.00 & Re>2000\end{cases} \quad \text{(A-11)}$$

The Reynolds numbers are defined as:

$$Re_L=\frac{Re_{SL}}{\theta}=\frac{\rho_L u_{SL}D}{\mu_L\theta},\qquad Re_G=\frac{\rho_G u_G D}{\mu_G} \quad \text{(A-12)}$$

The wetted wall fraction θ and the liquid holdup α_L, are calculated from empirical correlations developed by Hart et al. [38] for gas-liquid flow in horizontal smooth pipes:

$$\frac{\alpha_L}{1-\alpha_L} = \frac{u_{SL}}{u_{SG}} \left\{ 1 + 10.4 \cdot Re_{SL}^{-0.363} \sqrt{\frac{\rho_L}{\rho_g}} \right\} \tag{A-13}$$

$$\theta = 0.52\alpha^{0.374} + 0.26 \cdot \left\{ \frac{u_L^2 \rho_L}{\alpha_L^2 g D \left(\rho_L - \rho_G\right)} \right\}^{0.58} \tag{A-14}$$

The void fraction α_G, follows from the liquid holdup fraction α_L:

$$\alpha_G = 1 - \alpha_L \tag{A-15}$$

Geometrical models

For the calculation of the different liquid heights in the junction Ottens, uses a linear combination of the film model and the gutter model shown in Figure A-2.

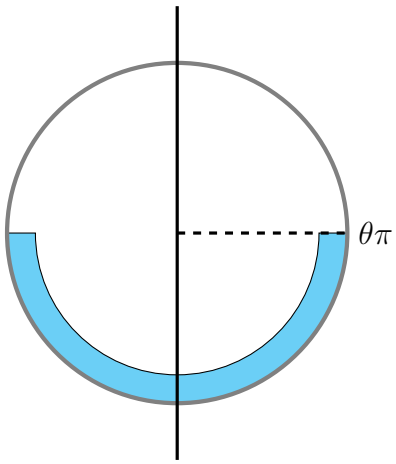

(a) Geometry of the film model, where θ is the wetted wall fraction.

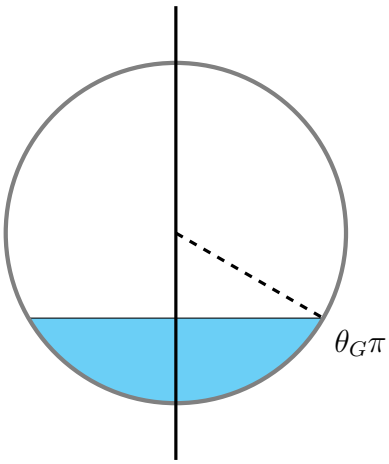

(b) Geometry of the gutter model, where θ_G is the gutter angle.

Figure A-2

The height of the centre of mass of the liquid is defined by:

$$z_L = \frac{\int_S \rho z \mathrm{dS}}{\int_S \rho \mathrm{dS}} \tag{A-16}$$

where ρ is constant for the incompressible liquid.

The linear combination of the film model and the gutter model is defined as:

$$z_L = \frac{\theta - \theta_G}{\theta + \theta_G} z_F + \frac{2\theta_G}{\theta + \theta_G} z_{Gu} \tag{A-17}$$

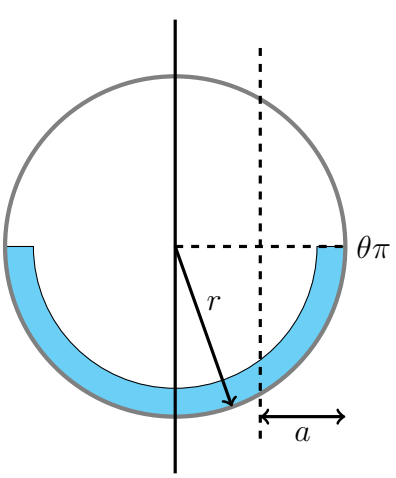

(a) The polar coordinate system used in the film model.

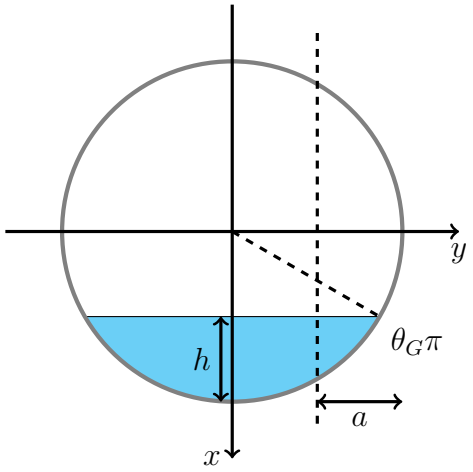

(b) The Cartesian coordinate system used in the gutter model.

Figure A-3

Film model

In the calculations with the film model, the polar coordinates shown in Figure A-3a are used. The wetted wall fraction denoted by θ, is determined by Equation A-14.

The part of the cross sectional area covered with liquid, is bounded by the following relations:

$$r_1 = \frac{D}{2}\sqrt{1-\frac{\alpha_L}{\theta}}, \qquad r_2 = \frac{D}{2}, \qquad \phi_1 = -\theta\pi, \qquad \phi_2 = \theta\pi \tag{A-18}$$

The formula for the height of the liquid in this coordinate system is:

$$z_F = \frac{D}{2} - \frac{\int_{\phi_1}^{\phi_2}\int_{r_1}^{r_2}\rho r^2\cos(\phi)\mathrm{d}r\mathrm{d}\phi}{\int_{\phi_1}^{\phi_2}\int_{r_1}^{r_2}\rho r\mathrm{d}r\mathrm{d}\phi} \tag{A-19}$$

In Equation A-3 a distinction is made between $z_{1,2}$ and $z_{1,3}$. The two heights correspond to the two portion of the incoming fluid flowing in the run (2) and branch arm (3), respectively. These areas are divided by a dividing plane indicated by the vertical dashed line in Figure A-3.

First the value of a, which is the distance between the right side of the pipe and the dividing plane is calculated. The following relation is used:

$$A_{L,Br} = \lambda_L A_{Film} = \lambda_L \frac{D^2\pi}{4}\alpha_L \tag{A-20}$$

This is equal to the area bound by:

$$r_1 = \frac{D}{2}\sqrt{1-\frac{\alpha_L}{\theta}}, \qquad r_2 = \frac{D}{2}, \qquad \phi_1 = \arcsin\left(\frac{\frac{D}{2}-a}{\frac{D}{2}}\right), \qquad \phi_2 = \theta\pi \tag{A-21}$$

which result in the following surface integral:

$$A_{L,Br} = \int_{\phi_1}^{\phi_2} \int_{r_1}^{r_2} r\mathrm{d}r\mathrm{d}\phi = \frac{1}{2}\left[\frac{D^2}{4} - \frac{D^2}{4}\left(1 - \frac{\alpha_L}{\theta}\right)\right]\left(\theta\pi - \arcsin\left(\frac{\frac{D}{2} - a}{\frac{D}{2}}\right)\right) \tag{A-22}$$

Now the height of the center of mass of the liquid film flowing into the branch arm can be calculated with the value of a, the boundaries in A-21 and the formula below.

$$z_{F,Br} = \frac{D}{2} - \frac{\int_{\phi_1}^{\phi_2}\int_{r_1}^{r_2} \rho r^2 \cos(\phi)\mathrm{d}r\mathrm{d}\phi}{\int_{\phi_1}^{\phi_2}\int_{r_1}^{r_2} \rho r\mathrm{d}r\mathrm{d}\phi} \tag{A-23}$$

For the calculation of the liquid height $z_{1,2}$, the same equations are used where a is swapped with c:

$$c = \frac{D}{2} - a \tag{A-24}$$

Gutter model

Using the symmetry in the gutter model, the height of the center of mass of the cross sectional area covered with liquid is calculated using the following integral boundaries:

$$x_1 = \frac{D}{2} - h, \qquad x_2 = \frac{D}{2}, \qquad y_1 = 0, \qquad y_2 = \sqrt{\frac{D^2}{4} - x^2} \tag{A-25}$$

with,

$$h = \frac{D}{2} - \frac{D}{2}\cos(\theta_G\pi) \tag{A-26}$$

For the Cartesian system, the centre of mass integral is written as:

$$z_{Gu} = \frac{D}{2} - \frac{\int_{x_1}^{x_2}\int_{y_1}^{y_2} \rho x\mathrm{d}y\mathrm{d}x}{\int_{x_1}^{x_2}\int_{y_1}^{y_2} \rho\mathrm{d}y\mathrm{d}x} \tag{A-27}$$

In calculating the height of the portion of the liquid flowing towards the branch arm, the same a is taken as in the film model.

$$x_1 = \frac{D}{2}\cos\left(\theta_G\pi\right), \qquad x_2 = y_2^2, \qquad y_1 = \frac{D}{2} - a, \qquad y_2 = \frac{D}{2}\sin(\theta_G\pi) \tag{A-28}$$

are inserted into the following integral:

$$z_{Gu,Br} = \frac{D}{2} - \frac{\int_{y_1}^{y_2}\int_{x_1}^{x_2} \rho x\mathrm{d}x\mathrm{d}y}{\int_{y_1}^{y_2}\int_{x_1}^{x_2} \rho\mathrm{d}x\mathrm{d}y} \tag{A-29}$$

Similar as in the film model, the variable c is introduced for the run arm.

Energy loss factors

Important in the ADSM is the empirical closure for the energy loss factors k in Equation A-4. For the gas phase Ottens et al. use relations for the loss factor based on work by Ito and Imai [36] for single phase turbulent gas flow in impacting T-junctions:

$$k_{12,G} = 0.59 + \left(1.18 - 1.84\sqrt{R} + 1.16R\right)(1-\lambda_G) - \left(0.68 - 1.04\sqrt{R} + 1.16R\right)(1-\lambda_G)^2 \tag{A-30}$$

$$k_{13,G} = 0.59 + \left(1.18 - 1.84\sqrt{R} + 1.16R\right)\lambda_G - \left(0.68 - 1.04\sqrt{R} + 1.16R\right)\lambda_G^2 \tag{A-31}$$

In which R is the rounding radius from the inlet to the branch arm. No relations were found in the literature by Ottens et al. or by the present author for the loss factors of the liquid layer in stratified wavy flow in a junction. In their work Ottens et al., performed a multi-parameter non-linear fit with the following model:

$$k_{12,L} = \left(a_1 + \frac{a_2}{1+Re_{L,2}} + a_3\kappa\right)k_{12_G}, \qquad k_{13,L} = \left(a_4 + \frac{a_5}{1+Re_{L,3}} + a_6\kappa\right)k_{13_G} \tag{A-32}$$

Using a data set of 89 experimental data points, obtained for an impacting T-junction at atmospheric conditions with diameter 0.0295 $[m]$, u_{SG} = 15.7-15.8 $[m/s]$ and u_{SL} = 0.00063-0.030 $[m/s]$ the a_i values become: a_1=a_4=-1.109, a_2=a_5=-13.77 and a_3=a_6=1.646.

Appendix B

Pictures of the setup

In this section, pictures of the key elements of the Severe Slugging Loop are shown. The pictures are listed along the path of the air and water flow trough the system.

Figure B-1: Pump P-145 and control valve FCV-300 that regulates the liquid flow rate.

(a) Gas mass flow controller FIC-110 that extracts the air from the STCA air supply.

(b) Buffer vessel V-103 for the air.

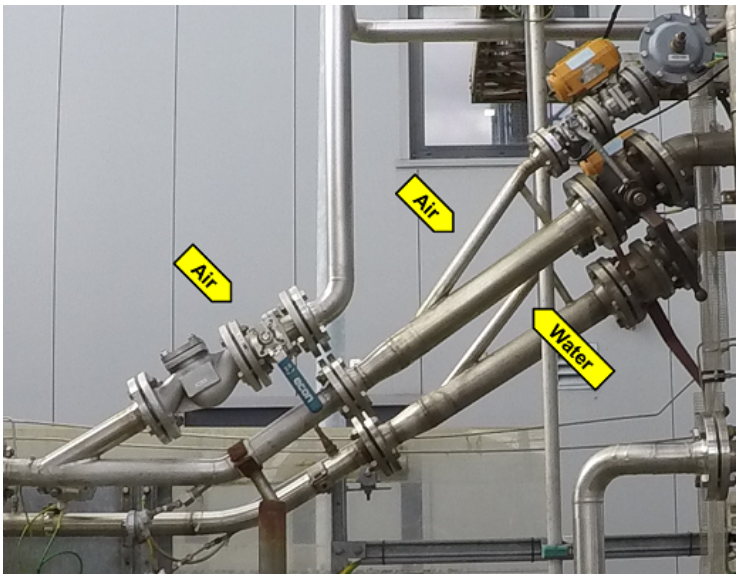

Figure B-3: The air and water are combined in this double Y-sprout inlet device.

Figure B-4: 180° bend connecting both halves of the 100 $[m]$ flowline.

Figure B-5: Second halve of the flowline containing the inclined perspex section and the horizontal section towards the T-junction.

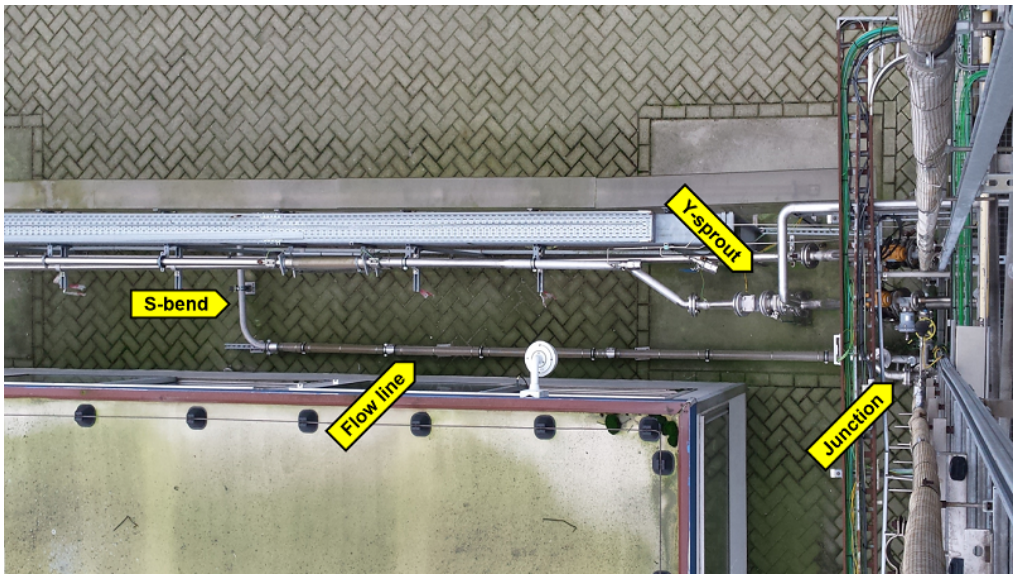

Figure B-6: Top view of the S-bend towards the horizontal section upstream of the junction.

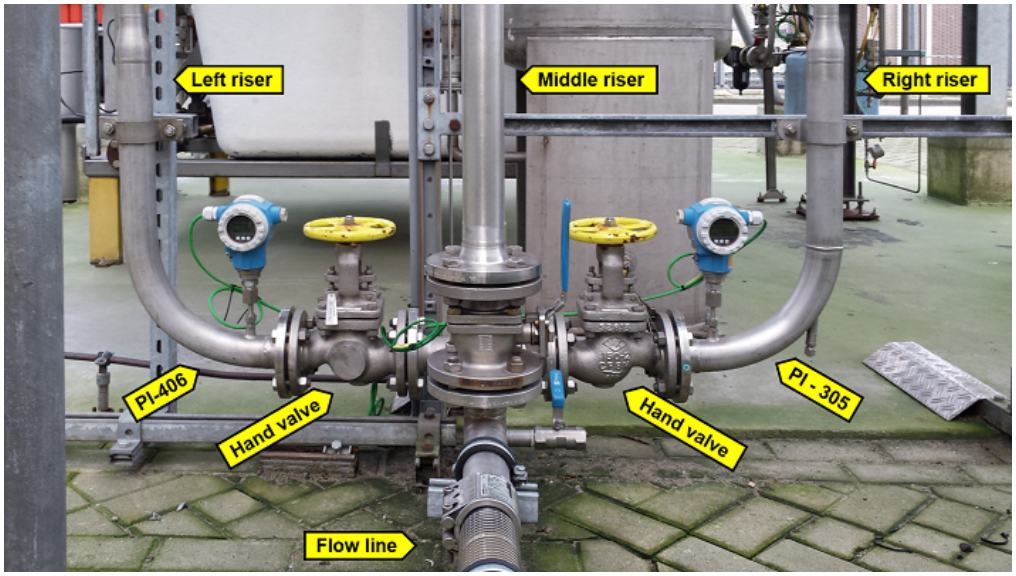

Figure B-7: Impacting T-junction which splits the mixture into the left and the right riser.The middle riser is not used in this research.

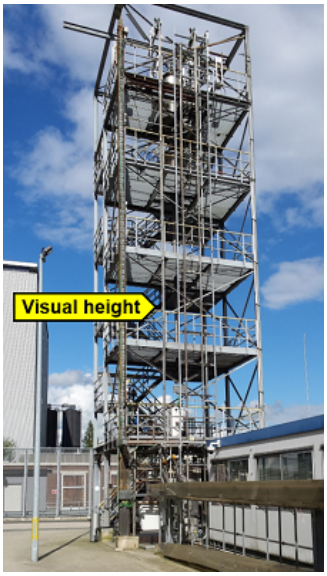

(a) Tower construction which supports the vertical risers. Flow pattern visualizations are taken at the height indicated with the arrow.

(b) Right riser head configuration with pressure indicator PI-311 followed by a choke valve FCV-310.

Figure B-9: Top section where the flow from both risers is combined.

(a) Final pipe segment of the top section and separator vessel V-201. The air is released in the atmosphere and the water flows down into vessel V-202.

(b) Vessel V-202 serves as a temporary water storage tank upstream of the pump.

Bibliography

[1] W. van der Gronden, "Experiments and modelling of twophase flow in a single flowline with two risers using a symmetric splitter," Master's thesis, Delft University of Technology, 2013.

[2] M. Ottens, A. de Swart, H. Hoefsloot, and P. Hamersma, "Gas-liquid flow splitting in regular, reduced and impacting T junctions," *Impianistica Italiana*, vol. 8, pp. 23–33, 1995.

[3] K. Hong, "Two-phase flow splitting at a pipe tee," *Journal of Petroleum Technology*, vol. 30, pp. 290–296, 1978.

[4] P. Prickaerts, "Controlling the split of a two phase gas-liquid flow from a single flowline to a dual riser," Master's thesis, Delft University of Technology, 2011.

[5] H. Van den Akker and R. Mudde, *Fysische transportverschijnselen.* Delft University Press, 2008.

[6] S. W. Churchill, "Friction-factor equation spans all fluid-flow regimes," *Chemical Engineering*, vol. 84, pp. 91–92, 1977.

[7] J. van 't Westende, *Droplets in annular-dispersed gas-liquid pipe-flows.* PhD thesis, Delft University of Technology, 2008.

[8] R. IJzermans and R. Lacy, "Technical description Shell Flow Correlations," Tech. Rep. GS.09.51663, Shell Global Solutions, 2009.

[9] G. B. Wallis, "One-dimensional two-phase flow," *AIChE Journal*, 1969.

[10] Y. Taitel and A. Dukler, "A model for predicting flow regime transitions in horizontal and near horizontal gas-liquid flow," *AIChE Journal*, vol. 22, pp. 47–55, 1976.

[11] C. E. Brennen, *Fundamentals of multiphase flow.* Cambridge University Press, 2005.

[12] J. Lea, H. Nickens, and M. Wells, *Gas well deliquification.* Gulf Professional Publishing, 2008.

[13] D. van Nimwegen, *The effect of surfactants on gas-liquid pipe flows.* PhD thesis, Delft University of Technology, 2015.

[14] S. Hwang, H. Soliman, and R. L. Jr, "Phase separation in impacting wyes and tees," *International Journal of Multiphase Flow*, vol. 15, pp. 965 – 975, 1989.

[15] A. El-Shaboury, H. Soliman, and G. Sims, "Two-phase flow in a horizontal equal-sided impacting tee junction," *International Journal of Multiphase Flow*, vol. 33, pp. 411 – 431, 2007.

[16] B. Azzopardi and P. Whalley, "The effect of flow patterns on two-phase flow in a T junction," *International Journal of Multiphase Flow*, vol. 8, pp. 491 – 507, 1982.

[17] B. Azzopardi, A. Purvis, and A. Govan, "Annular two-phase flow split at an impacting T," *International Journal of Multiphase Flow*, vol. 13, pp. 605 – 614, 1987.

[18] R. Chin, "Wet-steam splitting in a dead end tee," Tech. Rep. WRC-885, Shell Development Company, 1984.

[19] J. Hart, P. Hamersma, and J. Fortuin, "Phase distribution during gas-liquid flow through horizontal dividing junctions," *Nuclear Engineering and Design*, vol. 126, pp. 293 – 312, 1991.

[20] A. El-Shaboury, H. Soliman, and G. Sims, "Current state of knowledge on two-phase flow in horizontal impacting tee junctions," *Multiphase Science and Technology*, vol. 13, pp. 139 – 178, -.

[21] S. Chien and M. Rubel, "Phase splitting of wet steam in annular flow through a horizontal impacting tee junction," *SPE Production Engineering*, vol. 7, pp. 368–374, 1992.

[22] T. Ellison, D. Hatziavramidis, B. Sun, D. Gidaspow, *et al.*, *Computational fluid dynamics (CFD) model for phase separation at branching tee junctions.* Society of Petroleum Engineers, 1997.

[23] R. Worthen, "CFD simulations to predict gas-liquid flow splitting from a single flowline to two vertical risers," Tech. Rep. SR.14.13794, Shell Global Solutions, 2014.

[24] W. Yang and R. Menon, "Development of a rigorous modeling tool to analyze multiphase flow splitting," Tech. Rep. GS.07.53547, Shell Global Solutions, 2007.

[25] S. Sarkar, A. Singh, and P. Moeleker, "Evaluation of OpenFOAM for modeling multiphase flow splitting in T-junctions 2010," Tech. Rep. GS.10.53274, Shell Technology India, 2010.

[26] B. J. Azzopardi, "Phase separation at T junctions," *Multiphase Science and Technology*, vol. 11, pp. 223–329, 1999.

[27] A. Elazhary and H. Soliman, "Single- and two-phase pressure losses in a horizontal mini-size impacting tee junction with a rectangular cross-section," *Experimental Thermal and Fluid Science*, vol. 41, pp. 67 – 76, 2012.

[28] K. Hong and S. Griston, "Two-phase flow splitting at an impacting tee," *SPE Production & Facilities*, vol. 8, pp. 184 – 190, 1995.

[29] M. Ottens, H. C. Hoefsloot, and P. J. Hamersma, "Transient gas-liquid flow in horizontal T-junctions," *Chemical Engineering Science*, vol. 56, pp. 43 – 55, 2001.

[30] R. Lahey, "Current understanding of phase separation mechanisms in branching conduits," *Nuclear Engineering and Design*, vol. 95, pp. 145–161, 1986.

[31] N. Saba and R. Lahey, "The analysis of phase separation phenomena in branching conduits," *Int. J. Multiphase Flow*, vol. 10, pp. 1 – 20, 1984.

[32] S. Hwang, H. Soliman, and R. Lahey, "Phase separation in dividing two-phase flows," *International Journal of Multiphase Flow*, vol. 14, pp. 439 – 458, 1988.

[33] G. Groote and G. Haandrikman, "Experiments and simulations for the smart choke control of transient slugs," Tech. Rep. GS.06.52467, Shell Global Solutions, 2006.

[34] R. Malekzadeh, R. Henkes, and R. Mudde, "Severe slugging in a long pipeline-riser system: Experiments and predictions," *International Journal of Multiphase Flow*, vol. 46, pp. 9 – 21, 2012.

[35] A. Rajkotwala and P. R. Esquivel, "Validation and improvement of the Shell Flow Correlations for vertical flows," 2015.

[36] H. Ito and K. Imai, "Energy losses at 90° pipe tee junctions," *Journal of the Hydraulics Division*, vol. 09, pp. 1353–1369, 1973.

[37] R. B. Bird, W. E. Stewart, and E. N. Lightfoot, *Transport phenomena. 1960.* Madison, USA, 1960.

[38] J. Hart, P. Hamersma, and J. Fortuin, "Correlations predicting frictional pressure drop and liquid holdup during horizontal gas-liquid pipe flow with a small liquid holdup," *International Journal of Multiphase Flow*, vol. 15, pp. 947 – 964, 1989.